FAR-INFRARED SYNCHROTRON-BASED SPECTROSCOPY OF PROTON TUNNELLING IN MALONALDEHYDE

by

Edward Scott Goudreau

Bachelor of Science (Major in Physics and Chemistry, Honours in Physics), University of New Brunswick, 2014

A Thesis Submitted in Partial Fulfilment of
the Requirements for the Degree of

Master of Science

in the Graduate Academic Unit of Physics

Supervisors:	Dennis Tokaryk, PhD, Department of Physics Stephen Ross, PhD, Department of Physics
Examining Board:	Abdelhaq Hamza, PhD, Department of Physics, Chair Dennis Tokaryk, PhD, Department of Physics Stephen Ross, PhD, Department of Physics Sambhu Ghosh, PhD, Department of Physics David Magee, PhD, Department of Chemistry

This thesis is accepted by the
Dean of Graduate Studies

THE UNIVERSITY OF NEW BRUNSWICK

October, 2016

Abstract

Although the internally hydrogen-bonded species malonaldehyde ($C_3O_2H_4$) is considered an important prototype molecule for intramolecular proton transfer, its far-IR spectrum is not well understood. Using high-resolution spectra obtained from the Canadian Light Source synchrotron in Saskatoon, Saskatchewan, I have made significant progress in understanding its low-energy vibrational structure. A new rotational characterization of the vibrational ground state tunnelling-split pair is presented here, which benefits from these new IR measurements covering a more complete range of rotational parameter space than was reported previously. Full rotational analyses have been performed for three low-energy vibrational states at 241, 390, and 405 cm^{-1} and these states (as well as states at 273 and 282 cm^{-1}) have been conclusively matched to early microwave measurements [W. F. Rowe, Ph.D. Thesis, Harvard University, 1975]. Progress has been made toward developing a theoretical treatment of malonaldehyde using the Generalized Semi-Rigid Bender Hamiltonian to describe the large-amplitude tunnelling motion.

to my parents,
for support and encouragement

Acknowledgements

I would like to thank my supervisors, Dr. Dennis Tokaryk and Dr. Stephen Ross, for excellent instruction and guidance throughout this project; Dr. Brant Billinghurst, the Far-IR beamline scientist at the Canadian Light Source, for his assistance in data collection; Dr. David Magee and Dr. James Tait, who helped in performing the chemical synthesis of malonaldehyde; Dr. Colin Western, who developed the PGOPHER program that was used extensively during this project; Dr. Fumiyuki Ito, who provided the *ab initio* calculations that were used in the theoretical modeling; and Dr. Keiichi Tanaka, for providing preliminary data from an earlier study.

I would also like to thank David Milley, a long-time friend, for many hours of thought-provoking conversation and for providing an outside perspective on my work.

Table of Contents

List of Tables

List of Figures

Chapter 1

Introduction

1.1 - Review of Experimental Work on Malonaldehyde

Malonaldehyde ($C_3O_2H_4$) is a 9-atom planar molecule which possesses an asymmetric intramolecular hydrogen bond between the hydroxyl and formyl groups in its enol form, as seen in figure 1.1.1.

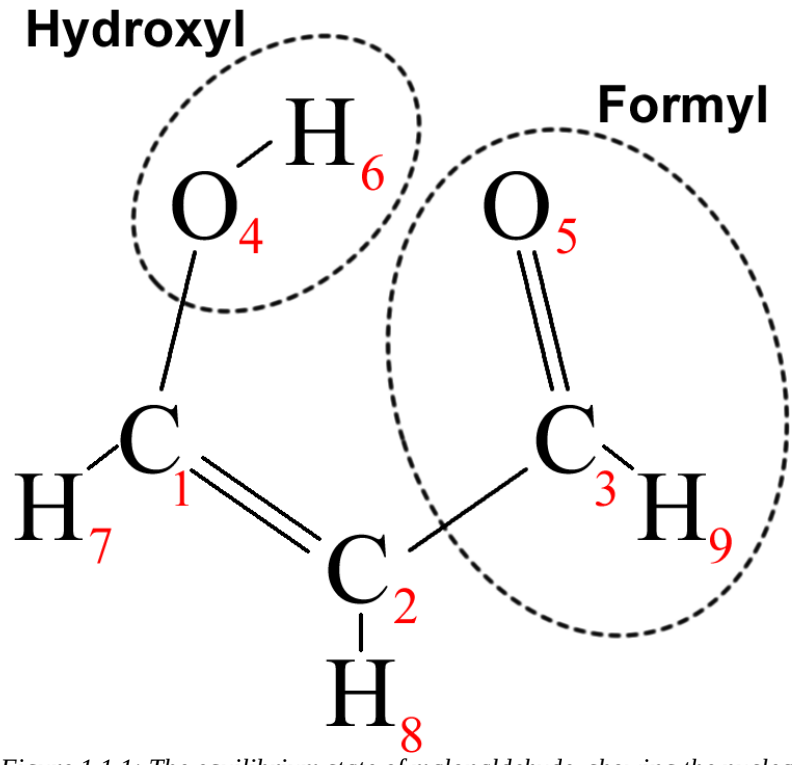

Figure 1.1.1: The equilibrium state of malonaldehyde, showing the nuclear labeling that will be used throughout this thesis.

The earliest spectroscopic measurements of gas-phase malonaldehyde were made by E. Bright Wilson's group and reported in a series of papers from 1976 to 1984 in which they performed a thorough microwave (pure rotational) study of the ground vibrational state and other low-lying states **[1-4]**. In particular, the 1975 doctoral thesis of Walter Rowe **[5]** contains characterizations and approximate frequencies of eight low-lying vibrational states including the ground state. At the time the structure of

malonaldehyde was largely unknown. The gas-phase molecule was believed to primarily exist in a hydrogen-bonded enol form, although it remained to be determined whether the hydrogen bond was symmetric (resulting in a C_{2v} structure) or asymmetric (resulting in a C_s structure). Many *ab initio* **[6-9]** and semi-empirical **[8, 10-12]** calculations of the time indicated that gas-phase malonaldehyde should have an asymmetric hydrogen bond, although some studies suggested otherwise **[13]**. Using relative intensity measurements, Wilson's group determined that there was a very low energy state not consistent with a molecular vibration. The existence of this state, which they measured directly at low resolution to be at about 21 cm^{-1} **[2]**, was strong evidence of tunnelling splitting in the molecule. This indicated an asymmetric hydrogen bond with a low-energy barrier to proton transfer of about 6.6 kcal/mol or 2308 cm^{-1} based on their measurements **[3]**. This conclusion was further supported by the observation of a 3:1 ratio of intensities resulting from nuclear spin symmetric effects due to indistinguishability of the H_7 and H_9 nuclei (as labeled in figure 1.1.1). This intensity ratio was reversed in the 21 cm^{-1} state, indicating that the molecule was gaining C_{2v} character due to the tunnelling effect, as the two states would become degenerate in the absence of tunnelling and the spin weighting would disappear. Experimental studies performed by other groups supported the conclusion that the hydrogen bond was asymmetric **[14-16]**.

In addition to their work on the parent molecule, Wilson *et al.* also measured and analyzed the pure rotational spectra of a large number of isotopically substituted species. Additionally, they were able to directly measure a small number of lines connecting the lowest two tunnelling states of the D_6D_8 isotopologue (where in this notation D_n indicates a deuterium substitution of the hydrogen atom H_n) using microwave-microwave double

resonance **[3]**. Their final value of the ground state splitting (21.583 cm^{-1}) and D_6D_8 splitting (2.88357 cm^{-1}) were determined by analyzing the interactions between the two tunnelling components **[4]**. This large reduction in splitting of the deuterated species is due to the higher mass of the deuterium nucleus in the tunnelling position, resulting in a lower energy of the particle in the potential well and consequently a lower probability of tunnelling. Their final fittings of the parent and D_6D_8 isotopologues **[4]** were done using a Watson A-reduced Hamiltonian with quartic centrifugal distortion terms and two interaction terms connecting the tunnelling components. These interaction terms are $[F + F''\hat{J}^2][\hat{J}_a\hat{J}_b + \hat{J}_b\hat{J}_a]$, with parameters F and F" (called F_J in this work), and will be discussed further in section 2.10.

Smith, Wilson and Duerst (hereafter referred to as SWD) performed an infrared study in 1983 in which they took a survey of vibrational states up to 4000 cm^{-1} for the parent molecule and a number of deuterated isotopologues including D_6D_8 **[17]**. There they proposed two alternative assignments of the observed bands, both of which assigned the lowest-energy fundamental to a band at 252 cm^{-1}, and one of these was later supported by theory **[18, 19]**. SWD's assignments were compared to calculations by Bicerano *et al.* **[20]** and unpublished results by John Pople, resulting in disagreements of up to 612 cm^{-1} in the parent molecule **[17]**.

From 1976 to 1981, Seliskar and Hoffmann published a series of papers on the electronic spectrum of malonaldehyde **[14, 21, 22]**, in which they reported the observation of a number of hot bands arising from excited vibrations of the ground electronic state in the 200-300 cm^{-1} range. The electronic spectrum was also studied later by Arias *et al.* in 1997 using degenerate four-wave mixing **[23]**. In addition to their

electronic work, Seliskar and Hoffmann performed an infrared study in 1982 **[24]** at higher resolution than was used by SWD. Their vibrational assignments are not as complete as those of SWD and there are a number of discrepancies between the sets of assignments. Neither of these groups were able to assign the individual tunnelling splitting components belonging to the observed bands. Splitting was observed by Seliskar and Hoffmann for the pair of bands near 506 and 512 cm^{-1} and for the pair near 384 and 390 cm^{-1} but they were unable to determine which components of the tunnelling-split ground and upper states were involved in each band.

In 1991, Firth *et al.* measured the gas-phase spectrum near 21 cm^{-1} with the intention of finding transitions connecting the two tunnelling components of the parent molecule's ground state **[25]**, but they were unable to measure these lines due to the inherent weakness of the tunnelling-rotation spectrum. Instead, they measured a number of pure rotational lines with high values of J from both ground state components. They performed another rotational fitting using their own measurements along with the lines measured by Wilson's group **[1-4]**, adding Watson A-reduced sextic distortion terms (except for h_J) to the Hamiltonian due to the higher J values present in their new lines. The resulting molecular parameters were generally considered to be in agreement with the microwave results **[4]**, although the authors noted the particularly large differences in the values of F and F'' (25 and 37 standard errors, respectively). Firth *et al.* noted that the sampling of J-K_a space produced by Wilson *et al.*'s microwave measurements and their far-IR lines was limited, and that their fitted parameters might lack predictive power outside the regions they sampled. In particular, the region of $J > 20$ and $K_a < 5$ is not well represented in their data.

The tunnelling-rotation spectrum of malonaldehyde was finally measured by Baba *et al.* in 1999, along with a number of new pure rotational lines near 21 cm^{-1} **[26]**. There they published a new fitting of the malonaldehyde ground state components combining their measurements with those of Firth *et al.* **[25]** and Wilson *et al.* **[1-4]**. Their Hamiltonian did not contain the h_K and h_{JK} distortion terms used by Firth *et al.*, but did include an additional K_a-dependent vibrational coupling term, F_K. With the addition of the tunnelling-rotation lines, Baba *et al.* determined a very precise value of the splitting, 21.58313829(63) cm^{-1} **[26]**. The resulting rotational constants were deemed consistent with those of Wilson's group. My comparison of Baba *et al.*'s constants with those of Firth *et al.* **[25]** showed a much lower level of consistency, with most parameters falling outside 5 standard deviations. In particular, the d_J and d_K distortion parameters are over 300 standard deviations away from those of Firth *et al.* for both ground state components.

The first high-resolution (FWHM linewidth $\leq$ 0.0015 cm^{-1}) rotation-vibration spectrum of malonaldehyde was obtained and analyzed by Duan and Luckhaus in 2004 **[27]**. They performed an IR-diode laser jet study of the ν_6 (C-O-H bend / symmetric C=C, C=O stretch) a-type fundamental near 1594 cm^{-1}. Due to the low concentration of malonaldehyde in their molecular jet, the resulting population was mostly in the lower ground state tunnelling component, meaning that their observations primarily correspond to transitions from that lower ground state level to the lower component of the ν_6 excited tunnelling pair. They were able to assign over 100 lines from this band, making use of the 3:1 nuclear spin weightings and matching lower state combination differences with the ground state description provided by Baba *et al.* **[26]**. The authors performed a fitting of the upper state with the same Hamiltonian used by Baba *et al.* for the ground state,

although they fixed the sextic distortion constants and the three interaction constants to the ground state values. The fitted upper state quartic distortion parameters were large compared to the ground state, and from this they concluded that the upper state is perturbed. They tentatively assigned a number of weaker lines to the band connecting the upper ground state component to the upper ν_6 component, which allowed them to calculate a reduction in splitting of 0.03 cm^{-1} in the ν_6 vibration compared to the ground state.

Cryogenic matrix isolation studies have been performed on malonaldehyde by various groups since 1989 when Firth *et al.* studied the IR (270-4000 cm^{-1}) and UV spectral regions of the molecule trapped in an argon matrix **[28]**. They showed that tunnelling motion was inhibited under matrix isolation conditions, resulting in no observable tunnelling splitting. A similar study was performed in the 400-4000 cm^{-1} range by Chiavassa *et al.* in 1992 using argon, krypton and xenon matrices **[29]**, although they did not confirm the elimination of splitting reported by Firth *et al.*

In 2006, Wassermann *et al.* obtained FTIR spectra of malonaldehyde at room temperature, in jet expansions (Ar and He carrier gases, 2 cm^{-1} resolution) and in an argon matrix (0.1 cm^{-1} resolution) **[30]**. They were able to experimentally determine the tunnelling splitting of four excited vibrational states near 767, 893, 1452 and 1594 cm^{-1}. The splittings in the 893 and 1452 cm^{-1} modes were reduced to about 5 cm^{-1}, while the splittings in the other two modes remained mostly unchanged. They drew attention to the large discrepancy between their experimentally determined splittings and various calculated results **[31-34]**.

In 2010 and 2013, Lüttschwager *et al.* performed a detailed gas-phase IR (2 cm^{-1} resolution) and Raman (1 cm^{-1} resolution) study of malonaldehyde using supersonic jet expansion and matrix isolation techniques (Ne, Ar, Xe, N_2 - 0.12 cm^{-1} resolution) covering the 200-3200 cm^{-1} region **[35, 36]**. They initially examined the C-O-H in-plane bending motion with the intention of locating a mode that enhances the tunnelling splitting, as other experiments had only shown reduction of splitting with vibrational excitation. After successfully measuring the C-O-H bend splitting to be 69 cm^{-1} (the largest splitting observed in malonaldehyde) **[35]**, they then measured the tunnelling splitting for a large number of excited vibrations. They provide assignments for a total of 14 excited vibrations using their own measurements and previous observations **[36]**. Comparing these experimental splittings to theoretical predictions, they found that the work of Hammer and Manthe **[37]** produced the closest agreement. They proposed two alternative and tentative assignments for the low-frequency ring opening/closing mode (which they call $\nu O\cdots O$), both of which place one tunnelling component at 241 cm^{-1}. The first, corresponding to a b_2-symmetry fundamental (using C_{2v} labels), assigns the other component at 184 cm^{-1}, resulting in a 57 cm^{-1} splitting. In this case, a-type bands would be observed at 184 and 220 cm^{-1} and b-type bands would be observed at 163 and 241 cm^{-1}. The second assignment, corresponding to an a_1-symmetry fundamental, places the other component at 506 cm^{-1}, resulting in a 265 cm^{-1} splitting. In this case, a-type bands would be observed at 220 and 506 cm^{-1} and b-type bands would be observed at 241 and 484 cm^{-1}. They also assigned the lowest frequency out-of-plane mode to a pair at 273 and 282 cm^{-1} with a splitting of 9 cm^{-1}.

1.2 - Review of Theoretical Work on Malonaldehyde

Due to its recognition as a prototypical system for intramolecular proton tunnelling and the abundance of experimental data for comparison, a large number of theoretical studies have been performed on malonaldehyde **[6-13, 18-20, 29, 31-34, 37-100]**. Malonaldehyde is a 9-atom system with 21 vibrational degrees of freedom, meaning that purely quantum mechanical treatments of the molecule in its full dimensionality are computationally expensive. During the time when most of the computational work was done on malonaldehyde, such calculations were not feasible. Instead, many researchers made use of various levels of semi-classical techniques **[31, 32, 38-55]** such as the model developed by Makri and Miller in 1989 **[38]** and the instanton approach (for example, in Refs. **[46, 54]**), which are based on describing the motion in a classical potential well and accounting for the probability of tunnelling to the other well using the WKB approximation. Some authors **[39, 40]** note that the instanton method neglects some effects of anharmonicity in the tunnelling mode, a problem which becomes worse for low potential barriers.

Many of the early attempts at semi-classical modeling of malonaldehyde still used reduced-dimensionality approaches to lessen computational expense **[41]** with the first 21-dimensional instanton treatment being made by Smedarchina *et al.* in 1995 **[42]**, although they used a simplified version of the instanton theory and a simple (Hartree-Fock level) potential energy surface (PES). Smedarchina *et al.* determined the tunnelling splitting to be 19.7 and 2.6 cm^{-1} for the regular and deuterated (at the tunnelling position) molecule, respectively. This full-dimensional calculation showed that heavy-atom motion makes a significant contribution to the tunnelling splitting. This conclusion was

supported by the work of Sewell, Thompson and Guo **[31, 43]** using the Makri-Miller model, who compared 15-dimensional (in plane) and 21 dimensional semi-empirical (based on measurements by Wilson *et al.*) PESs, resulting in tunnelling splitting values of 24.5 cm^{-1} **[43]** and 21.8 cm^{-1} **[31]** for the ground state, respectively, although their barrier height was quite high (10.0 kcal/mol or 3500 cm^{-1}) **[31]**. Sewell *et al.* also calculated frequencies and tunnelling splittings for excited vibrational states, and noted that the largest splitting was predicted for the lowest-frequency in-plane mode (the O···O ring opening/closing mode). Mil'nikov *et al.* **[44, 45]** applied the instanton theory using a PES calculated at the coupled cluster level (CCSD(T), (aug)-cc-pVTZ), resulting in a splitting of 21.2 cm^{-1} and a more reasonable barrier of 3.81 kcal/mol or 1333 cm^{-1} **[45]**. Benderskii *et al.* developed the perturbative instanton approach in a series of papers from 1997 to 2001. Many of these use malonaldehyde as a test case **[32, 46-48]**, and in their 2000 paper **[48]** they use this method with a fully multidimensional PES to calculate the normal mode frequencies, tunnelling splittings and a barrier height of 4.3 kcal/mol or 1504 cm^{-1}.

Coupling of the small-amplitude vibrational modes to the tunnelling motion can be treated using either the sudden (tunnelling is fast compared to other vibrations) or adiabatic (tunnelling is slow compared to other vibrations) approximation. The sudden approximation fixes the small-amplitude coordinates to their equilibrium values as proton tunnelling proceeds, whereas the adiabatic approximation allows the small-amplitude coordinates to assume a new equilibrium position at each point on the tunnelling path. In 2012, Smedarchina *et al.* developed a variant of the instanton method ("rainbow instanton") that is intermediate between the sudden and adiabatic approximations,

allowing it to handle a wide range of frequencies in the coupled modes **[40]**. The tunnelling path is also heavily dependent on whether the small-amplitude motions couple in a sudden or adiabatic way, following the minimum energy path (MEP) if the behavior is adiabatic and diverging from the MEP in the sudden case **[32]**. The tunnelling path was investigated in detail by Tautermann *et al.* in 2002 **[49, 50]**, where they concluded that the tunnelling path lies surprisingly close to the MEP.

Early quantum *ab initio* treatment of proton tunnelling dynamics in malonaldehyde were handled with a reaction path approach **[7, 20]**, using one coordinate to represent the proton transfer motion and letting the other coordinates adjust adiabatically at each point along the path. In 1986, Carrington and Miller **[56]** were the first to employ a two-dimensional reaction surface description, using the distances from each oxygen atom to the tunnelling proton as large-amplitude coordinates. This work was soon followed by other reduced dimensionality reaction surface descriptions **[57-64]**. The ground state tunnelling splittings produced using these models ranged from 9 **[57]** to 60 **[56]** cm^{-1}, although the calculations also gave high barrier heights of 6-10 kcal/mol (2100-3500 cm^{-1}), even when the splittings were in agreement with experiment.

In 2001, Tuckerman and Marx demonstrated the significant contribution of heavy-atom quantization in the tunnelling splitting **[65]**. In 2013, Siebrand *et al.* introduced a set of rules to determine whether exciting a given vibrational mode will increase or decrease the tunnelling splitting **[66]**. These rules explain the experimental **[36]** and theoretical **[37]** observations that most excited vibrations result in a decrease in splitting.

In 1998, Tayyari and Milani-Nejad performed vibrational frequency calculations at the MP2 level of theory **[67]** and used these results to reassign the experimental spectrum of malonaldehyde and its deuterated isotopologues taken by SWD **[17]**. These reassignments were supported by the work of Spanget-Larsen in 1999 **[68]**. In 2003, Tayyari *et al.* were able to obtain very good agreement with the experimental splitting (20.8 and 22.8 cm^{-1}, using MP2/6-31G** and B3LYP/6-311++G** respectively) and molecular geometry using a two-dimensional potential **[69]**. Unlike the work of Carrington and Miller **[56]**, and of Shida *et al.* **[57, 58]**, they treated the other coordinates non-adiabatically (fixing them at equilibrium as the C-O-H bending and O-H stretching coordinates were varied). Based on this success, they argued that the tunnelling in malonaldehyde is a two-dimensional process and does not involve significant motion of the heavy-atom frame.

The full-dimensional PES calculated using advanced *ab initio* theory at the CCSD(T) level by Wang *et al.* in 2008 **[70]** has a potential barrier of 4.11 kcal/mol (1438 cm^{-1}) and is considered to be the best available **[71]**. It has since been used in a number of multi-configuration time-dependent Hartree calculations **[37, 71-74]**, the most recent of which was performed by Schröder and Meyer in 2014 **[71]** and involves calculations of vibrational frequencies and tunnelling splittings that are compared to the most recent experimental assignments by Lüttschwager *et al.* **[36]**. The lowest energy modes are predicted by Schröder and Meyer to be at 252, 270, 385 and 523 cm^{-1} as compared to Lüttschwager *et al.*'s assignments of 184 (or 241 in their alternative assignment), 273, 390 and 512 cm^{-1} where the given states are the lower tunnelling components of each pair. Although the position of the lowest state from Ref. **[71]** matches well with Lüttschwager

et al.'s alternative assignment, the splittings in this case do not agree since Lüttschwager *et al.* proposes a splitting of 265 cm^{-1} while Schröder and Meyer calculate it to be 64.2 cm^{-1}. This splitting is close to that of Lüttschwager *et al.*'s lower-splitting assignment, but then the lowest state is at 184 cm^{-1} which is not in agreement with Schröder and Meyer. The other tunnelling splittings produced by Schröder and Meyer match the observations quite well and are consistent with the calculations of Hammer and Manthe **[37]**.

The most recent calculation of the vibrational frequencies of malonaldehyde, without splitting of excited states, was reported by Mizukami *et al.* in 2014 **[75]**, along with tunnelling splitting values of 21.0(4) and 3.2(4) cm^{-1} for the regular and deuterated isotopologues which are in good agreement with experiment.

1.3 - Goals of this Project

Other than the study of the tunnelling-split band pair near 1594 cm^{-1} by Duan and Luckhaus **[27]**, the infrared vibrational spectrum of malonaldehyde has not yet been explored at rotational resolution. Furthermore, the most recent set of vibrational assignments in the region below 500 cm^{-1} **[36]** contains some ambiguities and is not in good agreement with theoretical calculations. The available theoretical results vary considerably and there are many different and conflicting ideas about how the proton tunnelling should be modeled. Additional high-resolution spectra in the far-IR region, particularly below 500 cm^{-1}, were needed to begin resolving these ambiguities and to provide additional data for comparison with future computational work.

In this study, rotationally resolved Fourier transform infrared (FTIR) spectra of malonaldehyde were obtained in the 100 - 1600 cm^{-1} region using the Far-IR beamline at

the Canadian Light Source synchrotron in Saskatoon, Saskatchewan, Canada. A synchrotron was used as the source for this experiment due to a number of advantages that it provides. First, the synchrotron produces light across a large range of frequencies, allowing easy access to the region below 1000 cm^{-1} which is normally difficult using FTIR spectroscopy with a conventional source. It also produces a very narrow beam of light, which allows small aperture sizes to be used without a significant loss of radiation. This means that the greatest advantage is attained when operating at the highest resolution, when small apertures are required.

A secondary goal of this project was to describe the proton transfer using the generalized semi-rigid bender (GSRB) Hamiltonian **[101]**, which is a model for treating a large-amplitude vibrational motion along with the rotational degrees of freedom. Although the GSRB was not used in this project, a number of steps were accomplished in preparation for its use. In particular, the minimum energy path was determined using a two-dimensional potential energy surface with the O_4-O_5 and O_4-H_6 distances as coordinates (as labeled in figure 1.1.1).

Chapter 2

Spectroscopic Background

2.1 - The Use of Symmetry in Molecular Systems

All molecules can be classified by using groups which represent their symmetry under certain operations. A molecular symmetry (MS) group consists of permutations (which exchange identical nuclei) and the inversion operation (which inverts the coordinates of all nuclei and electrons) as well as their products (permutation-inversion operations). Each of these operations results in a configuration indistinguishable from the starting configuration and leaves the molecular Hamiltonian unchanged. The notation (12) will be used to indicate a transposition of nuclei 1 and 2 and more complex permutations will be indicated by products of transpositions. The inversion operation is denoted E^* and permutation-inversion operations will be written as a permutation with an asterisk added to the end, for example $(12)^*$. Another symmetry group that is used is the point group, which is composed of rotations, reflections through a plane of symmetry and the inversion operation, all of which apply only to the nuclei. The molecular symmetry group is used here to describe malonaldehyde instead of the point group for reasons that will be explained in the next section.

The symmetry operations of either of these groups can be mapped to a group of matrices which obey the same multiplication table as the symmetry group. This mapping represents an isomorphism if it is one-to-one or a homomorphism if it is many-to-one. The matrix group is then called a representation of the symmetry group. Most representations can be put in block-diagonal form, with each matrix element of the group having the same block structure as the other elements. Such representations are called

reducible representations and each set of corresponding blocks forms another representation. Representations that cannot be put in block-diagonal form and reduced in this way are called irreducible representations. There are a small number of unique irreducible representations for any group (the same as the number of classes of symmetry operations) and their properties are summarized in character tables. Character tables have columns corresponding to the group operations and rows corresponding to the irreducible representations of the group. The elements of the table are the characters (traces) of the matrices that make up each representation. For one-dimensional representations (including all of those used to describe malonaldehyde) the characters are the single elements of the matrices and can only take the values ±1 since all symmetry operations must return the nuclei to their original positions when applied twice. Any function that describes a molecule must transform in a way that obeys the MS group multiplication table. That is, for a function F and symmetry operations O_1, O_2 and O_3, if $O_1O_2 = O_3$ then $(O_1O_2)(F) = O_3(F)$. Therefore, such a function must transform identically to one of the irreducible representations of the group. For the cases considered here (one-dimensional irreducible representations) either O(F) = F or O(F) = -F for any symmetry operation O.

When solving the Schrödinger equation for a complex molecular system, the problem is typically separated into sets of similar degrees of freedom (translational, rotational, vibrational, electronic) and these are at first solved independently. These solutions do not necessarily transform in a way that is allowed by the molecular symmetry (as an irreducible representation). Linear combinations must be formed to ensure that they have the correct symmetry, and these new solutions are then said to have been symmetrized. The solutions to the Schrödinger equations for each of these parts are

then multiplied together to give an approximate solution for the molecule. These approximate solutions to the full Schrödinger equation can then be used as a basis set for a matrix description of the Hamiltonian, which can then be diagonalized to give the true wavefunctions and energies for the molecule.

2.2 - Structure and Symmetry of Malonaldehyde

When malonaldehyde is in its equilibrium state, the hydrogen-bonded proton occupies a position with unequal distance from each of the two oxygen atoms and the molecule belongs to the C_s point group. The C_s point group has two irreducible representations as shown in the character table (table 2.2.1), with symmetry labels A' and A", which are respectively symmetric and anti-symmetric with reflection in the plane of the molecule (σ_h).

C_s	E	σ_h
A'	1	1
A"	1	-1

Table 2.2.1: Character table for the C_s point group.

The transition state of malonaldehyde, in which the proton is equidistant from both oxygen atoms, has a C_2 axis bisecting the O-H-O angle and thus belongs to the C_{2v} point group. The C_{2v} point group has 4 irreducible representations (table 2.2.2), of which two are symmetric (A_1 and B_2) and two are anti-symmetric (A_2 and B_1) with respect to reflection in the molecular plane. Additionally, two are symmetric (A_1 and A_2) and two are anti-symmetric (B_1 and B_2) with respect to rotation about the C_2 axis.

C_{2v}	E	C_2	σ_v	σ_h
A_1	1	1	1	1
A_2	1	1	-1	-1
B_1	1	-1	1	-1
B_2	1	-1	-1	1

Table 2.2.2: Character table for the C_{2v} point group. The σ_h operation is reflection in the molecular plane and σ_v is reflection in the perpendicular plane.

It is evident that the large-amplitude proton transfer process that occurs in malonaldehyde makes it ill-suited for description as a member of a single point group, since this would depend on whether it is in the equilibrium or transition state configuration. Instead, it is more appropriate to describe malonaldehyde as a member of the molecular symmetry group G_4 which accounts for the effects of such large-amplitude changes in structure (as described by Bunker and Jensen in chapter 3 of Ref. **[102]**). The G_4 MS group is isomorphic to the C_{2v} point group, although, as described above, the symmetry operations of the G_4 group consist of permutation and permutation-inversion operations instead of rotations and reflections (table 2.2.3). Operations such as (13)(45)(79), which connect the two equilibrium configurations of malonaldehyde, would not be symmetry operations of the molecule if proton tunnelling was unfeasible. The C_{2v} symmetry labels can still be applied to the symmetry species of G_4 since the groups are isomorphic, and it is these labels (A_1, A_2, B_1 and B_2) that will be used throughout this thesis.

G_4	E	(13)(45)(79)	(13)(45)(79)*	E*
A_1	1	1	1	1
A_2	1	1	-1	-1
B_1	1	-1	1	-1
B_2	1	-1	-1	1

Table 2.2.3: Character table for the G_4 molecular symmetry group. Numbers enclosed in parentheses represent cyclic permutations of the indicated nuclei (as labeled in figure 1.1.1). An asterisk indicates the inversion of the coordinates of all particles.

2.3 - Choice of Axis System and Representation

The positions of the nuclei and electrons in a molecule can be described using a set of Cartesian axes fixed in place relative to the experiment (the lab-fixed axes), in which the N nuclei have 3N degrees of freedom. We usually want to consider only the 3N-3 rotational and vibrational degrees of freedom, so a translationless second axis system is defined which is parallel to the lab-fixed frame but with its origin at the molecular center of mass (the molecular center of mass frame). Another axis system can then be defined for use in describing nuclear motion which is parallel to the lab-fixed frame but with the origin at the nuclear center of mass (the nuclear center of mass frame). For the nuclei of a non-linear molecule there are 3 rotational degrees of freedom and thus 3N-6 vibrations. It is also desirable to separate these two types of motion by defining an axis system that rotates with the molecule and has its origin at the nuclear center of mass (the molecule-fixed frame). The rotational position is then given by the Euler angles relating these rotating axes as defined in the lab-fixed frame to the axes of the nuclear center of mass frame.

The difficulty arises when attempting to define the molecule-fixed axes relative to the nuclear coordinates, since the vibrational motion causes the structure of the molecule to change over time. These vibrational motions can also contribute to the rotational angular momentum of the molecule, especially in the case of large-amplitude motion such as the proton tunnelling in malonaldehyde, making it impossible to truly separate the rotation from vibration. For any single rigid structure of a molecule we can define the principal axes of rotation, for which the moment of inertia tensor becomes diagonal.

One set of rotating axes that can be used for malonaldehyde is the set of principal axes of the structure for which all of the small-amplitude vibrational coordinates occupy their equilibrium positions and the tunnelling coordinate is at the value corresponding to the transition state (so that the tunnelling proton is equidistant from the two oxygen nuclei). This set of axes is indicated in figure 2.3.1 and is the one which will be used in this thesis. Since these are not the principal axes in the equilibrium state the moment of inertia tensor in this configuration will not be diagonal, instead having non-zero off-diagonal terms (products of inertia) connecting the two in-plane axes. The definition of the axes for other configurations is handled by using the Eckart conditions, which are a set of equations that minimizes the coupling between vibration and rotation. This process is discussed in detail by Wilson, Decius and Cross in chapter 11 of Ref. **[103]**.

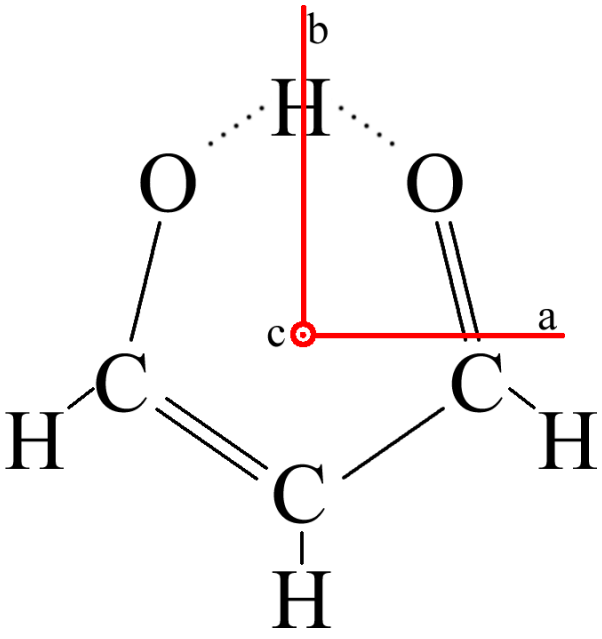

Figure 2.3.1: Principal axes of the transition state configuration of malonaldehyde.

By convention, the three principal axes of an asymmetric molecule are labeled a, b and c with the diagonal elements of the moment of inertia being in the order $I_a < I_b < I_c$. The rotational constants, being inversely proportional to the moment of inertia about each axis, are in the order A > B > C. There are six ways (called representations, not to be confused with matrix 'representations' of symmetry groups) in which these structurally determined principal axis labels can be assigned to the x, y and z Cartesian labels of the rotating axis system. In a convention established by Watson **[104]**, they are referred to as I, II or III as the z-axis is assigned to a, b or c respectively, and with a superscript r or l added to distinguish between the right-handed and left-handed way of assigning the other labels. The II^r representation (x = c, y = a, z = b) will be used exclusively in this thesis so that the z-axis corresponds to the C_2 symmetry axis in the transition state configuration. To avoid confusion between this use of the word 'representation' and its use for symmetry groups, the latter will be referred to as a 'symmetry representation' wherever there might be ambiguity between the two.

The rotational symmetry of a molecule can be represented by a number called the asymmetry parameter (κ), which is a function of the rotational constants (or principal moments of inertia) given by:

$$\kappa = \frac{2B - A - C}{A - C}$$

If B and C are equal, κ is -1 and the molecule is a prolate symmetric top. If A and B are equal, κ is 1 and the molecule is an oblate symmetric top. Malonaldehyde $(\kappa = -0.44)$ is a very asymmetric molecule, although it is more prolate than oblate.

2.4 - Vibrational Coordinates and Tunnelling Splitting

The 3N-6 vibrational degrees of freedom for a non-linear molecule are generally expressed as a set of independent normal coordinates. If the motion along each of these coordinates is a small-amplitude vibration, they can be approximated by non-interacting one-dimensional harmonic oscillators. The total vibrational wavefunction is then given by the product of the individual harmonic oscillator wavefunctions, and the total vibrational energy is the sum of their eigenvalues.

(2.1) $$\psi_{vib} = \psi_1 \psi_2 \ldots \psi_{3N-6}$$

(2.2) $$E_{vib} = E_1 + E_2 + \ldots + E_{3N-6}$$

These approximations are not valid in the case of large-amplitude motions such as the proton transfer in malonaldehyde. Motion along the proton tunnelling coordinate can not be described as that of a harmonic oscillator and it is not independent from the other vibrational modes. One consequence of this is that the excited states of the tunnelling mode are not evenly spaced in energy as they would be for a harmonic oscillator, but are

instead grouped into pairs. This grouping is the characteristic tunnelling splitting of such systems and it can be explained by considering the progression as the tunnelling barrier is gradually lowered from an infinitely high limit, so that tunnelling is unfeasible, to the low-barrier case that is actually observed.

In the infinite barrier case proton transfer does not occur and there are now two energetically equivalent versions of the molecule (figure 2.4.1), one with an O_4-H_6 bond and one with an O_5-H_6 bond. These two versions (A and B) are unable to interconvert and so exist independently. Each has an equivalent set of eigenstates ($|\psi_{An}>$ and $|\psi_{Bn}>$ respectively, for vibrational quantum number n) that describe the proton in a single potential well and have zero amplitude (and probability density) in the well corresponding to the other version, as explained in Ref. **[102]**. If these potential wells are treated as harmonic, the eigenstates are evenly spaced in energy.

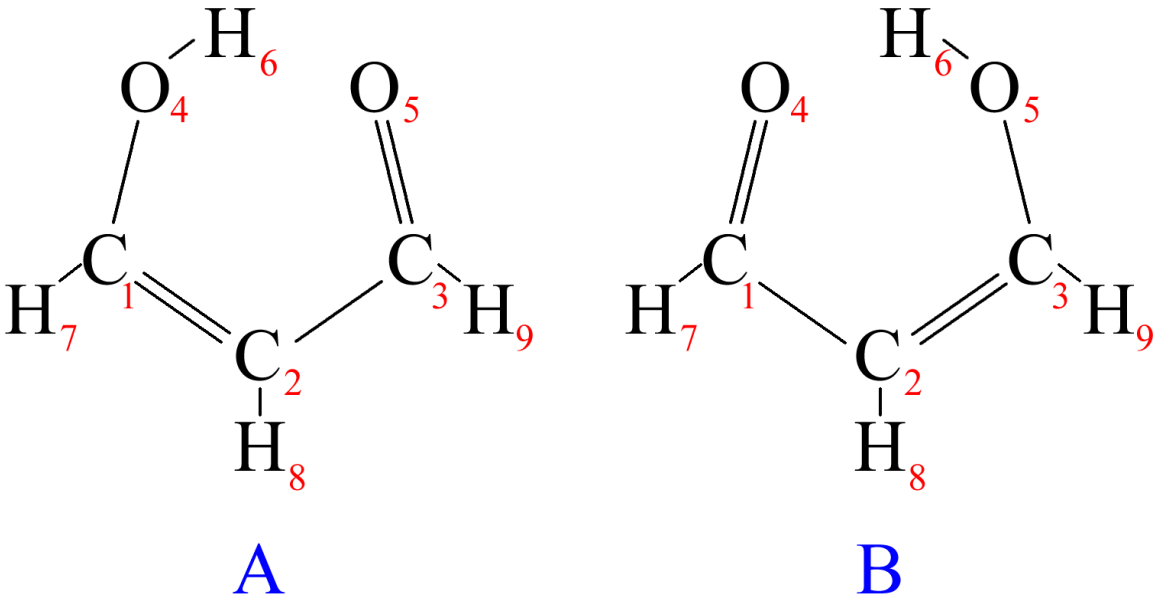

Figure 2.4.1: Energetically equivalent versions (A and B) of malonaldehyde connected by proton tunnelling.

If the barrier height is made finite, the $|\psi_{An}>$ and $|\psi_{Bn}>$ are each able to tunnel into the other well. The eigenstates interact with each other and each pair of equal n

forms the two superposed states $\frac{1}{\sqrt{2}}(|\psi_{An}> \pm |\psi_{Bn}>)$. The new set of eigenstates corresponding to this vibrational mode (the tunnelling mode) will appear grouped into pairs as shown in figure 2.4.2.

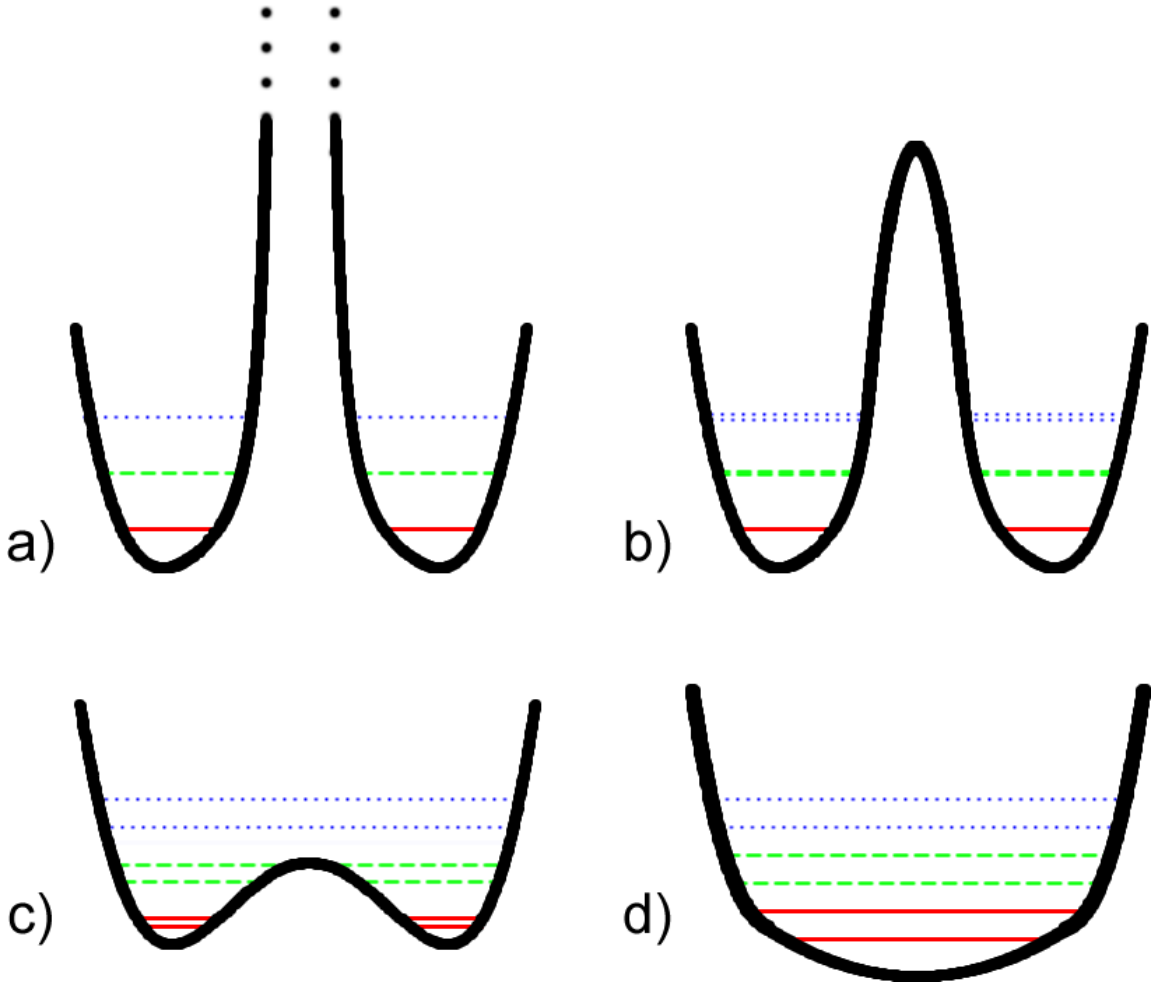

Figure 2.4.2: Energy levels of a double-well potential in the a) infinite-barrier, b) high-barrier, c) low-barrier and d) zero-barrier cases. In a), the levels are not split by tunnelling. b) and c) display tunnelling splitting of differing magnitudes. d) shows the wide single-well potential obtained from lowering the barrier to zero. The tunnelling mode in malonaldehyde has a barrier like that of c), where the ground state splitting is within about an order of magnitude of the vibrational state spacing.

The pairs will be closely spaced and approximately centered on the energy of $|\psi_{An}>$ or $|\psi_{Bn}>$ near the bottom of the potential well, becoming more widely spaced as the state energies approach and exceed the barrier height. If the barrier continues to be

lowered to zero, the states will once again become evenly spaced in energy (assuming harmonicity), but with a smaller spacing corresponding to the new wider single-well potential.

Examination of the tunnelling motion reveals that it is symmetric with respect to inversion and anti-symmetric with respect to the (13)(45)(79) and (13)(45)(79)* operations, belonging to the B_2 representation of the G_4 MS group. This can be seen by considering the effect of each operation on the O-H bond. If the molecule starts in version A (with an O_4-H_6 bond) then the (13)(45)(79) and (13)(45)(79)* operations convert it to version B, while the inversion operation leaves the version unchanged.

Each of the remaining 20 vibrational modes in malonaldehyde can be described as approximately harmonic for low vibrational excitation. However, each excited vibrational state ν_n is paired with the nearby combination state $\nu_n + \nu'$, where ν' is the tunnelling mode. These two states are referred to as the 'tunnelling components' of the vibration ν_n. The notation $\upsilon^{\upsilon'}$ will henceforth be used to refer to a state with vibrational quantum number υ in a given mode and υ' in the tunnelling mode. Combination states of two or more small-amplitude vibrations (called $\nu_1, \nu_2, \ldots \nu_n$) could be represented by the symbol $\upsilon_1\upsilon_2\ldots \upsilon_n^{\upsilon'}$, although such states will not be considered in this thesis. The ground state will be denoted 0^0 and its upper tunnelling component is then 0^1. The term 'fundamental' will refer to a vibrational transition from either of these two states to the 1^0 or 1^1 states of a single mode. The 0^1 state for malonaldehyde is located near 21 cm^{-1} above the ground state and will have a Boltzmann population very close to that of the ground state at temperatures near 0 ^oC, as was the case for the spectra that are used in this work. The 0^2

and 0^3 states forming the next pure tunnelling mode pair have not yet been experimentally identified.

Since the tunnelling coordinate is not independent from the other modes, the energy of a combination state including the tunnelling mode can not be approximated by the sum in equation (2.2). That is, the energy of the 1^1 combination state, denoted $E(1^1)$, will in general be different than the sum of the 0^1 and 1^0 state energies. Instead, the tunnelling splitting in the excited state, $E(1^1) - E(1^0)$, will depend on how the potential along the tunnelling coordinate changes as a result of the motion associated with the excited small-amplitude mode. It is expected that the tunnelling splitting in excited vibrational states will vary considerably from the ~21 cm^{-1} splitting observed in the ground state, and this has proven to be true as shown in Ref. **[36]**.

2.5 - Rotational State Labeling of Asymmetric Molecules

The rotational states of an asymmetric molecule (A > B > C) are eigenfunctions of the squared total rotational angular momentum operator $\hat{J}^2$ with quantum number J, but they are not eigenfunctions of $\hat{J}_z$ (the z-component of $\hat{\vec{J}}$ in the molecule-fixed frame) in any representation. The use of J alone is not enough to uniquely identify a state, so it becomes necessary to use $\hat{J}_z$ quantum numbers corresponding to the prolate (A > B = C) and oblate (A = B > C) symmetric top limits as additional labels. The following description abbreviates some of the points derived in chapter 11 of Ref. **[102]**.

For a symmetric top molecule, the rotational Hamiltonian can be simplified due to the presence of two identical rotational constants, allowing it to be expressed in terms of the angular momentum operators $\hat{J}^2$ and $\hat{J}_z$ in a representation where the z-axis is the

symmetry axis. The wavefunctions are then simultaneous eigenfunctions of $\hat{J}^2$ and $\hat{J}_z$ with quantum numbers J and k. The total angular momentum and its z-axis projection are thus both conserved quantities in the absence of perturbing fields. The wavefunctions are also eigenfunctions of the z-component of $\hat{J}$ in the lab-fixed frame (with quantum number m), but this operator does not appear in the field-free Hamiltonian so it does not contribute to the energy. Since the $\hat{J}_z$ operator appears squared in the Hamiltonian, the eigenvalues of $\hat{H}$ only depend on the absolute value of k, which we call K. In the prolate case the I^r representation is used which means that the z label is assigned to the a-axis, and in the oblate case the III^r representation is used which means that the z label is assigned to the c-axis. K and k can then be called K_a and k_a in the prolate case and K_c and k_c in the oblate case.

The asymmetric top Hamiltonian (used for malonaldehyde) can not be simplified in the same way since the three moments of inertia all have different values. Instead it is expressed in terms of the operators $\hat{J}^2$ and $\hat{J}_z$ along with the squared ladder operators $(\hat{J}^+)^2$ and $(\hat{J}^-)^2$, which raise and lower k by 2. Since the ladder operators do not mix states of different J, J remains a good quantum number and the total angular momentum is still conserved in the absence of external fields. However, the presence of these ladder operators means that the asymmetric top Hamiltonian is not diagonal in the basis of either prolate or oblate symmetric top eigenfunctions, instead having off-diagonal elements connecting states which differ in k by 2 quanta. For each block of given J (and m) in the Hamiltonian, smaller sub-blocks can be formed by using combinations of the symmetric top eigenfunctions with common K (k being K or -K). Four of these sub-blocks are formed depending on the parity of K and whether the combinations are made by adding

or subtracting the equal-K eigenfunctions. Diagonalizing the Hamiltonian matrix to obtain the asymmetric top eigenfunctions results in mixing of these basis functions within each of the sub-blocks (although not between them). This mixing involves basis functions with different values of K_a (using the prolate basis) or K_c (using the oblate basis). This demonstrates that neither K_a nor K_c are good quantum numbers for an asymmetric molecule.

If we were to smoothly distort an asymmetric molecule by adjusting the value of B so that it becomes a prolate symmetric top (for B = C) or an oblate symmetric top (for B = A) then the energy of each of its states will also have to vary smoothly so that they become the states $|J,K_a\rangle$ in the prolate case and $|J,K_c\rangle$ in the oblate case. This allows the states in the asymmetric case to be labeled as $J_{Ka,Kc}$ where the K values are taken from these symmetric top limits. Figure 2.5.1 illustrates this correspondence and also shows that each $|J,K_a\rangle$ state with $K_a > 0$ in the prolate limit splits into two states as the symmetry is broken. These eventually map to states with K_c values of $J - K_a$ and $J - K_a + 1$ in the oblate limit. The $K_a = 0$ states only map to the $K_c = J$ oblate states. This demonstrates that the symbol $J_{Ka,Kc}$ uniquely labels the asymmetric top states and establishes the restrictions that $K_a + K_c$ must equal either J or J + 1 and that K_a and K_c must be $\leq J$.

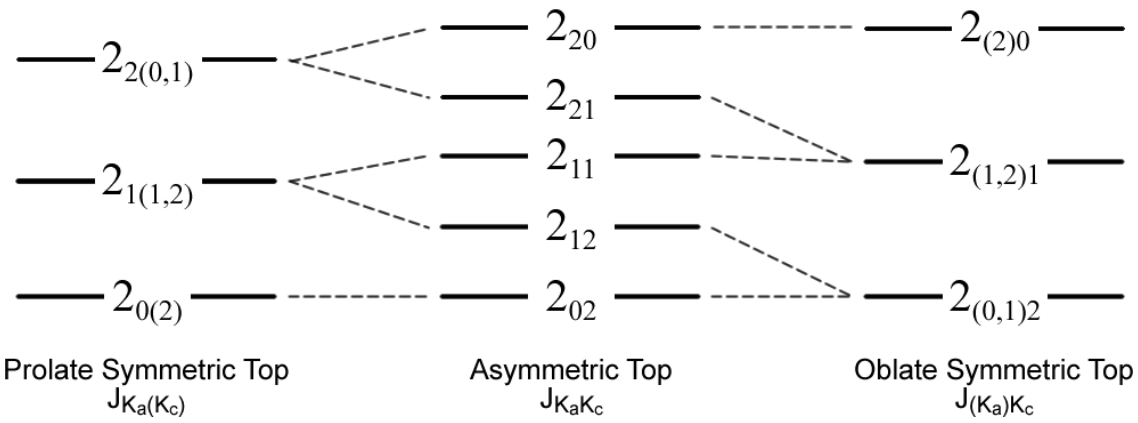

Figure 2.5.1: Rotational states (only J = 2 is shown) as a molecule is distorted from a prolate to an oblate symmetric top. In the asymmetric region, both K_a and K_c must be used to label a state.

2.6 - Rotational and Vibrational Selection Rules

A molecule exposed to light is in the presence of oscillating electric and magnetic fields, and these fields can interact with the charged particles in the molecule causing transitions between states. The electric field can be expressed as:

$$\vec{E} = \mathrm{Re}[\vec{E}_0 \exp(i\vec{k} \cdot \vec{r} - \omega t)]$$

and the expansion of $\exp(i\vec{k} \cdot \vec{r})$ produces a series of terms which can be put in the form of effective electric and magnetic multipole moments. The electric dipole contribution which results from the constant term in the expansion is usually dominant (unless it vanishes due to symmetry), and the resulting transitions are the most intense. The intensity of an electric dipole transition is proportional to the square of the transition dipole moment integral M_{ij}:

$$(2.3) \quad M_{ij} = \langle \Psi_i | \hat{\mu} | \Psi_j \rangle = \langle \Psi_i | \hat{\mu}_a | \Psi_j \rangle + \langle \Psi_i | \hat{\mu}_b | \Psi_j \rangle + \langle \Psi_i | \hat{\mu}_c | \Psi_j \rangle$$

where Ψ_i and Ψ_j are the two states involved in the transition and a, b and c designate the molecule-fixed axes. Transitions are forbidden if this integral vanishes and allowed otherwise. In many cases only one of the terms on the right of equation (2.3) will be non-

zero, and the resulting transitions are called a-type, b-type or c-type based on the remaining component of $\hat{\mu}$.

The electric dipole moment can be written as a sum of the permanent dipole moment $\hat{\mu}_p$ and an oscillating term $\hat{\mu}_v$. The permanent dipole moment is defined as the dipole moment when all of the vibrational coordinates (Q_1, Q_2, ...) are zero, so it only depends on the rotational coordinates (the Euler angles α, β and γ). The $\hat{\mu}_v$ term depends on the both the rotational and vibrational coordinates since the dipole moment oscillates with the changing geometry. As a result, M_{ij} can be written:

$$M_{ij} = < \Psi_i \,|\, \hat{\mu}_p(\alpha,\beta,\gamma) + \hat{\mu}_v(\alpha,\beta,\gamma,Q_1,Q_2,...) \,|\, \Psi_j >$$

For M_{ij} to be non-zero, the integrand must depend on the coordinates of integration (since Ψ_i and Ψ_j are orthogonal for $i \neq j$). In a pure-rotational transition, $\hat{\mu}_v$ can be neglected since it is small compared to $\hat{\mu}_p$ which depends on the rotational coordinates:

$$M_{ij\text{-}rot} \approx < \Psi_{r,i} \,|\, \hat{\mu}_p(\alpha,\beta,\gamma) \,|\, \Psi_{r,j} >$$

where Ψ_r are the rotational wavefunctions. For malonaldehyde, the equilibrium permanent dipole moment is along the b-axis (the z-axis using the II^r representation), and so the pure rotation spectrum consists of only b-type transitions.

For a vibrational transition the permanent dipole moment term vanishes since it does not depend on the vibrational coordinates, leaving only the $\hat{\mu}_v$ term. This means that vibrational transitions depend on the change in dipole moment along the vibrational coordinates involved in the transition rather than on the permanent dipole moment:

$$M_{ij\text{-}vib} = \langle \Psi_{rv,i} | \hat{\mu}_v(\alpha,\beta,\gamma,Q_1,Q_2,...) | \Psi_{rv,j} \rangle$$

where Ψ_{rv} are the rotation-vibration wavefunctions. The vibrational symmetry will determine which components of $\hat{\mu}_v$ vanish. Vibrational bands can then be called a-type, b-type or c-type bands if a single component remains, or hybrid bands if more then one component is non-zero. The overall rotational contour of a vibrational band differs with each band type. Of particular note is that bands of b-type do not have the intense and easily recognizable Q-branch region that characterizes the a- and c-type bands. This makes b-type bands more difficult to recognize in the spectrum.

It can be shown (as in chapter 14 of Ref. **[102]**) that M_{ij} will vanish according to the vanishing integral rule if $\Gamma(\Psi_i) \otimes \Gamma(\mu_\alpha) \otimes \Gamma(\Psi_j)$ does not contain the totally symmetric representation for an electric dipole component $\vec{\mu}_\alpha$ (where $\Gamma(F)$ is the symmetry representation of a function F). The component $\vec{\mu}_\alpha$ which satisfies this condition can be determined for a given vibrational transition using the character table by matching the symmetry of the transition with that of the electric dipole. Vectors along each axis of the molecule can be assigned symmetry labels based on how they transform under the MS group operations and these special labels are often included in character tables (these are added to the G_4 character table in table 2.6.1). From this we can see that the a, b and c axes (y, z and x in the II^r representation), and thus the corresponding electric dipole components, have B_2, A_1 and B_1 symmetry, respectively. The symmetry of a transition between two vibrational states with labels Γ'' and Γ' can be found by determining the symmetry of the direct product of the representations $\Gamma'' \otimes \Gamma'$ (see table 2.6.2).

G_4	E	(13)(45)(79)	(13)(45)(79)*	E*	
A_1	1	1	1	1	b
A_2	1	1	-1	-1	
B_1	1	-1	1	-1	c
B_2	1	-1	-1	1	a

Table 2.6.1: G_4 character table with the symmetry of a vector along each axis indicated on the right.

The symmetry can then be found for each vibrational transition from the ground 0^0 (A_1) and 0^1 (B_2) pair to the 1^0 and 1^1 pair corresponding to vibrations of each symmetry species (where the symmetry of the 1^1 level is given by $\Gamma \otimes B_2$ for a vibration of symmetry Γ). Comparing these with the symmetry of the dipole moment vectors gives the vibrational band types and the results are summarized in figure 2.6.1.

G_4	A_1	A_2	B_1	B_2
A_1	A_1	A_2	B_1	B_2
A_2	A_2	A_1	B_2	B_1
B_1	B_1	B_2	A_1	A_2
B_2	B_2	B_1	A_2	A_1

Table 2.6.2: Multiplication table for the G_4 MS group.

Four vibrational bands are expected for each of the in-plane fundamentals (of A_1 and B_2 symmetry). Two of these will be a-type bands ($0^0 \rightarrow 1^1$ and $0^1 \rightarrow 1^0$ for vibrations of A_1 symmetry; $0^0 \rightarrow 1^0$ and $0^1 \rightarrow 1^1$ for those of B_2 symmetry) and two will be b-type bands ($0^0 \rightarrow 1^0$ and $0^1 \rightarrow 1^1$ for vibrations of A_1 symmetry; $0^0 \rightarrow 1^1$ and $0^1 \rightarrow 1^0$ for those of B_2 symmetry). Two c-type bands are expected for each of the out-of-plane fundamentals ($0^0 \rightarrow 1^0$ and $0^1 \rightarrow 1^1$ for vibrations of B_1 symmetry; $0^0 \rightarrow 1^1$ and $0^1 \rightarrow 1^0$ for those of A_2 symmetry) with the other possible transitions being forbidden.

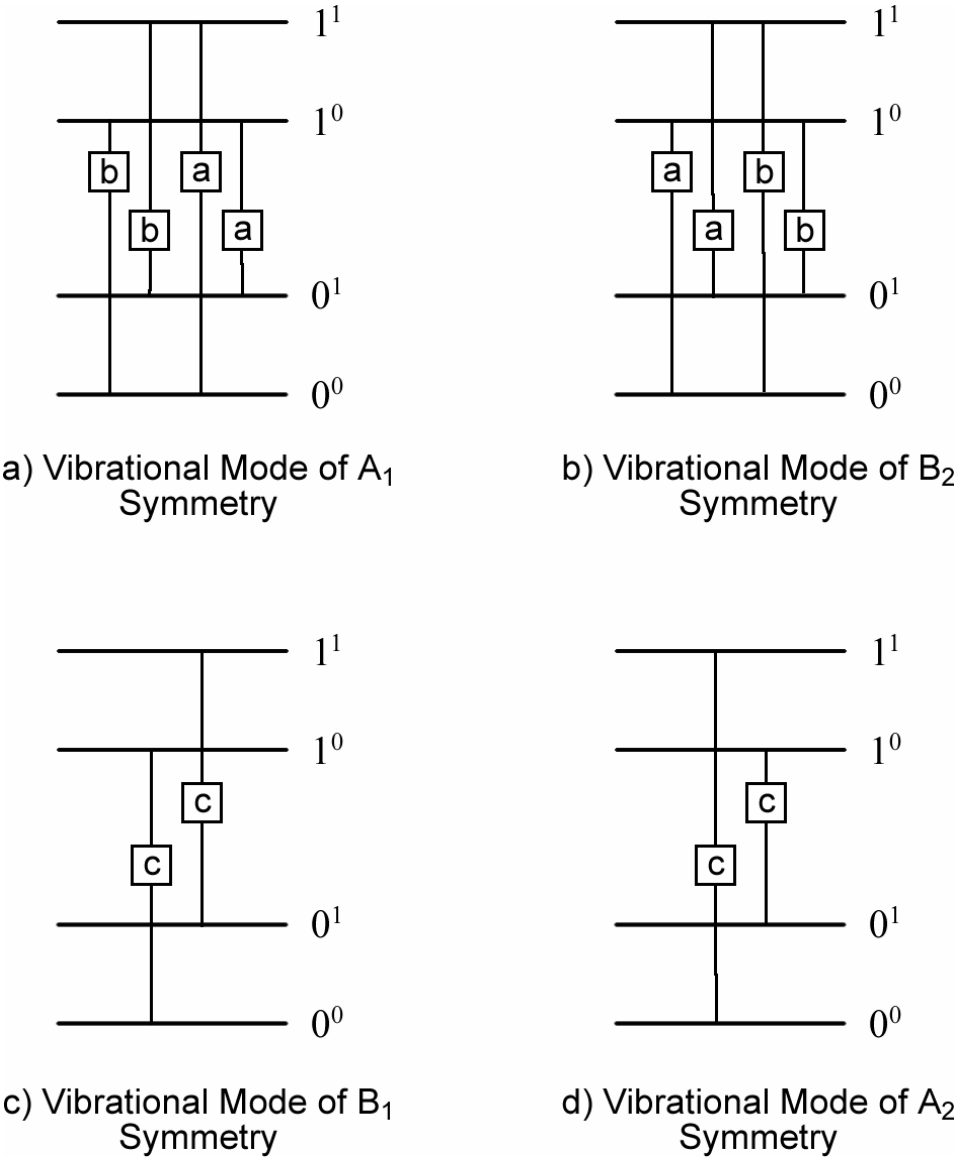

Figure 2.6.1: Selection rules and band types for vibrational fundamentals of malonaldehyde. This figure was inspired by figure 2 in Ref. ***[24]****.*

A vibrational transition between two states with rotational labels $J_{Ka,Kc}$ and $J'_{Ka',Kc'}$ is allowed in the electric dipole approximation only if ΔJ is -1, 0 or 1, and these cases are respectively called P, Q and R transitions. The allowed changes in the indices K_a and K_c depend on whether the transition is a-type, b-type or c-type. In a-type transitions, ΔK_a is even (0, ±2...) and ΔK_c is odd (±1, ±3...). In b-type transitions, both ΔK_a and ΔK_c are odd. In c-type transitions, ΔK_a is odd and ΔK_c is even. In all of these cases, the transitions with

the smallest allowed change in each K value are the most intense and only these are observed in this work.

2.7 - Nuclear Spin Statistical Effects

The total wavefunction of a molecule must be symmetric with respect to the exchange of two identical bosons and anti-symmetric with respect to the exchange of two identical fermions. Any allowed total wavefunction of malonaldehyde must then be anti-symmetric to the G_4 group operation (13)(45)(79) since nuclei 7 and 9 are fermions and the rest are bosons. From this, the character table (table 2.2.3) shows that the total wavefunction can only be of B_1 or B_2 symmetry depending on its parity (symmetry with respect to E^*). Therefore, a given rovibronic wavefunction of malonaldehyde can only combine with an appropriate nuclear spin wavefunction so that the product has one of these two symmetries.

Following the process described in chapter 8 of Ref. **[102]**, the two possible spin-½ eigenfunctions (in the form $|S, m_s>$) are $|\frac{1}{2}, \frac{1}{2}>$ (called α) and $|\frac{1}{2}, \frac{-1}{2}>$ (called β). For a nucleus n, the spin functions will be denoted α^n and β^n. The combined H_7 and H_9 spin functions are then given by:

$m_s = 1$ $\quad \alpha^7\alpha^9$

$m_s = 0$ $\quad \alpha^7\beta^9$, $\beta^7\alpha^9$ $\quad$ or $\quad \frac{1}{\sqrt{2}}(\alpha^7\beta^9 \pm \beta^7\alpha^9)$ when symmetrized

$m_s = -1$ $\quad \beta^7\beta^9$

The $m_s = \pm 1$ functions are unchanged by all G_4 operations and have A_1 symmetry, while the $m_s = 0$ functions generate the reducible representation $A_1 \oplus B_2$. Combining

these together gives the representation $3A_1 \oplus B_2$. The remaining four spin functions belonging to the H_6 and H_8 nuclei are unaffected by any G_4 operations and are of A_1 symmetry. Combining these with the symmetry representation of the H_7 and H_9 spins gives a total nuclear spin representation of $4A_1 \otimes (3A_1 \oplus B_2)$, which reduces to $12A_1 \oplus 4B_2$ since A_1 is the totally symmetric representation. Rovibronic wavefunctions of B_1 and B_2 symmetry that must combine with an A_1 nuclear spin function to produce a valid product will have a weighting of 12, and rovibronic wavefunctions of A_1 and A_2 symmetry that must combine with a B_2 nuclear spin function will have a weighting of 4, resulting in a 3:1 ratio.

The ground state electronic wavefunction of malonaldehyde is of A_1 symmetry and is totally symmetric. The 0^0 and 0^1 vibrational states are of A_1 and B_2 symmetry as described above, and only transitions originating from these states will be considered. Finally, the symmetry of the rotational states $J_{Ka,Kc}$ can be determined by separating them into four groups based on whether K_a and K_c are respectively even (e) or odd (o). These groups and their symmetries are ee (A_1), eo (B_1), oe (B_2) and oo (A_2). The final nuclear spin weightings for the 0^0 and 0^1 rovibronic wavefunctions are given in table 2.7.1, where it is apparent that a 3:1 alternating intensity pattern should appear in the spectrum. As shown, the rotational state weightings only depend on the sum of K_a and K_c, with the weighting of the ee and oo states ($K_a + K_c$ even) being the opposite of the eo and oe states ($K_a + K_c$ odd).

Vibrational Symmetry	K_aK_c Parity	$K_a + K_c$ Parity	Spin Weighting
A_1	ee	even	4
	oo		
	eo	odd	12
	oe		
B_2	ee	even	12
	oo		
	eo	odd	4
	oe		

Table 2.7.1: Nuclear spin weightings for malonaldehyde vibrational states of A_1 and B_2 symmetry.

2.8 - Rotational Energy Level Structure

In the rigid-rotor approximation the energy of a set of states with common K_a or common K_c will increase with J, and for a common value of J the energy will increase with K_a and decrease with K_c (as shown in Ref. **[102]**). The spacing between the two states of common J and K_a (with K_c being J - K_a and J - K_a + 1) and of common J and K_c (with K_a being J - K_c and J - K_c + 1) will vary considerably and in many cases one of the two pairs will appear to be degenerate at experimental resolution. This apparent degeneracy will have consequences for the observed intensities in the spectrum since the two states will necessarily have opposite spin weightings (being a pair of even and odd $K_a + K_c$). Alternating intensities will not be observed within a region where this apparent degeneracy occurs and will appear only when it is lifted.

In the case of apparent degeneracy, the rotational states can be labeled using only the set of prolate or oblate symmetric top quantum numbers as J_K for K being K_a or K_c. This indicates that the apparent degeneracy occurs when the molecule is, in a sense, behaving like a symmetric top. If the molecule is in a state with K_a or K_c being close to J then most of the angular momentum is about the z-axis of a prolate or oblate symmetric

top. In this case the average structure of the molecule over multiple rotations about the z-axis will be close to that of a symmetric top as the x and y components of the moment of inertia are averaged together. From this informal argument it would be expected for K_a to be closer to a good quantum number for states of high K_a and similarly for K_c.

This conclusion can also be reached mathematically by considering the form of the asymmetric top rotational Hamiltonian. When expressing the Hamiltonian in the basis of prolate symmetric top wavefunctions, the off-diagonal terms take the form:

$$< J, k_a - 2 | (J^+)^2 | J, k_a > = \{[J(J+1) - (k_a - 1)(k_a - 2)][J(J+1) - k_a(k_a - 1)]\}^{1/2} \hbar^2$$

$$< J, k_a + 2 | (J^-)^2 | J, k_a > = \{[J(J+1) - (k_a + 1)(k_a + 2)][J(J+1) - k_a(k_a + 1)]\}^{1/2} \hbar^2$$

Looking at the limit of high J and K_a (= $|k_a|$), both of these reduce to:

$$< J, k_a - 2 | (J^+)^2 | J, k_a > \approx < J, k_a + 2 | (J^-)^2 | J, k_a > \approx [J^2 - k_a^2] \hbar^2$$

These off-diagonal terms become smaller as K_a increases, resulting in wavefunctions that are closer to those of a prolate symmetric top. K_a then becomes closer to being a good quantum number as in the prolate case and K_c becomes less important. As a result, the two J_{Ka} states (with K_c = J - K_a or K_c = J + 1 - K_a) must become degenerate in the limit of high J and K_a. A similar argument can be applied if the asymmetric top Hamiltonian is expressed in the oblate symmetric top basis, with the result that the two J_{Kc} states must be degenerate in the limit of high J and K_c.

For a given J there must be a transition region of intermediate K values where the states group as J_{Ka} pairs at higher energy (high K_a, low K_c) and J_{Kc} pairs at lower energy (high K_c, low K_a). In this region, the pairs must break up and reform as they rearrange, resulting in the appearance of the 3:1 intensity alternation as the apparent degeneracy is

broken. Since the states are no longer grouped into pairs, this region will appear much less structured in the spectrum.

2.9 - Parameters in the Rotational Hamiltonian

The rotational Hamiltonian for an asymmetric rigid rotor is:

$$\hat{H}_{rot} = A\hat{J}_a^2 + B\hat{J}_b^2 + C\hat{J}_c^2$$

where the rotational constants A, B and C are inversely proportional to the moments of inertia about their respective axes. As the rotational angular momentum of a molecule increases, its structure will change as a result of centrifugal distortion. The resulting dependence of the moments of inertia (and therefore the rotational constants) on angular momentum can be accounted for in the Hamiltonian by adding higher order terms in $\hat{\vec{J}}$ and $\hat{J}_z$. A full set of such terms can be found by applying the appropriate symmetry conditions for the general Hamiltonian and for an asymmetric molecule (as is done by Watson in Ref. **[104]**). However, as is shown by Watson, the corresponding physical parameters are not all independently determinable by experiment. The energy eigenvalues that can be measured using spectroscopic techniques are dependent on a reduced set of constants which, as Watson demonstrated, can be constructed by combining members of the larger set. There are two ways in which this is commonly done, called the asymmetric top reduction (A-reduction) and the symmetric top reduction (S-reduction). The A-reduction is used for very asymmetric molecules and can fail for near-symmetric tops since it contains terms which go to infinity in the symmetric case. Since malonaldehyde is highly asymmetric, the A-reduction is used in this work. The resulting Hamiltonian for the A-reduction is given as equation 68 (page 34) in Ref. **[104]**,

and includes quartic (Δ_J, Δ_{JK}, Δ_K, δ_J, δ_K) and sextic (Φ_J, Φ_{JK}, Φ_{KJ}, Φ_K, φ_J, φ_{JK}, φ_K) centrifugal distortion constants. Note that some authors refer to the quartic distortion constants as (D_J, D_{JK}, D_K, d_J, d_K) and the sextic distortion constants as (H_J, H_{JK}, H_{KJ}, H_K, h_J, h_{JK}, h_K).

2.10 - Coupling of Vibrational Tunnelling Components

In addition to the centrifugal distortion Hamiltonian described above, terms must be added to account for rotation-vibration interactions connecting the two tunnelling components of each vibrational state. These interactions can be thought of as arising as a consequence of the chosen axis system. As mentioned above (section 2.3), the moment of inertia tensor in the equilibrium state is not diagonal, instead taking the form:

$$I = \begin{bmatrix} I_{xx} & 0 & 0 \\ 0 & I_{yy} & I_{yz} \\ 0 & I_{yz} & I_{zz} \end{bmatrix}$$

where I_{yz} is a product of inertia given by $I_{yz} = -\sum_i m_i y_i z_i$ and the sum is over all of the particles in the molecule.

The contribution from I_{yz} appears in the rotational Hamiltonian as a term of the form $\hat{H}_{vr} = F\{\hat{J}_a, \hat{J}_b\}_+$ where $\{\hat{J}_a, \hat{J}_b\}_+$ is the anti-commutator of $\hat{J}_a$ and $\hat{J}_b$ (that is, $\hat{J}_a\hat{J}_b + \hat{J}_b\hat{J}_a$). This term is mathematically identical in form to that of a second-order Coriolis interaction between the two states, and results in the same effect on the system. For many of the tunnelling pairs, the interaction is strong enough to necessitate the use of higher order terms in $\hat{\vec{J}}$ and its components. Including these terms, the full vibration-rotation interaction Hamiltonian used in this thesis is:

$$\hat{H}_{vr} = F\{\hat{J}_a, \hat{J}_b\}_+ + F_J \hat{J}^2\{\hat{J}_a, \hat{J}_b\}_+ + F_B\{\hat{J}_a, \hat{J}_b^3\}_+$$

where the constant F_J is called F" in previous work on malonaldehyde.

Chapter 3

Experimental Methods

3.1 - Preparation of Malonaldehyde and Experimental Setup

Malonaldehyde sodium salt dihydrate (with Na^+ occupying the tunnelling site) was produced by acidic hydrolysis of 1,1,3,3-tetramethoxypropane as described by Trivella *et al.* in Ref. **[105]**. This intermediate step is necessary due to the instability of solid malonaldehyde, which rapidly polymerizes at temperatures above 0 °C. Synthesis of the sodium salt was performed with the assistance of Dr. David Magee[1] and Dr. James Tait[1] at the University of New Brunswick and it was then shipped to the Canadian Light Source (CLS) at the University of Saskatchewan. Malonaldehyde was then produced on site at the CLS by reacting the sodium salt with hydrochloric acid dissolved in diethyl ether. This step was carried out in a dry nitrogen flow and the reaction was kept below -40 °C as described in Ref. **[105]**. The cold sample was then pumped for about 3 hours to remove the solvent and HCl.

The malonaldehyde spectra that are used in the present work were acquired by Dr. Dennis Tokaryk prior to my involvement in the project. My visits to the CLS were in an attempt to synthesize a deuterated isotopologue of malonaldehyde with a deuteron in place of the tunnelling proton. This was attempted first by substituting the HCl in diethyl ether with DCl in diethyl ether, although this was unsuccessful, instead producing only the regular molecule. Wilson's group had reported making a number of deuterated isotopologues by coating the inside of the cell with D_2O and allowing for exchange with

[1] Department of Chemistry, University of New Brunswick

regular malonaldehyde **[2]**. We have also attempted this method, but we have been unable to verify the production of any deuterated isotopologues.

The Far-IR beamline at the CLS consists of a set of planar and ellipsoidal mirrors which accept and convey the synchrotron radiation from the storage ring to the spectrometer **[106]**. Taking advantage of the angular distribution of frequencies present in synchrotron radiation, the first of these mirrors has a 6 mm slot which allows higher-frequency components to pass through and be absorbed. The infrared light is then directed to an ellipsoidal mirror and through a diamond window (which transmits throughout the infrared region) separating the ultra high vacuum of the storage ring (about 10^{-10} Torr) from the rest of the beamline (less than 1 mTorr) **[107]**. The remaining four mirrors then bring the light to the spectrometer.

The beamline makes use of a Bruker IFS 125HR Fourier transform infrared spectrometer which has a maximum optical path length difference of 9.4 m, allowing it to achieve resolutions of 0.00096 cm^{-1} or better. The sample cell is a 2 m long White cell set up to produce a 72 m total path length. The temperature in the White cell can be adjusted using an attached chiller and was kept at 0 °C for acquisition of malonaldehyde spectra to avoid polymerization within the cell. This equipment can operate in the 12 to 10000 cm^{-1} range depending on the combination of beamsplitters, cell windows and detectors that are being used.

3.2 - Spectrum Acquisition and Processing

Malonaldehyde spectra were obtained in three different regions: 40 to 335 cm^{-1}, 330 to 550 cm^{-1} and 700 to 1800 cm^{-1}. The spectrum in the 40 to 335 cm^{-1} region was taken using a silicon bolometer, a 6 µm Mylar beamsplitter and polypropylene cell windows. The same beamsplitter and windows were used for the 330 to 550 cm^{-1} region, but with a copper-doped germanium (Cu:Ge) detector. The 700 to 1800 cm^{-1} spectrum was taken using a narrow-band MCT (mercury cadmium telluride) detector and with a potassium bromide (KBr) beamsplitter and windows.

Different gas pressures were used for each spectral region. The Si bolometer, Cu:Ge and MCT spectra were taken at gas pressures of 127, 65 and 50 mTorr respectively. The presence of a number of impurities is evident from the spectra, so the gas pressures reported here do not represent an amount of pure malonaldehyde.

The spectrum acquisition and processing was performed using the Bruker OPUS software **[108]**. For each spectral region, a large number of interferograms (200-300) were obtained, averaged and Fourier transformed to obtain a transmittance spectrum. About 300 low-resolution background scans were also obtained and the absorbance spectrum A was calculated using

$$A = -\ln\left(\frac{I}{I_0}\right)$$

where I is the transmittance spectrum and I_0 is the averaged transformed background transmittance.

Chapter 4

Analysis of the Malonaldehyde Far-IR Spectrum

4.1 - Techniques and Software

After the initial processing, much of the analysis and manipulation of the spectra was handled using the data analysis and graphing software Igor Pro **[109]**. For a particular spectral feature or region of interest, peak positions and intensities were obtained using an automated peak-picking algorithm and then used to construct a Loomis-Wood plot. This was done using a software package written for Igor Pro by Christopher Neese **[110]**.

A Loomis-Wood plot is an alternative way of viewing a spectrum in which it is split into a number of segments which are then stacked vertically in consecutive order. The width of the segments is expressed as an n^{th} order polynomial function of row number, where n is selected by the user. The utility of this method is that the segment width can be made to match the spacing of consecutive lines in a branch of increasing J, which results in the lines of that progression appearing in sequence vertically with one line on each row. This is accomplished by fitting the segment width function to a set of selected line positions belonging to a series. The row number then becomes an index called m which is equal to J+1 for R-branch lines and -J for P-branch lines. Other patterns of lines with similar spacing can then be readily identified.

When analyzing spectra it is useful to subtract line frequencies to form combination differences, which allow information about a single vibrational state to be extracted from transitions involving two vibrational states. One type of combination difference, called an R/P combination difference, can be calculated once P and R

branches are identified in a band. Pairs of R and P lines which share the same rotational upper state can be identified and subtracted, giving the energy difference between the two lower states. In malonaldehyde, the absolute J numbering and J_{KaKc} labeling of the transitions can then be confirmed by comparing these R/P combination differences with those calculated from previously reported microwave results for the ground state tunnelling pair **[26]**. Once enough assignments were made so that a good fitting of the transition frequencies to a Hamiltonian model could be obtained, the frequencies of unassigned transitions could be accurately calculated and the remaining assignments could be made on the basis of agreement between a predicted line position and an observed feature.

The SPFIT (fitting of transitions to a model) and SPCAT (calculation of transition frequencies and intensities from the model) programs developed by Pickett **[111]** were used for some of the preliminary work. However, most of the fitting and further assigning of the spectrum was done using the PGOPHER program developed by Colin Western **[112]**, which has similar functionality but with the addition of a visual interface and other useful features. In PGOPHER, the experimental spectrum can be displayed above a simulated spectrum using the current set of molecular parameters, and assignments can be made by comparison of the two. In addition to fitting the line positions, PGOPHER was also used for its ability to easily perform lower and upper state combination difference fitting. From a given line list, PGOPHER can automatically generate all possible combination differences for a specified vibrational state and these can be used instead of the transitions to characterize that state. Combination difference fitting is useful since only one vibrational state needs to be fitted, which is important if the other

vibrational state involved in the transition is perturbed or otherwise unable to be easily modeled.

4.2 - Overview of the Spectrum

Examination of the spectra has revealed the presence of a number of impurities in the sample. Many of the very intense widely spaced lines that appear throughout most of the spectra (in particular the low-frequency silicon bolometer region) are due to water in the sample cell and could not be avoided. There are also many bands of HNCS, the presence of which may be due to residual material from a previous unrelated experiment using the same equipment. Spectra of HNCS that were used to identify these bands were reported in Refs. **[113]** and **[114]**.

The region of the silicon bolometer spectrum from 165 to 245 cm^{-1} is given in figure 4.2.1. Although the spectrum was also taken from 40 to 165 cm^{-1}, no features were found in that region that could be attributed to malonaldehyde on the basis of band structure (line spacing, density and intensity). Additionally, no bands were observed or predicted below 184 cm^{-1} in the literature. In the region shown, the main features are the two bands near 184 and 220 cm^{-1} (as indicated by + signs). Both of these bands have a clear R-Q-P branch structure which identifies them as being a-type or c-type. These are consistent with the observations of others, in particular Lüttschwager *et al.* **[36]** who assigned them to the $0^0 \rightarrow 1^0$ (184 cm^{-1}) and $0^1 \rightarrow 1^1$ (220 cm^{-1}) transitions of the νO···O in-plane ring opening/closing mode (as defined in chapter 2, the notation $\upsilon^{\upsilon'}$ represents a state with vibrational quantum number υ in the small-amplitude mode being discussed and υ' in the tunnelling mode).

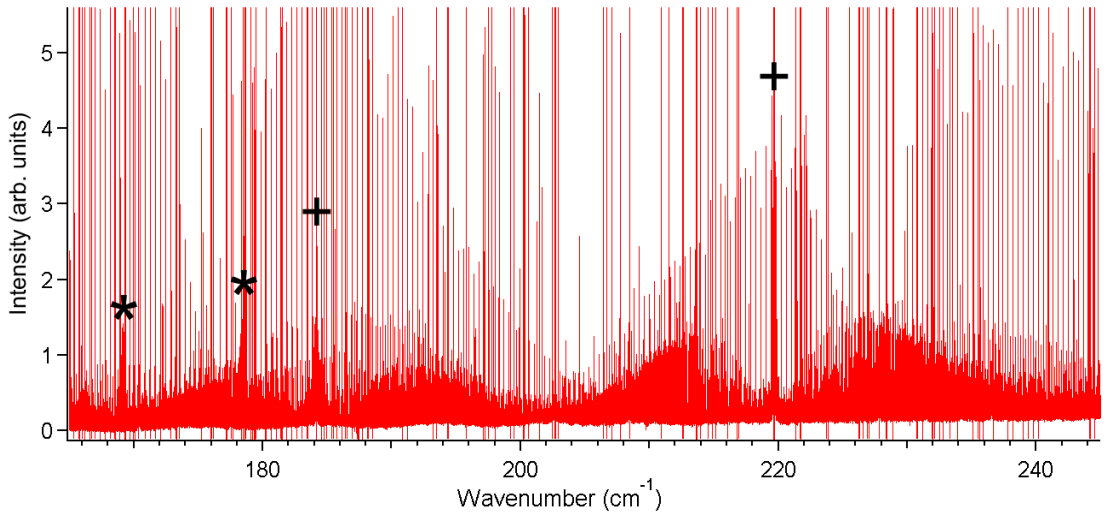

Figure 4.2.1: FTIR spectrum of malonaldehyde in the 165 to 245 cm^{-1} region. HNCS bands are indicated with asterisks (*). Bands assigned in Ref. ***[36]*** *are indicated by plus signs (+).*

The region of the silicon bolometer spectrum from 215 to 295 cm^{-1} is given in figure 4.2.2. There are two main features in this region (not including the 220 cm^{-1} band, which is included in figure 4.2.2 for scale) near 252 and 282 cm^{-1} (as indicated by + signs). The feature near 273 cm^{-1} is a band of HNCS. The bands at 252 and 282 cm^{-1} are also consistent with Ref. **[36]**, in which they are respectively assigned as the $0^1 \rightarrow 1^0$ and $0^0 \rightarrow 1^1$ transitions of an out-of-plane vibration (γC_cH, as labeled by Lüttschwager *et al.*). There are also some small features that can be seen near 256 and 269 cm^{-1}.

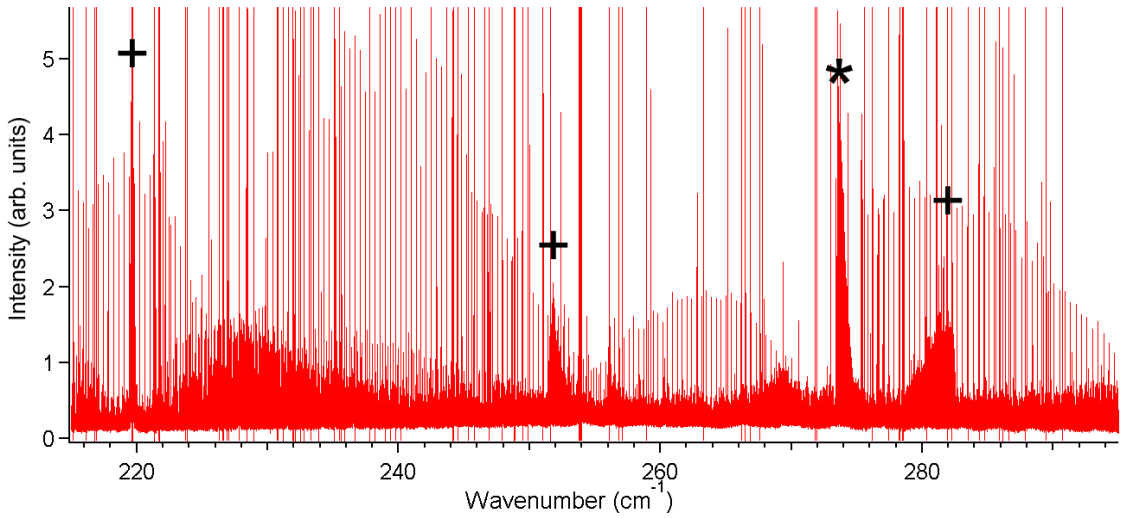

Figure 4.2.2: FTIR spectrum of malonaldehyde in the 215 to 295 cm^{-1} region. The asterisk indicates a band of HNCS (*). *Bands assigned in Ref.* ***[36]*** *are indicated by plus signs* (+).

The spectrum from 345 to 545 cm^{-1} (Cu:Ge detector range) is given in figure 4.2.3, where two features can be seen near 384 and 512 cm^{-1}. Both of these are actually closely spaced pairs of similarly-structured bands located at 384/390 cm^{-1} for the lower-frequency pair and 506/512 cm^{-1} for the higher-frequency pair (as indicated by + signs). The band structure indicates that they are either a- or c-type. This is consistent with Ref. **[36]** where the lower-frequency pair are assigned as the $0^1 \rightarrow 1^1$ (384 cm^{-1}) and $0^0 \rightarrow 1^0$ (390 cm^{-1}) transitions of an out-of-plane ring-bending mode, and the higher-frequency pair are assigned as the $0^0 \rightarrow 1^0$ (506 cm^{-1}) and $0^1 \rightarrow 1^1$ (512 cm^{-1}) transitions of an in-plane ring-bending mode. The baseline oscillations in the spectrum that are apparent in the higher-frequency region of figure 4.2.3 are channeling effects that result from accidental etalon-like behavior (multiple reflections and interference) in the beamline optics.

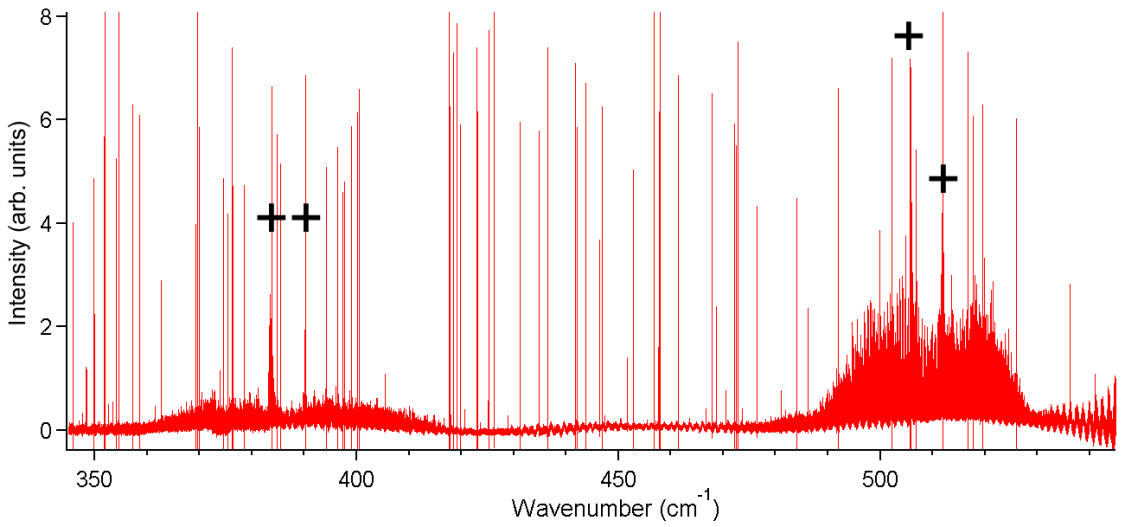

Figure 4.2.3: FTIR spectrum of malonaldehyde in the 345 to 545 cm^{-1} region. Bands assigned in Ref. ***[36]*** *are indicated by plus signs* (+).

The spectrum in the 700 to 1800 cm^{-1} region (MCT detector range) is shown in figure 4.2.4. Many of the features that can be seen, such as the bands at 1594 and 1658 cm^{-1}, correspond to assignments made by Lüttschwager *et al.* in Ref. **[36]**. The bands at 1267 and 1358 cm^{-1} were respectively assigned by Lüttschwager *et al.* as the $0^1 \rightarrow 1^0$ and $0^0 \rightarrow 1^1$ transitions of the C-O-H bending mode, with a tunnelling splitting of about 69 cm^{-1} in the upper state. Other features near 1267 cm^{-1} may correspond to the bands assigned by Lüttschwager *et al.* as excitations of the tunnelling components of a C_1-H_7 wagging mode. They assigned the bands at 964 and 1000 cm^{-1} as $0^1 \rightarrow 1^0$ and $0^0 \rightarrow 1^1$ transitions of a carbon-frame vibration and the bands at 878 and 883 cm^{-1} to the $0^0 \rightarrow 1^0$ and $0^1 \rightarrow 1^1$ transitions of an in-plane ring-bending mode. Figure 4.2.5 shows an expansion of the region from 735 to 1030 cm^{-1}, and it can be seen that there is another band under the unknown impurity near 766 cm^{-1}. Although the tunnelling components involved in the transition were not assigned in Ref. **[36]**, the band was observed by Smith *et al.* **[17]** and identified as a fundamental of the out-of-plane H_8 bending mode by Tayyari and Milani-Nejad **[67]**. The feature near 1452 cm^{-1} was assigned in Ref. **[67]** as a

C_1-C_2 stretching, H_7 and H_8 bending mode fundamental. The features that can be seen near 713, 772, 1106, 1535 and 1776 cm^{-1} are likely impurities based on their rotational structure which is not consistent with malonaldehyde, but they have not yet been identified.

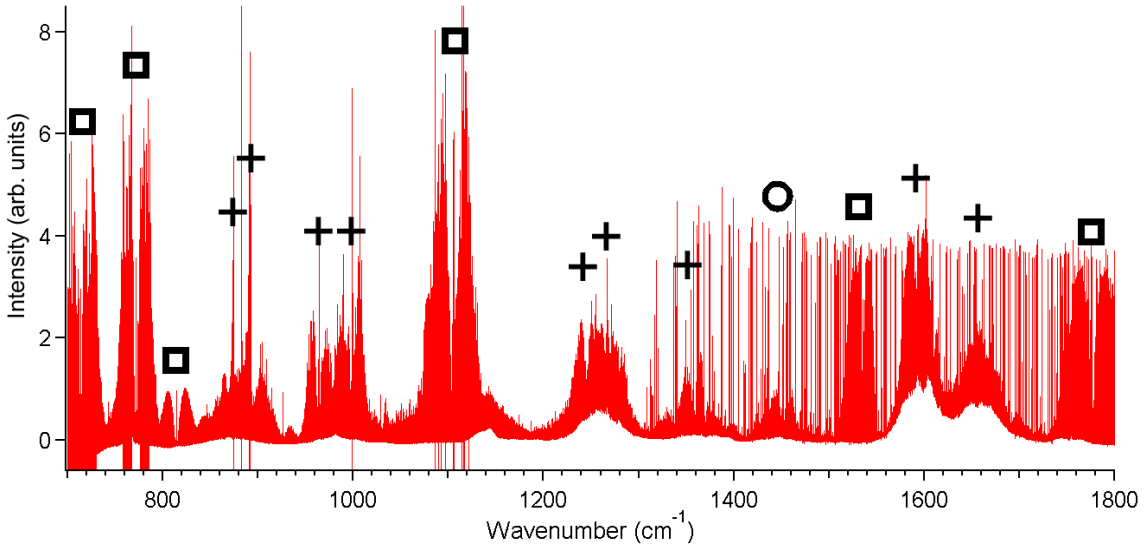

Figure 4.2.4: FTIR spectrum of malonaldehyde in the 700 cm^{-1} to 1800 cm^{-1} region. Bands assigned in Ref. ***[36]*** *are indicated by plus signs* (+)*, impurities by squares* (□) *and the circle* (○) *represents a band that was assigned in Ref.* ***[67]****.*

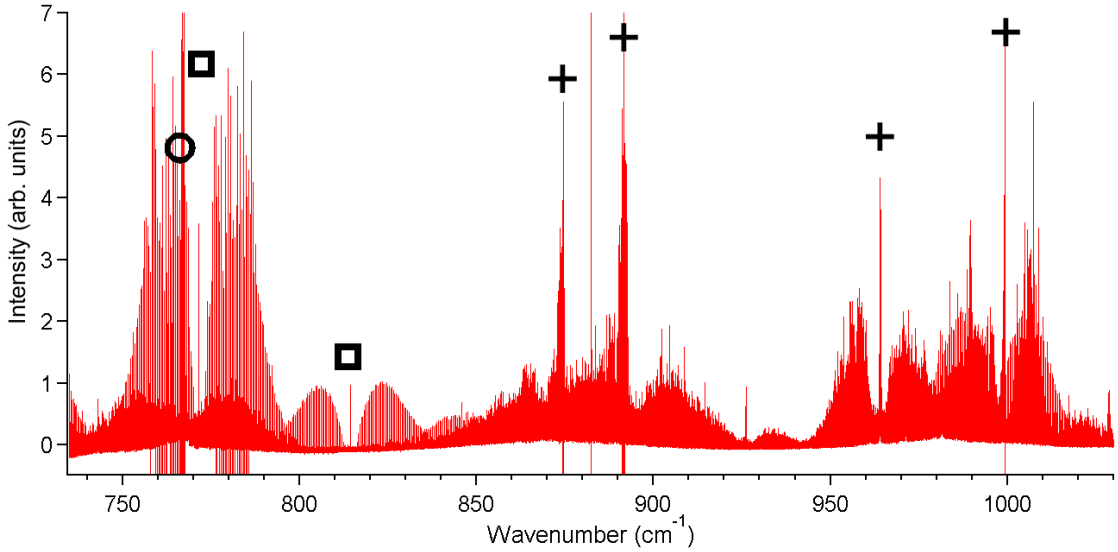

Figure 4.2.5: FTIR spectrum of malonaldehyde in the 735 cm^{-1} to 1030 cm^{-1} region. Bands assigned in Ref. ***[36]*** *are indicated by plus signs* (+)*, impurities by squares* (□) *and the circle* (○) *represents a band that was assigned in Ref.* ***[67]****.*

4.3 - Comparison with Ground State Combination Differences

The most recent and complete description of the malonaldehyde ground state tunnelling pair comes from the work of Baba *et al.* **[26]**, in which the authors measured the tunnelling-rotation spectrum of the ground state for the first time. Their fitting and resulting constants combined these measurements with the work of Wilson *et al.* **[1-4]** and Firth *et al.* **[25]**. In Ref. **[26]** the authors introduced the constant F_K as the coefficient of a "K_a dependent term" for the interaction between the tunnelling components of the ground state. The definition of this term was not given in their paper, so it was necessary to guess at the form of the term that was being used. A definition for a similar distortion term with a constant called C_K was given in the later work of Duan and Luckhaus **[27]** as

$$C_K\{\hat{J}_z^2,\{\hat{J}_x,\hat{J}_y\}_+\}_+$$

or $C_K\{\hat{J}_a^2,\{\hat{J}_b,\hat{J}_c\}_+\}_+$ in their chosen representation of I^r.

However, the definition of the undistorted interaction term given by Duan and Luckhaus as

$$C_{xy}\{\hat{J}_x,\hat{J}_y\}_+, \text{ or } C_{bc}\{\hat{J}_b,\hat{J}_c\}_+ \text{ in } I^r$$

is not in agreement with the interaction term as initially reported in Wilson *et al.*'s work and used by Baba *et al.* which involves $\hat{J}_a$ and $\hat{J}_b$ instead of $\hat{J}_b$ and $\hat{J}_c$. The definition that was used here in the initial calculations of combination differences was

$$F_K\{\hat{J}_a^3,\hat{J}_b\}_+$$

Any difference between this term and the one used by Baba *et al.* was not expected to have a great effect on the calculations. Although the F_K term was needed in the more precise microwave characterization, the infrared-derived combination differences that are

being compared to the microwave results are likely not precise enough to be sensitive to it.

Upon comparing combination differences from the initial assignments of the infrared bands, it became apparent that the infrared values would consistently drift away from the microwave values at high J (above about J = 30). The good agreement of the values at low J supported the validity of the assignments, making it unlikely that misassigned lines were responsible for the drift. Figures 4.3.1 and 4.3.2 show the drift for a number of a- and b-type bands for which initial assignments could be made. Figure 4.3.1 shows the bands that originate from the 0^0 ground state component and figure 4.3.2 shows the bands that originate from the 0^1 ground state component. Only the $K_a = 0$ series is shown for each band, since it was the most easily identifiable series of lines in the a- and b- type bands that were observed. The drift is greatest for the high-J lines of the 512 cm^{-1} band, where it reaches a magnitude of almost 0.007 cm^{-1} at J = 66, which is about 10 times larger than the experimental line width of 0.0007 cm^{-1}. It is clear from the figures that the drift is consistent across multiple a- and b-type bands originating from the same ground state, although it is less severe in bands coming from the 1^1 ground state.

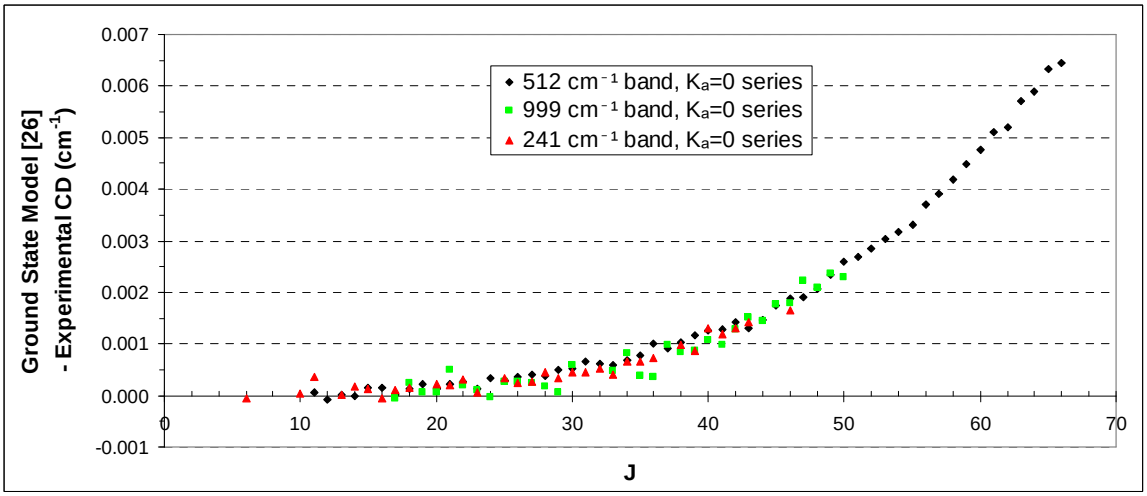

Figure 4.3.1: Experimental combination differences (CDs) from a- and b-type bands originating from the 0^0 ground state component subtracted from the equivalent difference in ground state energy levels calculated using the model from Ref. ***[26]****.*

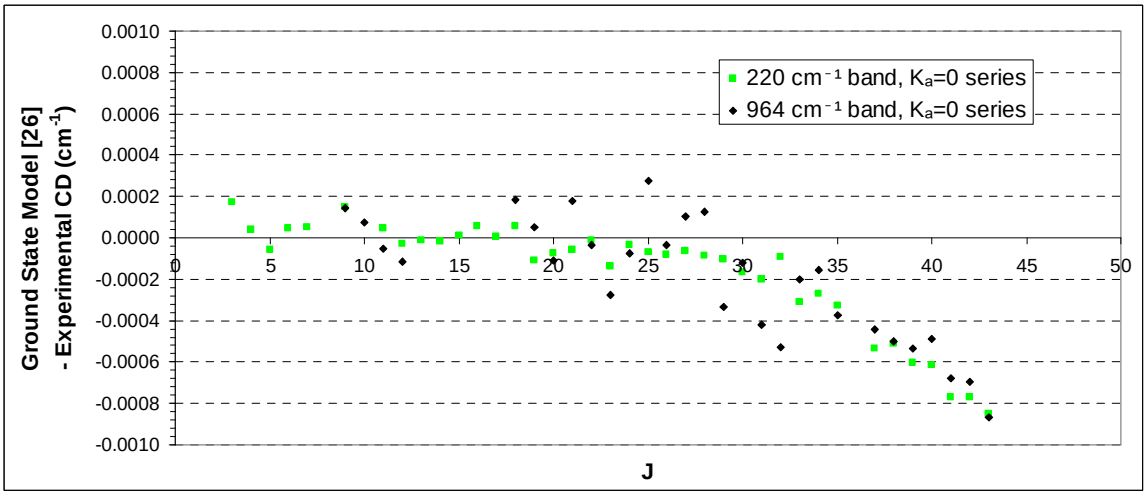

Figure 4.3.2: Experimental combination differences (CDs) from a- and b-type bands originating from the 0^1 ground state component subtracted from the equivalent difference in ground state energy levels calculated using the model from Ref. ***[26]****.*

Figure 4.3.3 compares the combination differences of the two c-type tunnelling components of the 384 cm^{-1} band to the microwave values. For these c-type bands (for which the high-K_a lines were the most easily identifiable) there is no evidence of drift and the combination differences are all within one line width of the microwave value (from Ref. **[26]**). However, the deviations are almost all positive (the experimental values are less than the model values) which indicates that the matches are not ideal.

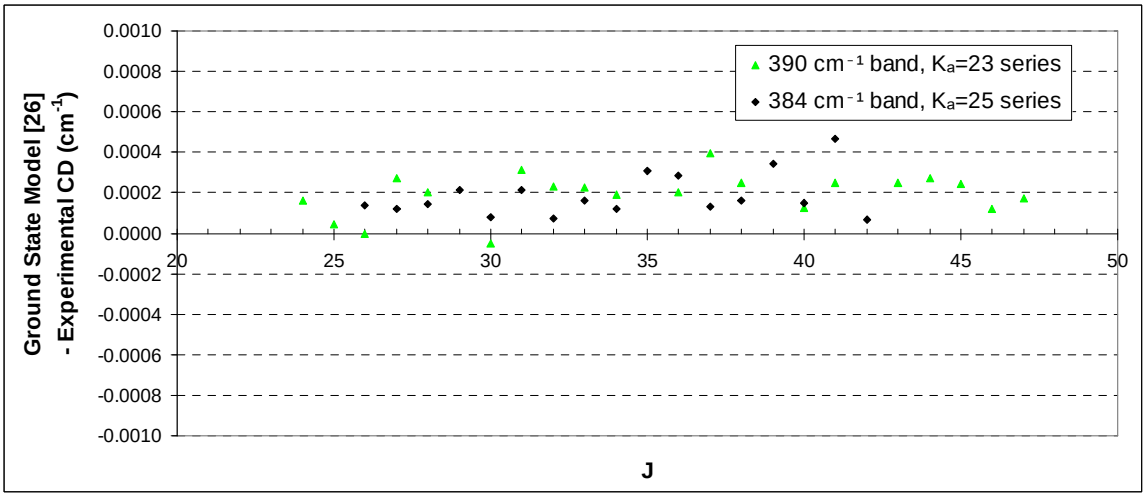

Figure 4.3.3: Experimental combination differences (CDs) from c-type bands originating from the 0^0 (390 cm^{-1} band) and 0^1 (384 cm^{-1}) ground state components subtracted from the equivalent difference in ground state energy levels calculated using the model from Ref. ***[26]****.*

4.4 - Recharacterizing the Ground State

In attempting to resolve the issue of the combination difference drift, it was necessary to make use of a preliminary line list previously obtained from an author of Ref. **[26]** by Dr. Stephen Ross, one of the supervisors of this thesis work. This line list included lines measured by the authors as well as those of the two prior ground state studies of Wilson *et al.* **[1-4]** and Firth *et al.* **[25]**. Although this information does not necessarily represent the final state of their work, it was noted that many of the lines from the two studies prior to theirs were weighted to zero, in particular a large number of those from the work of Firth *et al.*

In Ref. **[25]**, the authors mention that the current sampling of the ground state levels covers a limited range in J-K_a space. They illustrated this using a plot of J vs. K_a with the measured levels indicated for each of the ground state components. Similar plots have been constructed (figures 4.4.1 and 4.4.2), reflecting the addition of the measurements made by Baba *et al.* **[26]** and the removal of lines that were zero-weighted in their preliminary line list. These plots clearly demonstrate that the lines used in the

preliminary fitting reported by Baba *et al.* mostly cover the region of high K_a (close to J) and that the low-K_a region is not represented, particularly for high J. Since the combination difference drift was observed most severely in a- and b-type bands where the easily assigned lines correspond mostly to K_a values below 5, this provides a likely explanation. Many of the observed infrared lines in this work are in a quantum number range for which the previous ground state characterization from Ref. **[26]** is not reliable. It then became necessary to produce a characterization of the ground state that incorporated these new IR data.

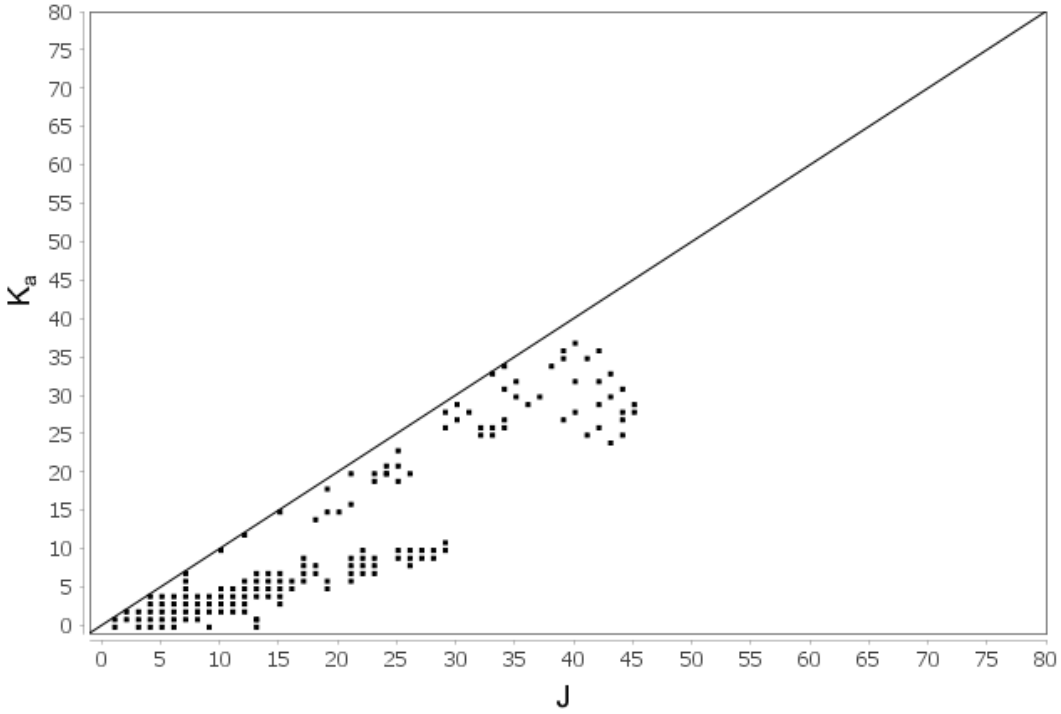

Figure 4.4.1: J-K_a space plot indicating the rotational levels in the 0^0 ground state component which were included in the preliminary line list from the authors of Ref. ***[26]****.*

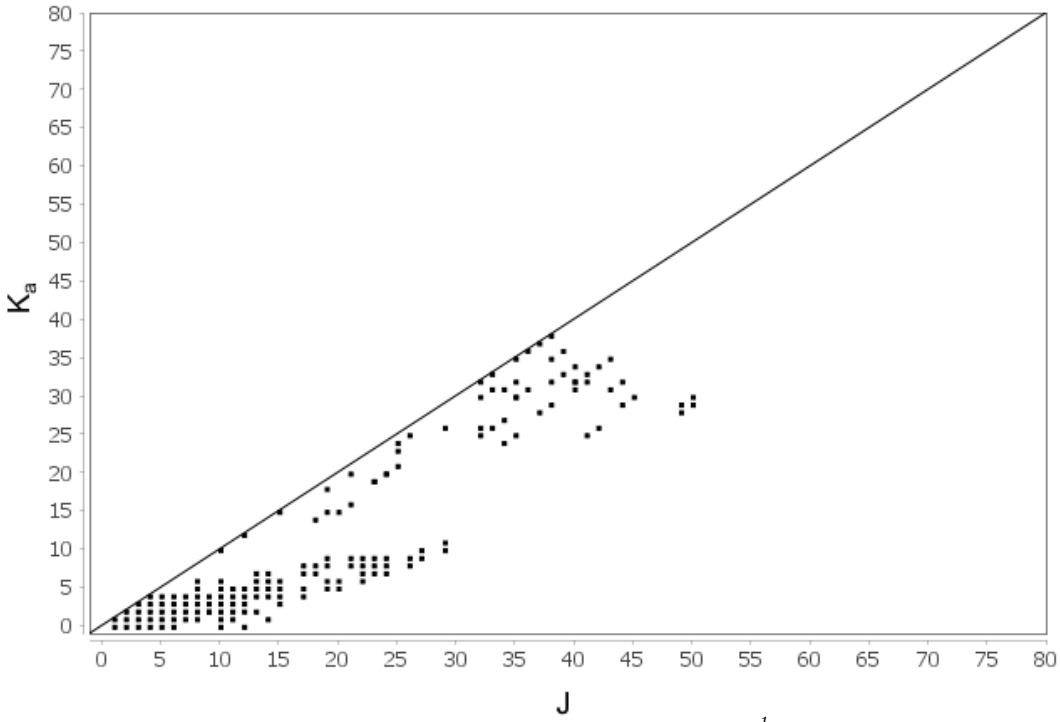

Figure 4.4.2: J-K_a space plot indicating the rotational levels in the 0^1 ground state component which were included in the preliminary line list from the authors of Ref. ***[26]****.*

The ground state characterization was first determined using only the infrared data by performing a lower state combination difference fitting with lines from a number of identified fundamental bands. This process was done in parallel with the assigning of the bands, so that new assignments were used to further update the ground state. Lines that were used in this fitting came from bands at 220, 241, 282, 384, 390, 506, 512, 766, 964 and 999 cm^{-1}, with the greatest contribution coming from the 220, 241, 384 and 390 cm^{-1} bands. Descriptions of each of these bands will be covered in later sections.

Residuals from this combination difference fitting were all within acceptable error and with no significant drift, demonstrating that the previous ground state characterization was not suitable for these new observations. All of the lines used in the preliminary line list from the authors of Ref. **[26]** were then included in the fitting. After verifying that the results were still consistent with the IR data, many of the lines reported

by Wilson *et al.* **[1-4]** and Firth *et al.* **[25]** that were not included in the preliminary line list from the authors of Ref. **[26]** were then added. The final ground state constants were obtained as part of a global fitting with the 241, 390 and 404 cm^{-1} states and will be presented in a later section along with a full description of the lines that were used.

With the addition of the new IR data, the characterization of the ground state presented here now covers a much wider range of J-K_a space (as shown in figures 4.4.3 and 4.4.4). It can also be seen from figures 4.4.5 and 4.4.6 that the drift in ground state combinations differences has been eliminated in the a- and b- type bands (note that the vertical scale of figure 4.4.5 is a factor of 7 smaller than that of figure 4.3.1). However, the combination differences for the c-type bands are still consistently less than the values calculated from the new ground state characterization (the comparison is unchanged from figure 4.3.3).

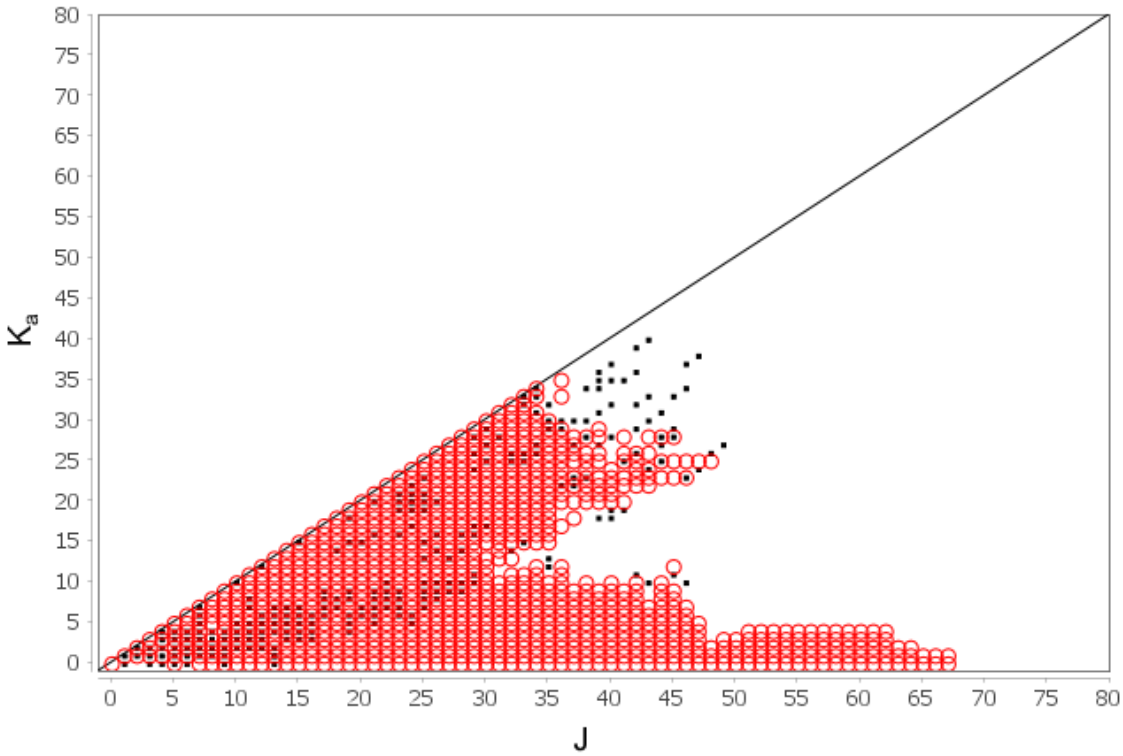

Figure 4.4.3: J-K_a space plot indicating measured levels in the 0^0 state. Black dots represent previously measured data from Refs. ***[1-4]****,* ***[25]*** *and* ***[26]****. Red circles represent data measured in this work.*

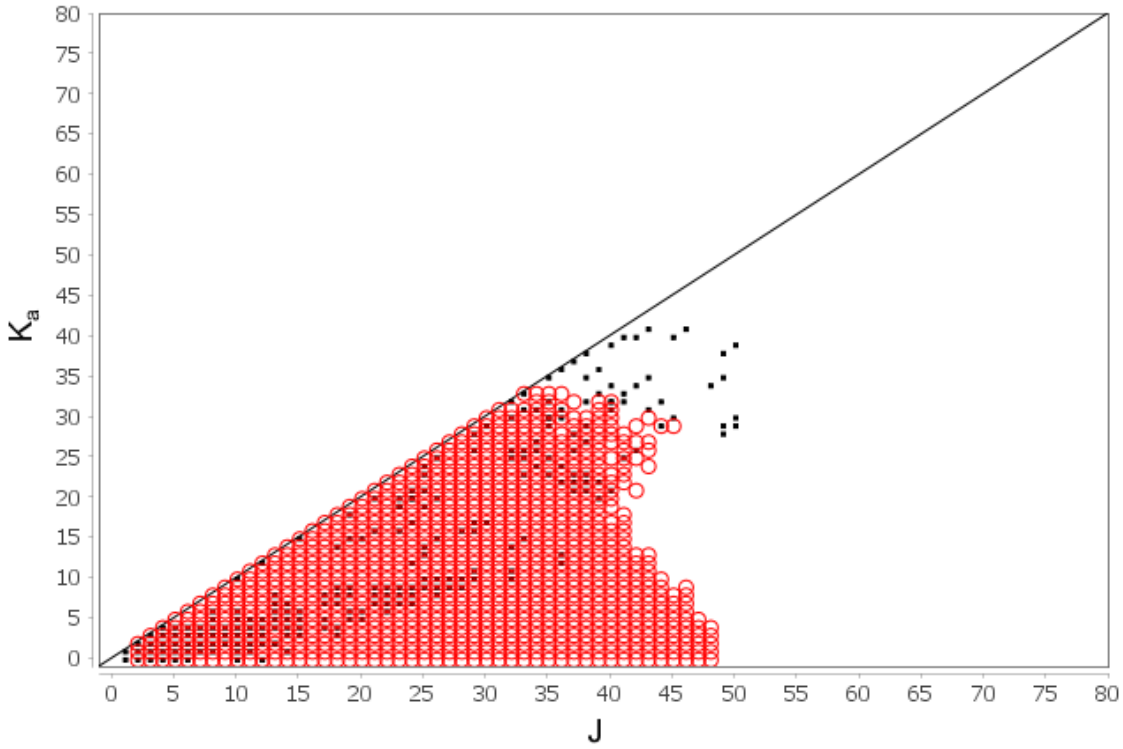

Figure 4.4.4: J-K_a space plot indicating measured levels in the 0^1 state. Black dots represent previously measured data from Refs. ***[1-4]****,* ***[25]*** *and* ***[26]****. Red circles represent data measured in this work.*

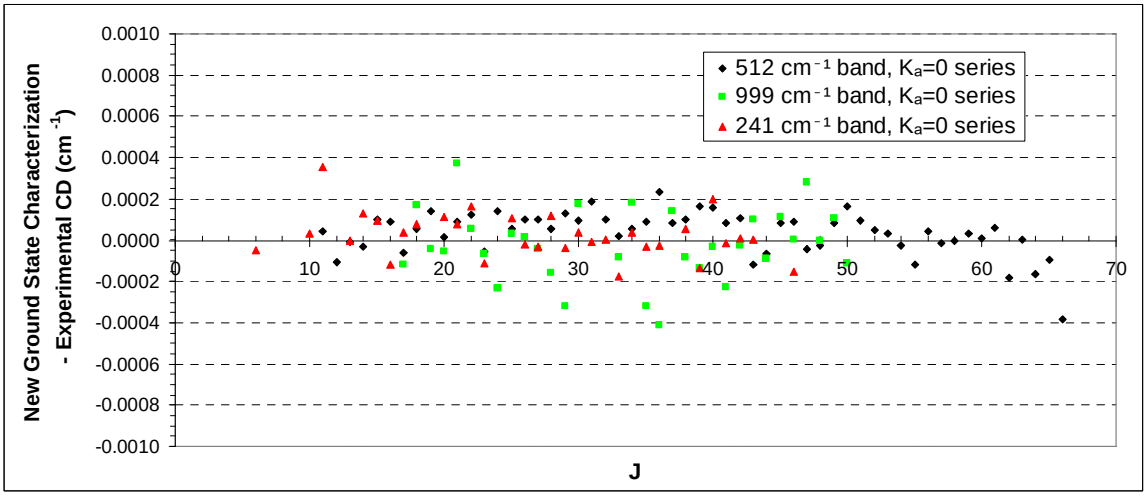

Figure 4.4.5: Experimental combination differences (CDs) from a- and b-type bands originating from the 0^0 ground state component subtracted from the equivalent difference in ground state energy levels calculated using the new characterization.

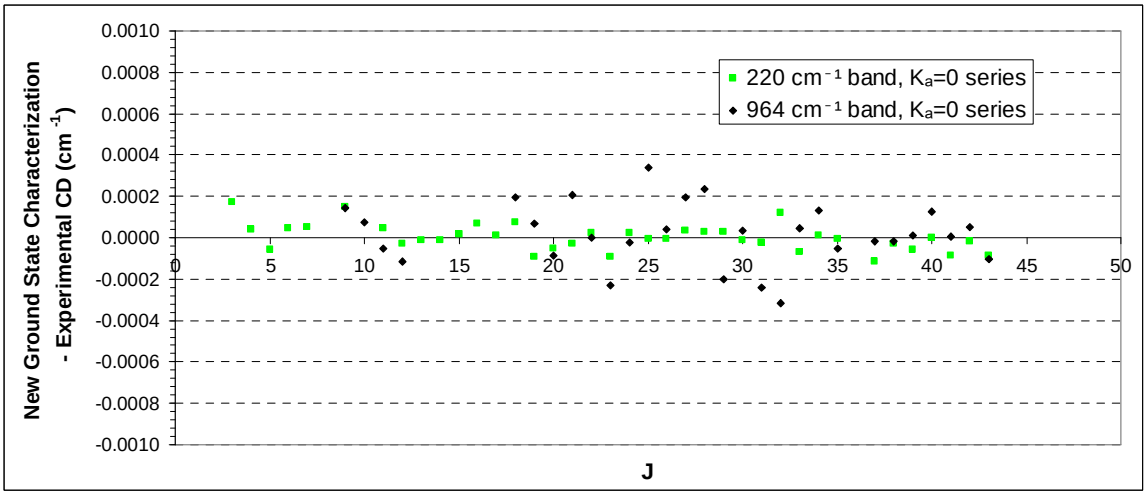

Figure 4.4.6: Experimental combination differences (CDs) from a- and b-type bands originating from the 0^1 ground state component subtracted from the equivalent difference in ground state energy levels calculated using the new characterization.

4.5 - Early Microwave Observations of Excited Vibrational States

The 1975 doctoral thesis of Walter Rowe **[5]** included an analysis of the pure-rotational spectrum of 8 vibrational states. While the two lowest-energy of these are clearly the ground state tunnelling pair, the other 6 states have since remained vibrationally unassigned. Rowe was able to calculate an approximate frequency for each of these states on the basis of relative intensities, although the high uncertainties in these values prevent them from being unambiguously matched to current infrared observations based on this alone. The 8 states observed by Rowe are presented in table 4.5.1 along with his estimates of their energy. To avoid ambiguity with infrared measurements, any vibrational state observed by Rowe will henceforth be referred to as R# where # is the vibrational frequency of the state as determined by Rowe.

Name used in this work	Planarity	Frequency (cm^{-1})
R0	In-plane	0.00
R16	In-plane	16 ± 14
R277	In-plane	277 ± 22
R293	In-plane	293 ± 8
R237	Out-of-plane	237 ± 20
R282	Out-of-plane	282 ± 9
R393	Out-of-plane	393 ± 59
R390	Out-of-plane	390 ± 35

Table 4.5.1: The 8 vibrational states observed by Rowe, showing frequency and planarity as determined in Ref. ***[5]****.*

For each of the states observed in Rowe's thesis, he presented an assessment of the planarity of each vibration based on calculations of the inertial defect. The inertial defect is a function of the principal moments of inertia given by $I_c - I_a - I_b$ and it provides a measure a molecule's planarity, with non-planar molecules having negative values and planar molecules having a value close to zero. Rowe suggested a possible grouping of these states into tunnelling split pairs based on having like planarity and similar frequency. These pairings are R0/R16, R277/R293, R237/R282 and R393/R390. In all cases where characterizations of these states based on Rowe's work were needed for comparison with infrared results, a new fitting of Rowe's reported line positions has been performed so that the results are consistent with the model used here. The constants that were obtained from these new fittings are in most cases not significantly different than those obtained by Rowe.

Figure 4.5.1 shows an energy level diagram of the states observed by Rowe **[5]** along with the vibrational assignments of Lüttschwager *et al.* **[36]** and a representative set of calculated state energies from the recent work of Schröder and Meyer **[71]**. All three groups are in agreement that there are a total of 8 states in the region shown, with two out-of-plane states near 400 cm^{-1} and four states (two in-plane and two out-of-plane)

between 150 and 350 cm^{-1}. This suggests a one-to-one correspondence between states from each group. The ground state pairs clearly match across each group, and it seems likely that the two out-of-plane states near 400 cm^{-1} are also equivalent. However, it is unclear how the states in the intermediate range correspond across the microwave, IR/Raman and theoretical data.

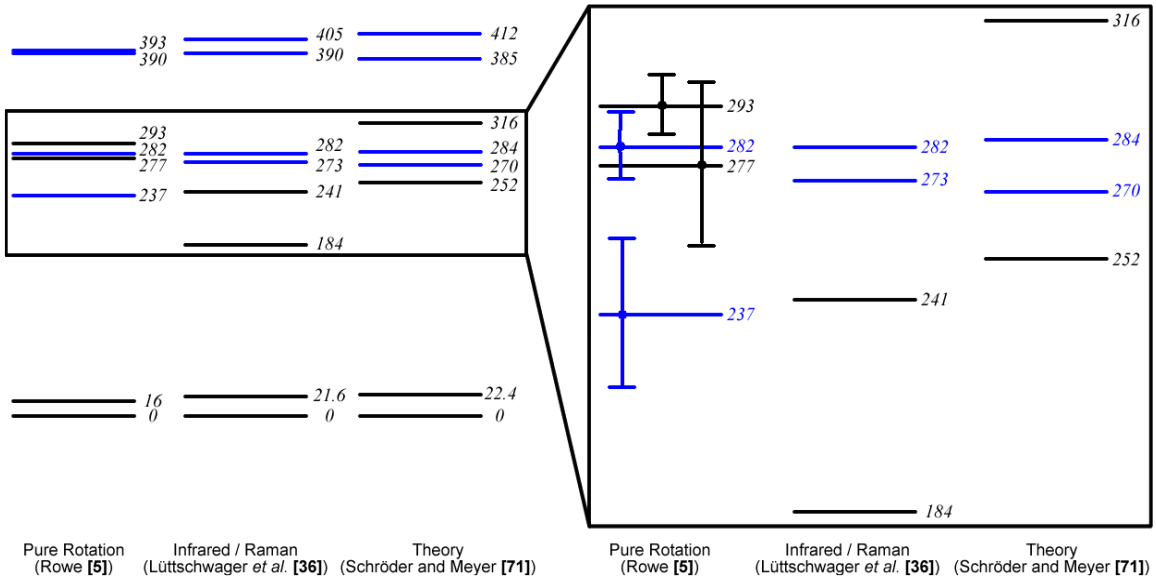

*Figure 4.5.1: Energy level diagram showing the 8 vibrational states observed by Rowe **[5]** along with the assigned states from Ref. **[36]** and calculated frequencies from Ref. **[71]**. Black and blue indicate in-plane and out-of-plane vibrations, respectively.*

4.6 - The 220 and 241 cm^{-1} Bands

Ground state combination difference comparisons using R and P lines from the 220 and 241 cm^{-1} bands confirm the assignments made by Lüttschwager *et al.* **[36]** that they correspond to transitions from each ground state component to a single state at 241 cm^{-1}. The observed rotational transitions also confirm that the 220 cm^{-1} band is a-type and the 241 cm^{-1} band is b-type, which indicates that the 241 cm^{-1} state is the 1^0 of a vibrational mode with A_1 symmetry or the 1^1 of a mode with B_2 symmetry (see figure 2.6.1). In either case, the vibrational mode is in-plane. As will be discussed in a later

section, the other tunnelling component of this state is likely higher in energy (and thus does not correspond to the 184 cm^{-1} band), suggesting that the mode is of A_1 symmetry.

A total of 2604 lines from the 220 cm^{-1} band and 1854 lines from the 241 cm^{-1} band were assigned, covering a wide range of J-K_a space. All of these are R and P lines since the 220 cm^{-1} Q-branch could not be resolved. Nuclear spin weightings were used in making assignments within the regions of intermediate K_a where the asymmetry doublets are split. These infrared lines could be fitted together with the pure rotational R237 lines from Ref. **[5]** (with the exception of two lines which were removed as likely misassignments) giving residuals that were within the experimental uncertainty of both sets of data. This provides confirmation that the R237 state observed by Rowe is the 241 cm^{-1} state observed here, and the 4 cm^{-1} difference is within Rowe's reported uncertainty in the frequency of R237 (table 4.5.1). Although the inertial defect reported by Rowe (and verified here - see table 4.9.2) is negative which indicates non-planarity, the infrared data provide strong evidence that the motion corresponding to this mode is in-plane. Fitting of the 241 cm^{-1} state was done without the use of coupling terms connecting it to the other tunnelling component. The success of the fitting even without these terms suggests that the splitting is greater than in the ground state or 390/405 cm^{-1} pairs for which coupling terms were required.

4.7 - The 384 and 390 cm^{-1} Bands

A comparison of R/P combination differences from the 384 and 390 cm^{-1} bands also supports the assignments of Lüttschwager *et al.* **[36]**, confirming that they are c-type

$0^0 \rightarrow 1^0$ and $0^1 \rightarrow 1^1$ transitions of an out-of-plane vibration. The vibrational selection rules of figure 2.6.1 show that the vibrational mode must be of B_1 symmetry.

A total of 1613 lines from the 384 cm^{-1} band and 1596 lines from the 405 cm^{-1} band were assigned, all of which are R and P branch lines. Fitting these states required the use of the full three-term interaction Hamiltonian described in section 2.10 since the splitting of about 15 cm^{-1} is similar in magnitude to the ground state splitting of about 21 cm^{-1}. The R390 and R393 pure rotation lines from Ref. **[5]** were included in the fitting for the 405 and 390 cm^{-1} states, respectively, giving residuals within experimental error for both infrared and microwave lines. This demonstrates that R390 is the 405 cm^{-1} state and R393 is the 390 cm^{-1} state which is well within the uncertainty in the frequency reported by Rowe (table 4.5.1). This is in agreement with Rowe's assessment based on the inertial defect that these vibrations are primarily out-of-plane.

4.8 - The 282 and 252 cm^{-1} Bands

The 282 and 252 cm^{-1} bands were assigned by Lüttschwager *et al.* **[36]** as the $0^0 \rightarrow 1^1$ and $0^1 \rightarrow 1^0$ transitions of an out-of-plane C_3-H_9 vibration (which they call γC_cH), with states at 273 and 282 cm^{-1}. Some P and R branch lines were identified for the 282 cm^{-1} band using a Loomis-Wood plot as shown in figure 4.8.1. Lower state R/P combination differences were calculated using these lines and the result was a match to the 0^0 ground state in agreement with the previous assignment. The transitions that were observed also confirmed that the band is c-type and that the branches that were identified correspond to sequences of K_c being 0 and 1. With only a small number of lines

corresponding to a narrow range of K_c values, it was not possible to obtain a proper fitting of the state.

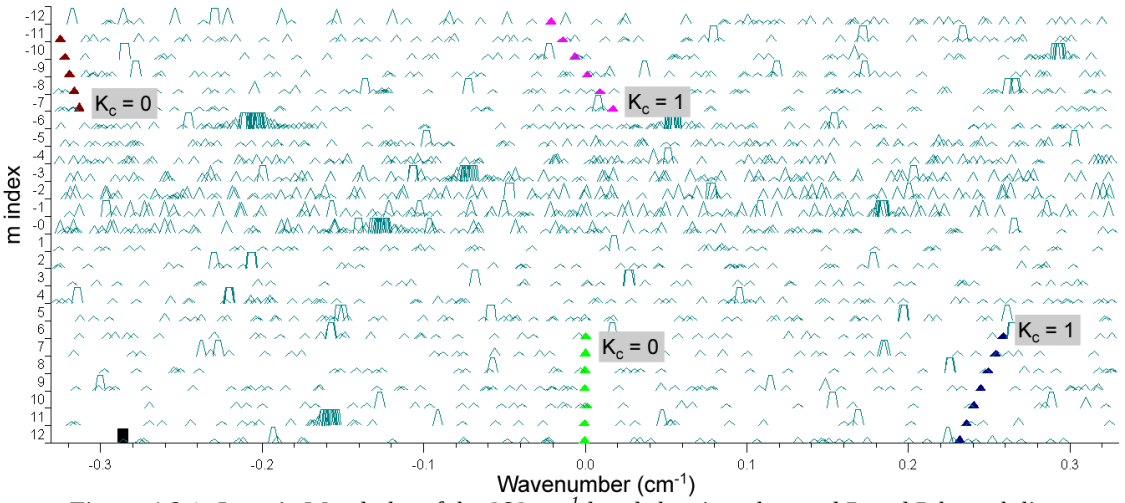

Figure 4.8.1: Loomis-Wood plot of the 282 cm^{-1} band showing observed R and P branch lines. The first line shown in each branch is as follows - P branch, K_c = 0: 277.498 cm^{-1}, K_c = 1: 277.829 cm^{-1} - R branch, K_c = 0: 286.318 cm^{-1}, K_c = 1: 286.577 cm^{-1}.

Of the low-frequency states observed by Rowe, the 282 cm^{-1} state was thought to likely correspond to one of R277, R282 or R293 since the others had been conclusively identified. Due to the large uncertainties in Rowe's calculations of their frequencies, the matching could not be done on the basis of this alone. Having determined that the 282 cm^{-1} band is c-type and originates from the 0^0 state, it was possible to simulate (using PGOPHER **[112]**) the three possible spectra corresponding to each of the remaining states observed by Rowe. Figure 4.8.2 shows the Q-branch region of the 282 cm^{-1} band with simulations of c-type bands connecting the 0^0 state to each of R277, R282 and R293. From these simulations, it can be seen that only the R282 upper state produces a spectrum with a structure resembling the actual measurement. Furthermore, the individual line positions in the low-J region of the Q-branch are in excellent agreement with the simulation (figure 4.8.3) and some assignments can even be made by inspection. This provides convincing evidence that the 282 cm^{-1} band is R282.

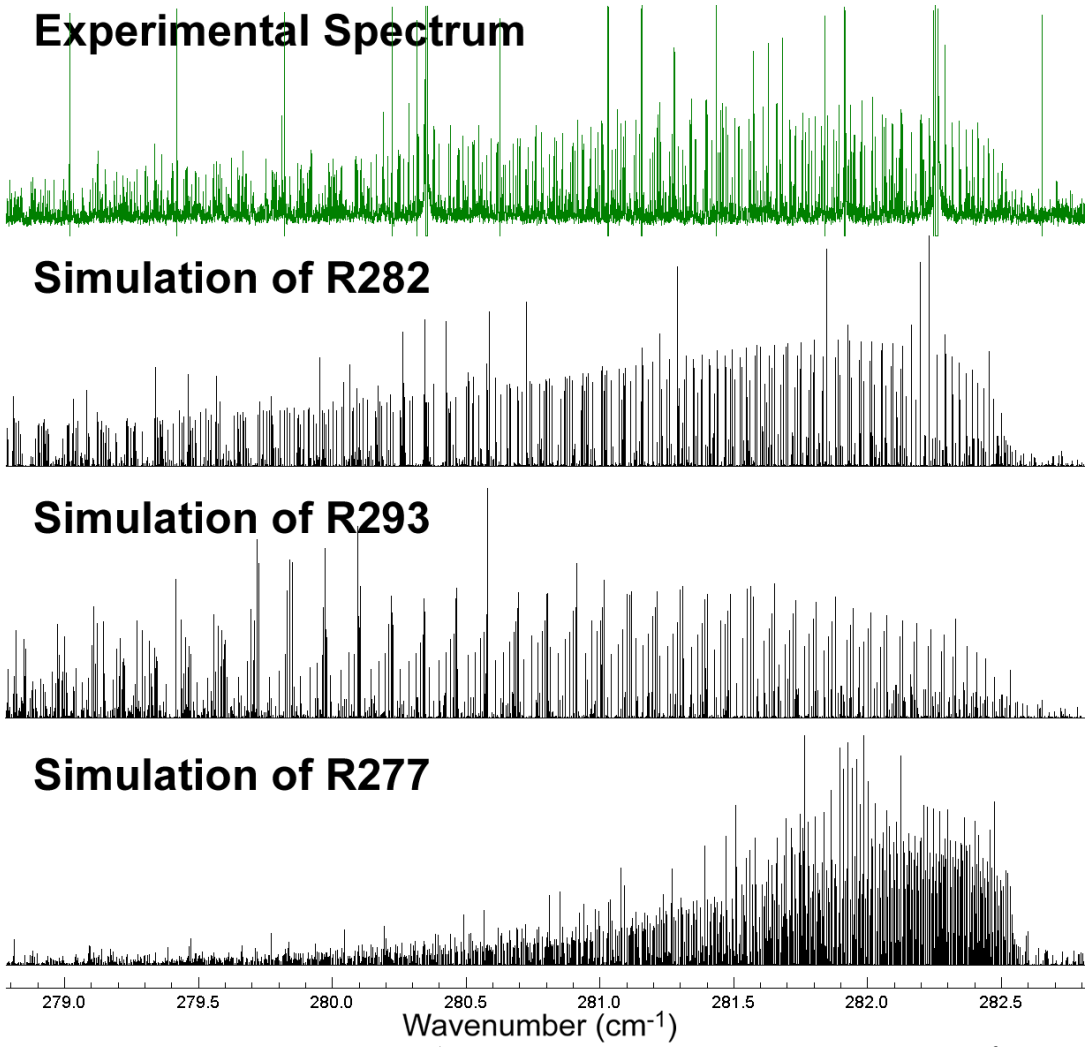

Figure 4.8.2: The Q-branch of the 282 cm^{-1} band (top) with simulations of c-type bands from 0^0 to each of R282, R293 and R277 from Ref. ***[5]****. The best agreement is for the simulation of R282.*

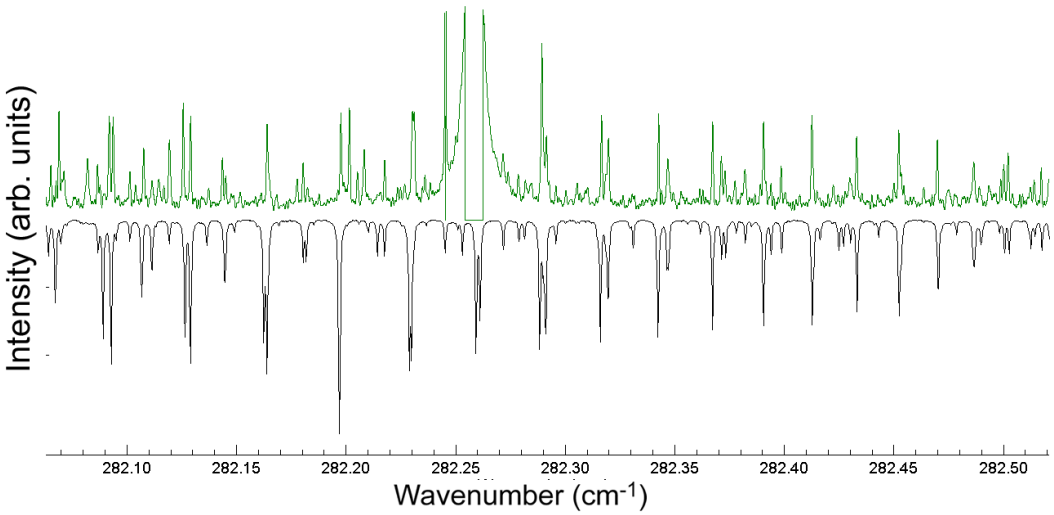

Figure 4.8.3: The low-J region of the 282 cm^{-1} band Q-branch showing the agreement between the actual spectrum (above) and a simulation (below) using Rowe's R282 line list ***[5]*** *as described in the text.*

If the assignment of the 252 cm^{-1} band from Ref. **[36]** is correct, then it should be a c-type band connecting 0^1 to the other tunnelling component of the 282 cm^{-1} state at 273 cm^{-1}. In that case, it would likely correspond to either R277 or R293. Using the same technique as described above for the 282 cm^{-1} band, c-type simulations of bands connecting 0^1 to both of these states as well as R282 are presented in figure 4.8.4. It can be seen from this comparison that only the R277 state produces a band with a similar structure to the observed Q-branch. Both of the other simulations produce Q-branches with higher-J lines proceeding to lower frequency which is the opposite of what is observed. Simulations were also made of a-type bands from 0^1 as well as a- and c-type bands from 0^0, but none of these produced bands resembling the actual spectrum.

As with the 282 cm^{-1} band, the low-J line positions of the Q-branch match excellently when the simulation is properly aligned (figure 4.8.5) and assignments of a number of Q-branch lines have been made by matching the experimental and simulated line positions.

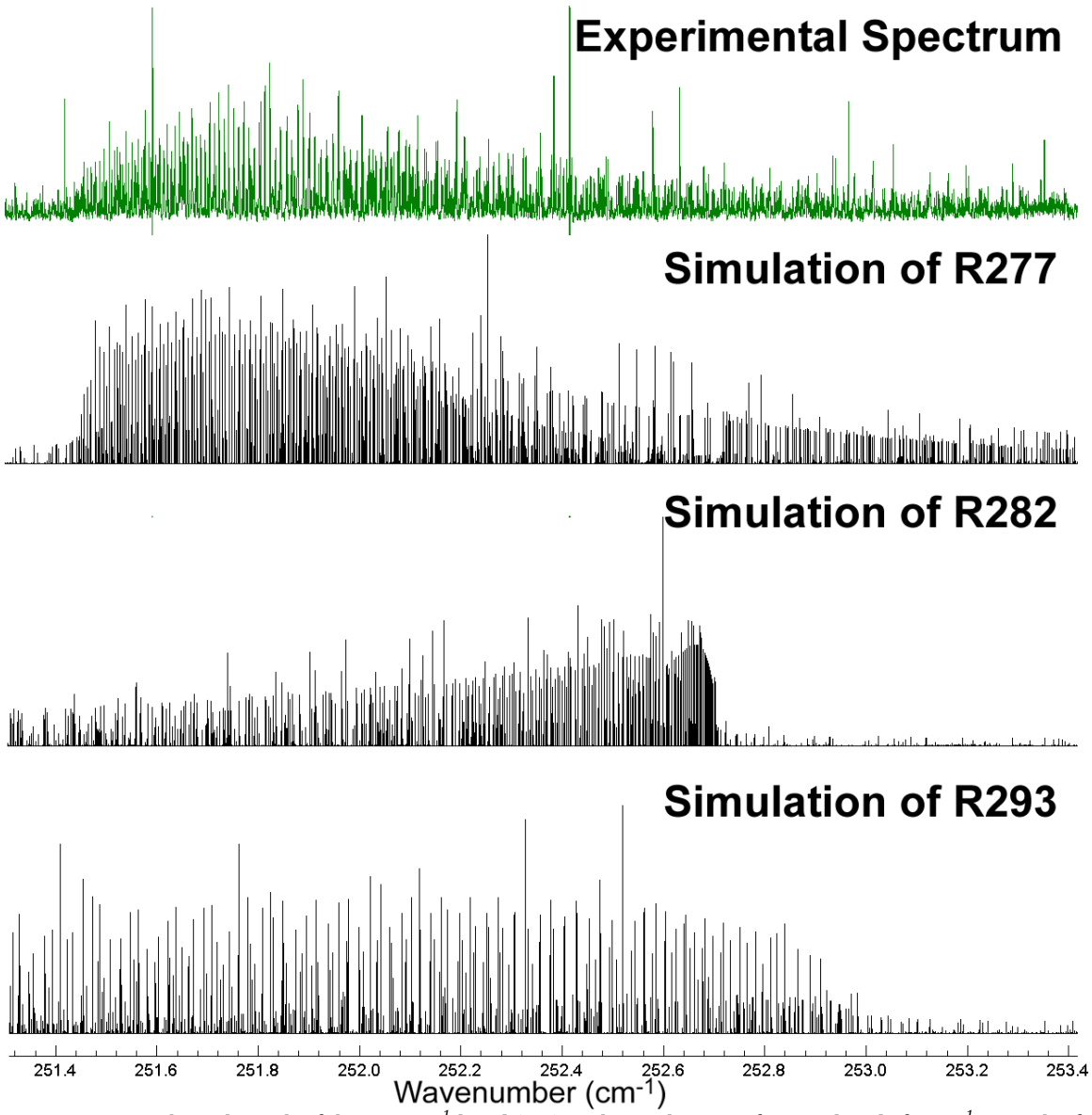

Figure 4.8.4: The Q-branch of the 252 cm^{-1} band (top) with simulations of c-type bands from 0^1 to each of R282, R277 and R293 from Ref. ***[5]****. The best agreement is for the simulation of R277.*

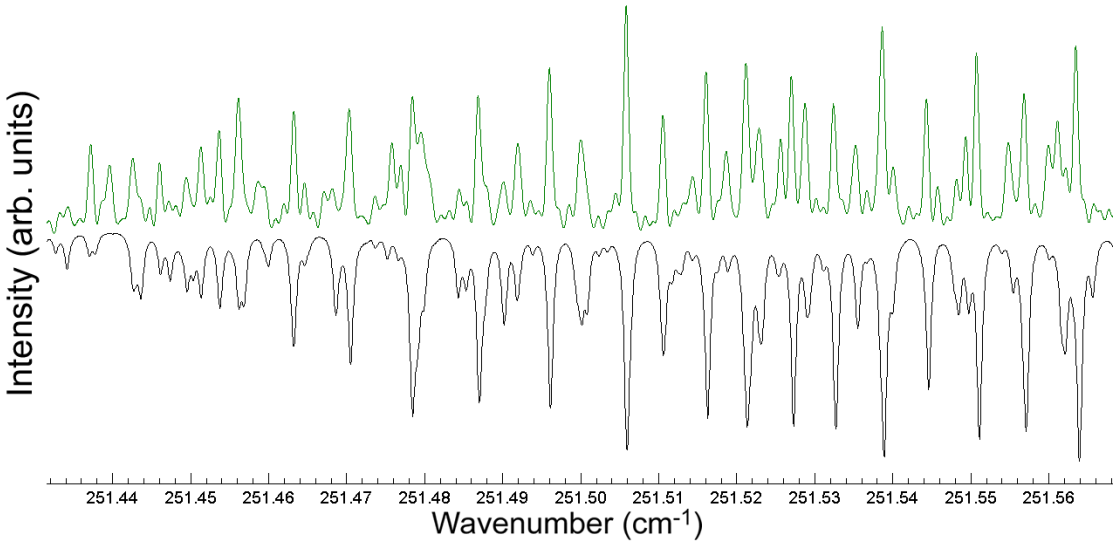

Figure 4.8.5: The low-J region of the 252 cm^{-1} band Q-branch showing the agreement between the actual spectrum (*above*) *and a simulation (below) using Rowe's R277 line list* ***[5]*** *as described in the text.*

4.9 - Global Fitting of the 0^0, 0^1, 241 cm^{-1}, 390 cm^{-1} and 405 cm^{-1} States

The final fitting of the ground state tunnelling pair, the 241 cm^{-1} state and the 390/405 cm^{-1} tunnelling pair was done as a combined multi-state fit. For each of these states the Hamiltonian model given in sections 2.9 and 2.10 was used, although some of the parameters were set to zero in cases where they were not well-determined by the fit. The ground state pair and the 390/405 cm^{-1} pair were both coupled using the full interaction Hamiltonian in section 2.10.

A summary of the various groups of lines and combination differences that were used in the fitting is given in table 4.9.1. Full lists of these lines and combination differences are provided as supplementary material (see appendix B). The included subset of ground state pure rotation and tunnelling rotation lines from the work of Wilson *et al.* **[1-4]**, Firth *et al.* **[25]** and Baba *et al.* **[26]** was determined to be consistent with the infrared data as described in section 4.4. A large number of infrared R and P lines from the 220, 241, 384 and 390 cm^{-1} bands were used, as well as the smaller but more precise

microwave line list from Rowe **[5]** for the 241, 390 and 405 cm^{-1} states. Finally, lower state R/P combination differences calculated using assigned lines from the bands connecting to states not included in the fitting (the 282, 512, 527, 766, 964 and 999 cm^{-1} states) were also used. The constants obtained for all five states are presented in table 4.9.2 along with values of the inertial defect.

States	Description	Number of Points	Uncertainty (10^{-6} cm^{-1} : MHz)
0^0	- Pure rotation **[2]**	73 (80)	1.7 : 0.05
0^1	- Pure rotation **[2]**	71 (77)	1.7 : 0.05
0^0	- Pure rotation **[4]**	12 (14)	6.7 : 0.2
0^1	- Pure rotation **[4]**	8 (12)	6.7 : 0.2
0^0	- Pure rotation **[25]**	63 (96)	10 : 0.3
0^1	- Pure rotation **[25]**	63 (90)	10 : 0.3
0^0	- Pure rotation **[26]**	26 (26)	1.4 : 0.043
0^1	- Pure rotation **[26]**	32 (32)	1.4 : 0.043
$0^0 \rightarrow 0^1$	- Tunnelling rotation **[26]**	36 (36)	1.4 : 0.043
241 cm^{-1}	- Pure rotation **[5]**	26 (28)	1.7 : 0.05
390 cm^{-1}	- Pure rotation **[5]**	31 (31)	1.7 : 0.05
405 cm^{-1}	- Pure rotation **[5]**	28 (28)	1.7 : 0.05
$0^1 \rightarrow$ 241 cm^{-1}	- Infrared lines, 220 cm^{-1} band	2604	200 : 6
$0^0 \rightarrow$ 241 cm^{-1}	- Infrared lines, 241 cm^{-1} band	1854	200 : 6
$0^1 \rightarrow$ 405 cm^{-1}	- Infrared lines, 384 cm^{-1} band	1613	200 : 6
$0^0 \rightarrow$ 390 cm^{-1}	- Infrared lines, 390 cm^{-1} band	1596	200 : 6
0^0	- Infrared CDs, 282 cm^{-1} band	54	280 : 8.5
0^1	- Infrared CDs, 506 cm^{-1} band	100	280 : 8.5
0^0	- Infrared CDs, 512 cm^{-1} band	350	280 : 8.5
0^0	- Infrared CDs, 766 cm^{-1} band	267	280 : 8.5
0^1	- Infrared CDs, 964 cm^{-1} band	111	280 : 8.5
0^0	- Infrared CDs, 999 cm^{-1} band	131	280 : 8.5

Table 4.9.1: Summary of data used in the multi-state fitting of the ground state tunnelling pair, the 241 cm^{-1} state and the 390/405 cm^{-1} tunnelling pair. For pure rotation and tunnelling rotation lines obtained from other sources, the number total number of lines from that source is given in parentheses. Uncertainty for the combination differences (CDs) were calculated using standard error propagation. Full line and combination difference lists are available (see appendix B).

	0^0	0^1	241	390	405
Origin (cm^{-1})		21.58313974(60)	241.0566119(75)	390.3009228(72)	404.770168(11)
A (cm^{-1})	0.328021705(19)	0.328429130(21)	0.328688600(48)	0.327745097(32)	0.327985762(49)
B (cm^{-1})	0.173870920(16)	0.172076495(18)	0.172567011(48)	0.173612366(16)	0.172433803(39)
C (cm^{-1})	0.113558211(16)	0.112852336(16)	0.113236969(36)	0.113540979(13)	0.113094568(39)
ΔK (10^{-6} cm^{-1})	0.263490(91)	0.15427(11)	0.09477(23)	0.24186(67)	0.16567(79)
ΔJK (10^{-6} cm^{-1})	-0.12851(10)	-0.07140(10)	0.01965(19)	-0.11335(66)	-0.07102(81)
ΔJ (10^{-6} cm^{-1})	0.0910848(92)	0.087027(10)	0.092564(46)	0.088805(53)	0.086279(74)
δK (10^{-6} cm^{-1})	0.059719(38)	0.018369(50)	-0.008244(69)	0.05163(31)	0.02359(35)
δJ (10^{-6} cm^{-1})	-0.0274796(86)	-0.0298190(95)	-0.029790(14)	-0.027372(25)	-0.028845(36)
ΦK (10^{-12} cm^{-1})		-1.186(95)	2.25(22)		
ΦKJ (10^{-12} cm^{-1})		1.83(12)	8.37(37)		
ΦJK (10^{-12} cm^{-1})		-0.410(42)	-11.65(18)		
ΦJ (10^{-12} cm^{-1})			-0.193(16)	0.646(18)	
φK (10^{-12} cm^{-1})		-0.745(36)	1.292(93)		
φJK (10^{-12} cm^{-1})		0.218(18)	4.681(80)		
φJ (10^{-12} cm^{-1})	-0.0229(24)	-0.0686(31)			
ID (10^6 amu Å^2)	4.04932(91)	3.30831(92)	-4.1298(22)	-2.47387(79)	-4.0477(22)
F (10^{-3} cm^{-1})	1.64209(27)			1.3718(17)	
F_J (10^{-8} cm^{-1})	-2.6322(85)			-3.69(11)	
F_B (10^{-8} cm^{-1})	5.0786(82)			7.49(11)	

Table 4.9.2: Vibrational frequency and rotational parameters for the ground state tunnelling pair, 241 cm^{-1} state and 390/405 cm^{-1} tunnelling pair. ID is the inertial defect. Fitting was done using the Watson A-reduced Hamiltonian in the I^r representation. Additional interaction parameters F, F_J and F_B are defined in section 2.10. Distortion parameters not given for a state were not be well-determined and were fixed to zero.

4.10 - The 184 cm^{-1} Band

The band at 184 cm^{-1} (figure 4.10.1) was assigned by Lüttschwager *et al.* **[36]** according to one of their assignment schemes as the $0^0 \rightarrow 1^0$ transition of the νO···O ring opening/closing mode. This would make it the second a-type band associated with this mode along with the 220 cm^{-1} band. The b-type $0^1 \rightarrow 1^0$ band would then occur at 163 cm^{-1}, but this band has not been seen in any earlier studies or in this work, although the other b-type band at 241 cm^{-1} was seen.

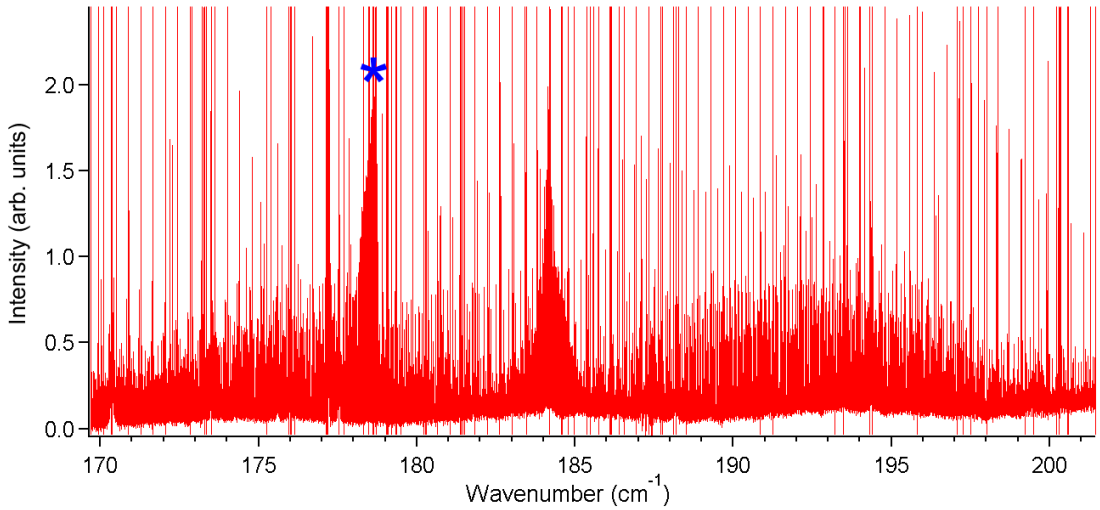

Figure 4.10.1: The 184 cm^{-1} band. The feature indicated by an asterisk is an HNCS impurity.

If the 184 cm^{-1} band originates from the 0^0 or 0^1 state, then the upper state would have to be at 184 cm^{-1} or 205 cm^{-1}. Since Rowe was able to measure the pure rotational spectrum of states ranging from 0 to 405 cm^{-1} in energy, any state near 184 cm^{-1} would have been sufficiently populated for it to be seen in his experiment. The rotational structure of the molecule in this state is not likely to be so distorted that it would have been unrecognizable to Rowe's analysis. Furthermore, the intensity of the pure rotational spectrum is dependent on the permanent electric dipole moment of the molecule which should not change much between states, so there does not seem to be any reason why this spectrum would have been anomalously weak.

If a state at 184 cm^{-1} was observed by Rowe the most likely candidate would be necessarily R293, since every other state that he reported has been convincingly assigned to a different energy on the basis of the arguments in the preceding sections. It does not seem likely that R293 is actually located at 184 cm^{-1} since Rowe's relative intensity calculation for this state has a reported uncertainty of only 8 cm^{-1} compared to the 109 cm^{-1} difference in energy. The possibility that the upper state of the 184 cm^{-1} band corresponds to R277 or R282 is also unlikely for the same reason, in addition to the above arguments for their location being elsewhere.

Using a Loomis-Wood plot, some branches of the 184 cm^{-1} band were able to be identified (figure 4.10.2). The structure of these branches is similar to that of other malonaldehyde a-type bands such as the 220 cm^{-1} band, and likely correspond to lines of low K_a. Upper and lower state combination differences were calculated using likely combinations of R and P lines, and these were compared to all other characterized states of malonaldehyde with no successful matches.

Based on the inability to match lower state combination differences and the fact that no state near 184 cm^{-1} was observed by Rowe, it seems very unlikely that the 184 cm^{-1} band is a fundamental of malonaldehyde. The line spacing and structure of the band indicate that it does conceivably belong to malonaldehyde. If this is the case, it must then be a hot band originating from an exited state that is relatively low in energy (below about 500 cm^{-1}) since it was observed under the experimental conditions of this work and Rowe's experiment as well as others. An examination of the low frequency region reveals that there is no pair of known states that are separated by 184 cm^{-1}. This leaves only states for which the energy is not known such as R293 or possibly the 0^2 or 0^3 excited

tunnelling states as possible explanations for this transition if it is associated with malonaldehyde.

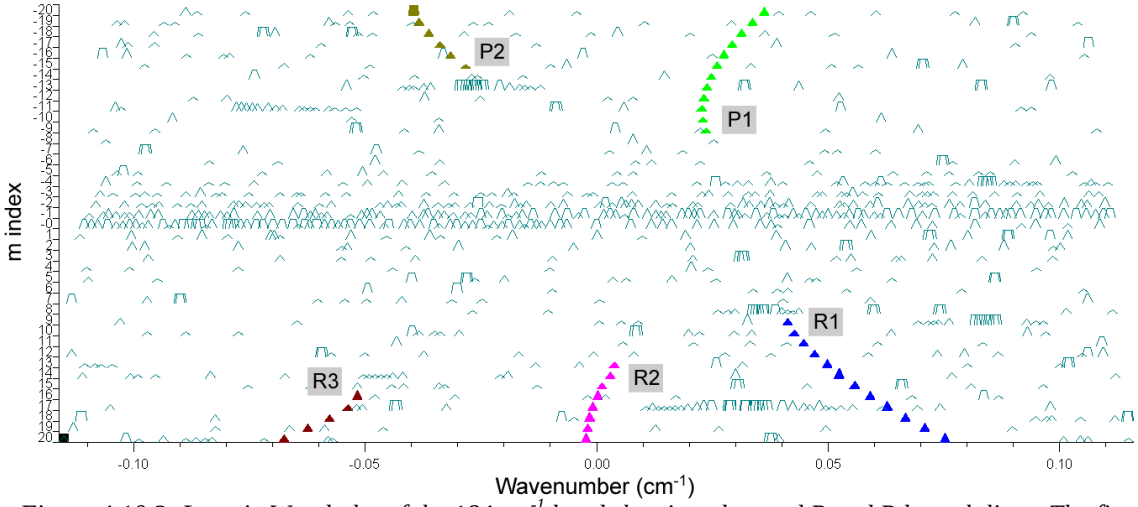

Figure 4.10.2: Loomis-Wood plot of the 184 cm^{-1} band showing observed R and P branch lines. The first line shown in each branch is as follows - P1: 182.305 cm^{-1}, P2: 180.955 cm^{-1}, R1: 186.347 cm^{-1}, R2: 187.230 cm^{-1}, R3: 187.871 cm^{-1}.

4.11 - The Identity of R293

If the 184 cm^{-1} state is not a fundamental, then it can not be the other tunnelling component of the 241 cm^{-1} state as was claimed by Lüttschwager *et al.* **[36]**. Since all of the low-frequency states should have been observed in Rowe's experiment, the remaining R293 state is almost certainly the 1^1 component of the 241 cm^{-1} mode. There is also the possibility that the 1^1 state is high enough in frequency that it was not populated in Rowe's work (as, for example, in the alternative assignment from Ref. **[36]**), although this is unlikely both due to the very large splitting that would be necessary and because there would be no other good explanation for the R293 state.

The problem with this proposed assignment is that Rowe's calculation for the frequency of R293 has an uncertainty of 8 cm^{-1}, and no other experiment has detected any state near this region (excluding the 282 cm^{-1} and 273 cm^{-1} states which are already

accounted for). If this state is the other tunnelling component of the 241 cm^{-1} state then there should be an a-type band to it from the 0^0 ground state, and this band should be visible in the spectrum as is the 220 cm^{-1} band. Although no features exist in the spectrum at 293 cm^{-1} (figure 4.11.1) that seem likely to be this transition, there is a feature that has yet to be identified at 269 cm^{-1}. Simulation of an a-type band from 0^0 to R293 with its origin at 269 cm^{-1}, along with simulations of the 282 and 252 cm^{-1} bands on either side, replicates the contour of the spectrum in this region fairly well (figure 4.11.2). Based on this, it seems possible that this could be the 0^0 to R293 transition. However, this would place R293 well outside the 8 cm^{-1} uncertainty range stated by Rowe. Additionally, there is no clear match between the line positions from this simulation to the observed spectrum as was the case with the 282 and 252 cm^{-1} bands.

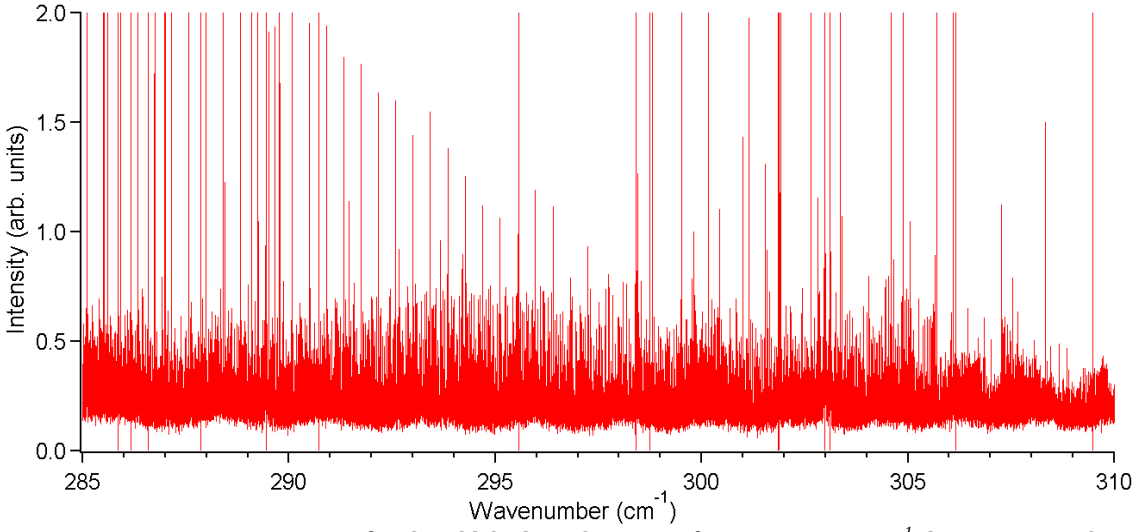

Figure 4.11.1: FTIR spectrum of malonaldehyde in the region from 285 to 310 cm^{-1} demonstrating that there are no likely vibrational bands near 293 cm^{-1}. The densely spaced lines in this region are the R-branch lines of the 282 cm^{-1} band.

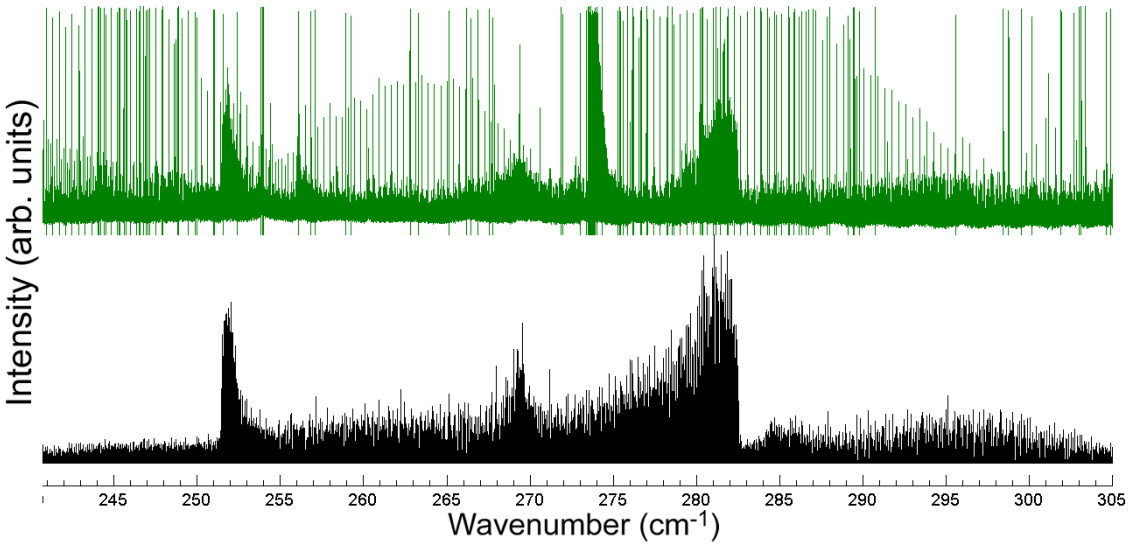

Figure 4.11.2: Simulation of an a-type band from 0^0 to R293 ***[5]*** *with its origin at 296 cm^{-1} (below) compared to the spectrum (above). The 252 and 282 cm^{-1} bands are also included in the simulation. The feature near 274 cm^{-1} is an HNCS impurity.*

Chapter 5

Theoretical Modeling of Malonaldehyde

5.1 - Describing Proton Transfer as a Large-Amplitude Motion

Although the standard Hamiltonian used in the preceding chapter is capable of describing the spectrum of malonaldehyde mathematically, it does not account for the large-amplitude tunnelling motion in a physically meaningful way. One of the goals of this project was a treatment of malonaldehyde using the generalized semi-rigid bender (GSRB) Hamiltonian **[101]** which allows for a single large-amplitude vibration (such as proton tunnelling in malonaldehyde) and can calculate the state energies corresponding to the rotational and large-amplitude degrees of freedom. Although this goal could not be completed during this thesis project, most of the required work has been done in preparation for use of the GSRB. This involved describing the proton tunnelling path, defining a coordinate for the tunnelling motion (called ρ) and determining the behavior of the geometrical parameters (bond lengths and angles) as this coordinate is varied. The GSRB does not account directly for the small-amplitude motions, instead allowing them to relax to equilibrium at each point along the large-amplitude coordinate. As a result, the large-amplitude motion is described as following the minimum energy path (MEP).

A set of 15 independent geometrical parameters, 8 bond lengths (B_1 to B_8) and 7 in-plane angles (A_1 to A_7), were used to describe the relative positions of the nuclei in the molecule and these are given in table 5.1.1 (with nuclear numbering corresponding to that of earlier figures such as figure 1.1.1). Malonaldehyde is known to be planar, so the six dihedral angles representing out-of-plane configurations have been fixed to either 0° or 180° to maintain planarity. These 15 parameters then account for the 15 vibrational

degrees of freedom for planar malonaldehyde and uniquely specify its configuration in a rotating center-of-mass reference frame.

Parameter	Definition	Parameter	Definition
B_1	C_3-H_9	A_1	O_5-C_3-H_9
B_2	C_3-O_5	A_2	C_2-C_3-O_5
B_3	C_2-C_3	A_3	C_3-C_2-H_8
B_4	C_2-H_8	A_4	C_1-C_2-C_3
B_5	C_1-C_2	A_5	C_2-C_1-H_7
B_6	C_1-H_7	A_6	C_1-O_5-O_4
B_7 (rOO)	O_4-O_5	A_7	C_1-O_4-H_6
B_8 (rOH)	O_4-H_6		

Table 5.1.1: Geometrical parameters used to describe planar malonaldehyde. B parameters are distances and A parameters are angles.

Two coordinates were identified as being most closely connected to the proton tunnelling motion. These are the O_4-H_6 distance (representing the movement of the proton from one oxygen atom to the other) and the O_4-O_5 distance (the opening and closing of the molecular frame). These coordinates will hereafter be referred to respectively as rOH and rOO. A set of *ab initio* geometry optimizations at the DFT-B3LYP level of theory using a 6-31++G(2df,p) basis set were performed by F. Ito **[115]** using the Gaussian 09 software package **[116]**. These calculations cover a grid of points which have a range of rOH from 0.86 to 1.22 Å and rOO from 2.16 to 3.76 Å, each in intervals of 0.02 Å (although not all rOO values within this range are included for a given rOH). Because the potential energy surface is symmetric (both equilibria are identical) calculations were only made for one side of the transition state. The values of rOH and rOO and the corresponding energies for each point form a two-dimensional potential energy surface for proton transfer.

5.2 - Finding the Minimum Energy Path

The code that was used to perform the calculations described in this section and the next is provided in appendix A. An initial calculation of the MEP was done by separating the two-dimensional *ab initio* surface into one-dimensional potential energy 'slices' each corresponding to a single value of either rOO (giving a potential energy curve along rOH) or rOH (giving a potential energy curve along rOO). Each of these slices could be fitted to a potential energy function of the form:

$$V(r) = V_e + a_2(r - r_e)^2 + a_3(r - r_e)^3 + \ldots \quad (5.1)$$

where r is either rOH or rOO, and V_e, r_e and the a_n are the parameters of the fit. Each slice was fitted to a function of order 6 (up to the a_6 term) and the highest order term was iteratively removed if the fit parameters were not all well-determined (if the uncertainty was greater than the parameter), down to a lowest order of 2. For each set of slices (of common rOH or rOO), the minima of the potential energy curves (r_e and V_e) combined with the common rOO or rOH value of each slice gives an estimate for the MEP. Both of these MEP estimates, one from the rOH-fixed calculations and one from the rOO-fixed calculations, are shown on the potential energy surface in figure 5.2.1.

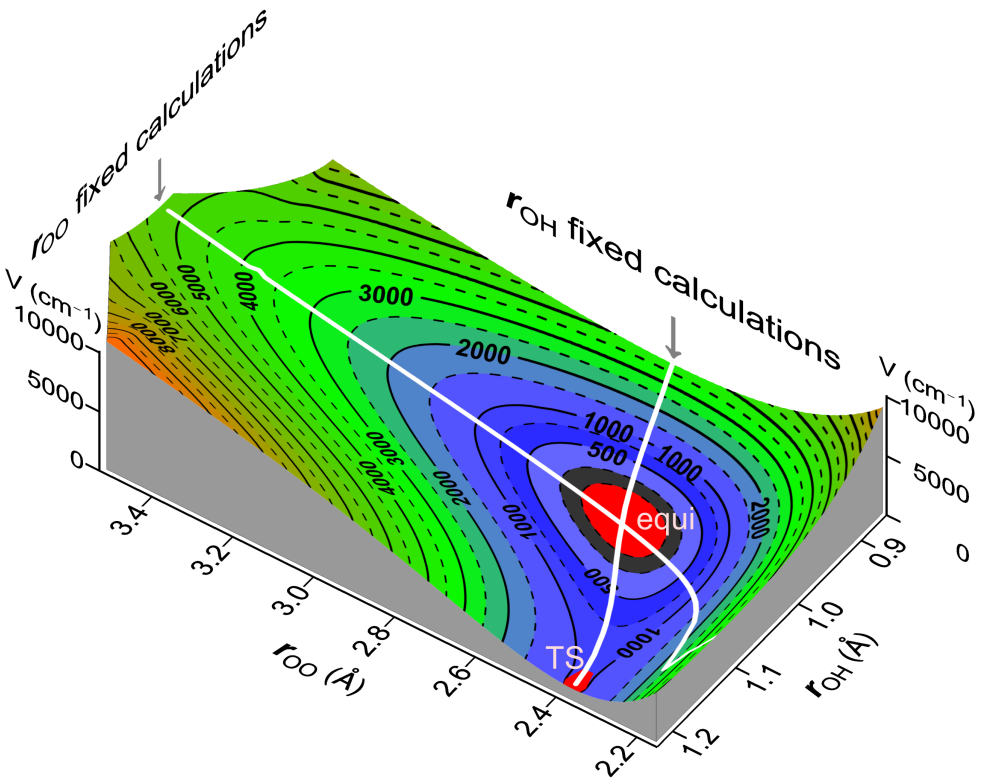

Figure 5.2.1: The ab initio *potential energy surface* ***[115]*** *showing the results of the rOH- and rOO-fixed calculations of the malonaldehyde MEP. TS and equi indicate the transition state and equilibrium state configurations.* (*Figure courtesy of Dr. S. Ross*)

It is clear from figure 5.2.1 that neither of these calculations result in a good estimate of the MEP across the entire surface. Instead, the rOO-fixed calculations are more reliable when the MEP is perpendicular to the rOO-fixed slices and the rOH-fixed calculations are more reliable when the MEP is perpendicular to the rOH-fixed slices. Near the equilibrium point, the MEP is not perpendicular to either slice and neither calculation is acceptable.

The next step was to generate potential energy slices that were perpendicular to the MEP at each point along it. This process was done iteratively starting with a 'guess' MEP that was constructed by combining the rOO-fixed points for rOH less than equilibrium and the rOH-fixed points for rOH greater than equilibrium. The guess MEP was first fitted to a function of the form:

$$rOO(rOH) = \frac{a_0 + a_1 rOH}{b_0 + b_1 rOH}$$

where the a_n and b_n are fit parameters. For each point on the guess MEP, a line was constructed which was perpendicular to the function where it is nearest to that point. Wherever this line intersected with one of the previously calculated rOH or rOO slices, the energy at the intersection was calculated using the fitted functions from (5.1). The set of points along this perpendicular slice were fitted to functions of the same form as equation (5.1) but in terms of distance along this line. The minimum energy and position of this function were then used as a new MEP point which replaced the one used from the guess MEP. Once this was done for each point on the guess MEP, the resulting new MEP was used as the guess for the next iteration. This was done until the results converged, which took about 10 iterations. The resulting final MEP is shown along with the rOH-fixed and rOO-fixed paths in figure 5.2.2.

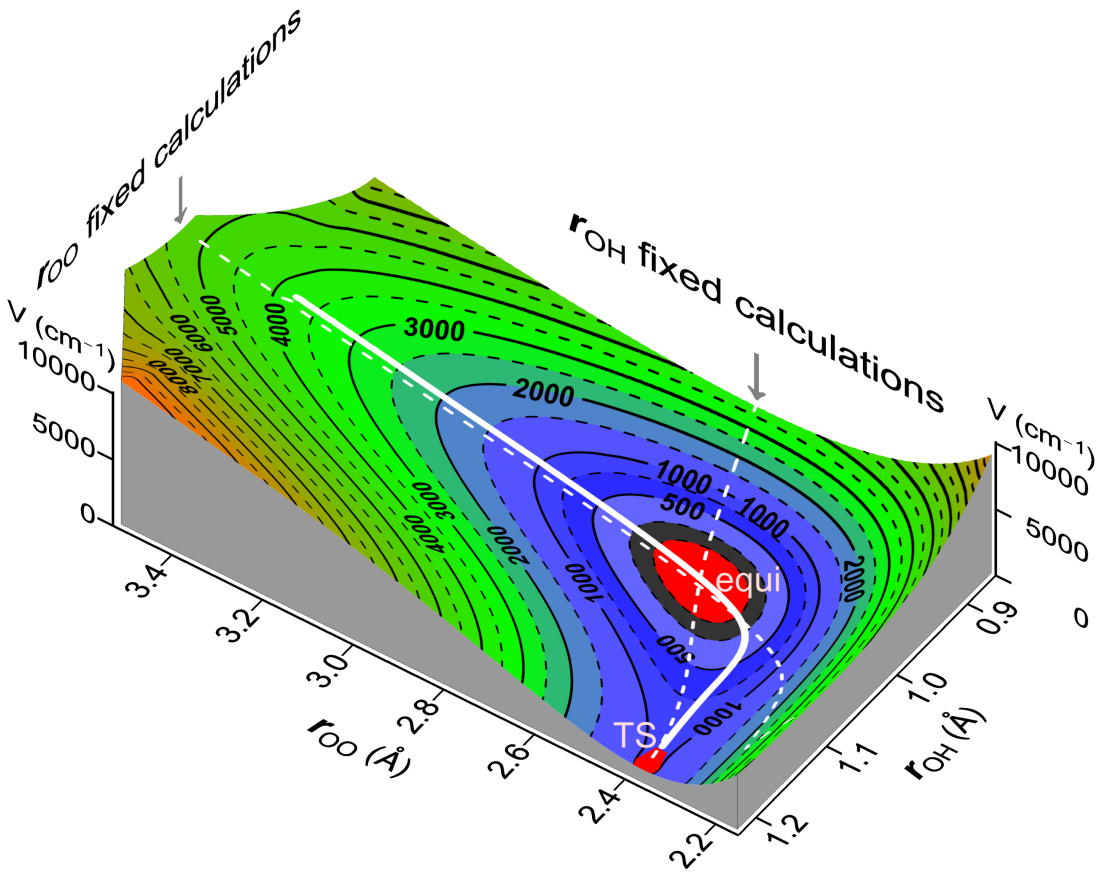

Figure 5.2.2: The ab initio *potential energy surface* ***[115]*** *showing the final MEP calculation* (*solid line*) *and the rOH- and rOO-fixed calculations* (*dashed lines*). *TS and equi indicate the transition state and equilibrium state configurations.* (*Figure courtesy of Dr. S. Ross*)

5.3 - Describing the Geometry Along the MEP

With the MEP determined, a definition for the tunnelling coordinate ρ could be found so that ρ varies smoothly and monotonically along the MEP and so that the potential energy and geometrical parameters vary smoothly with ρ. It is also required that ρ = 0 at the transition state. As of writing, the definition that is being considered is:

$$\rho(rOO, rOH) = (rOO - rOH) - (rOO_t - rOH_t)$$

where rOO_t and rOH_t are the values of rOO and rOH at the transition state (note that in appendix A ρ is defined as the difference between the C-C bonds on either side of the molecule, or B5 - B3). To determine the values of the parameters in table 5.1.1 at each

point along the MEP, a process was used that parallels the calculation of the MEP. For each parameter P, the *ab initio* points were used to construct a parameter surface of P which varies with rOH and rOO, where P is analogous to the energy in the MEP calculation. A set of rOH-fixed (a curve of P along rOO) and rOO-fixed (a curve of P along rOH) slices was then extracted. Each of these slices was fitted to a polynomial of maximum order 6, with higher-order terms being removed until the parameters were all well-determined as was done for the energy slices.

During the final iteration of the MEP calculation, at the step when the line is constructed perpendicular to the function fitted to the MEP of the previous iteration and points are obtained from the energy slices wherever the line intersects with one, the same process is performed for each of the other parameters. For each parameter slice that the perpendicular line intersects, the value of that parameter (and the position on the line) at the intersection with that slice is extracted from the polynomial fitted to that slice. Another polynomial is then fitted to these points to give the parameter P as a function of position along the line (or rOH and rOO). This function is then evaluated at the minimum of the corresponding energy slice (the new MEP point) to give the value of P at that point on the MEP.

The next step in this process is to describe the behavior of each of these parameters using a functional form that is compatible with the GSRB. As of writing, this step is currently ongoing. Once these functional forms are found, they will be used by the GSRB program to calculate the combined tunnelling-rotation state energies. It may also be possible for some functions used in the GSRB, such as the potential energy function or the MEP, to be fitted to the experimental data.

Chapter 6

Conclusions

The work presented here represents significant progress in analyzing the low-frequency (< 500 cm^{-1}) range of the far-IR spectrum of malonaldehyde. Fundamentals have been identified which correspond to all but one of the lowest six excited vibrational states measured by Rowe in 1975 **[5]** (as shown in table 6.1). Rowe's microwave observations have been of considerable assistance in assigning and fitting the infrared data, and have provided important insight into the low-frequency vibrational structure of the molecule.

The current results mostly support the assignments made recently by Lüttschwager *et al.* **[36]** except in the case of the 184 cm^{-1} band. Although Lüttschwager *et al.* tentatively assigned it as a fundamental of the νO···O mode along with the 241 cm^{-1} band as a tunnelling-split pair, the evidence shown here suggests that the 184 cm^{-1} band is not a fundamental, and that the other tunnelling component of the 241 cm^{-1} band lies elsewhere. It is likely that Rowe observed this state near 293 cm^{-1}, and if this does prove to be the case then microwave measurements and constants for it are available. Further investigation of the far-IR region with higher-quality spectra is necessary, particularly near 293 cm^{-1}, since vibrational transitions to the R293 state may be anomalously weak. The band at 184 cm^{-1} has not yet been conclusively identified and also remains as a point for further study of this system. Additionally, there are a number of overtones and combination bands that would be expected in the 400 to 600 cm^{-1} range which were not observed here.

A simultaneous five-state rotational fitting has been performed on the ground state tunnelling pair, the 241 cm^{-1} state and the 390/405 cm^{-1} tunnelling pair (see table 4.9.2). The precise energies of the 241, 390 and 405 cm^{-1} states have been determined for the first time, and the characterizations made by Rowe have been significantly expanded using infrared data. The ground state characterization presented here incorporates the measurements used in the previous work by Baba *et al.* **[26]** as well as a large range of infrared measurements and is now applicable over a much wider range of rotational J-K_a parameter space (as shown in figures 4.4.3 and 4.4.4).

Microwave (from Ref. **[5]**)		IR		
Frequency	Planarity	Frequency (present work)	Planarity (present work)	Assignment (from Ref. **[36]**)
0	In-plane	0	In-plane	Ground
16 ± 14	In-plane	21.58313974(60)	In-plane	
277 ± 22	In-plane	273	Out-of-plane	γC_cH
282 ± 9	Out-of-plane	282	Out-of-plane	
393 ± 59	Out-of-plane	390.3009228(72)	Out-of-plane	γring
390 ± 35	Out-of-plane	404.770168(11)	Out-of-plane	
237 ± 20	Out-of-plane	241.0566119(75)	In-plane	νO···O
293 ± 8	In-plane	-	In-plane	

*Table 6.1: Summary of the eight lowest vibrational states of malonaldehyde showing the correspondence between states measured by Rowe **[5]** and those measured in the infrared. The IR-determined frequency of Rowe's 293 cm^{-1} state has been left blank as it has yet to be determined and its planarity is assumed based on it likely being part of a tunnelling pair with the 241 cm^{-1} state. The vibrational assignments are those of Lüttschwager* et al. ***[36]***. *The 273 and 282 cm^{-1} states were not included in the multi-state fitting.*

The two states at 273 and 282 cm^{-1} have been identified as R277 and R282, which means that pure rotation lines and constants already exist for them. However, Rowe's description could be significantly improved by the addition of a full set of infrared assignments of the 252 (21 to 273 cm^{-1} transition) and 282 cm^{-1} bands which would cover a much wider range in J-K_a space. As of writing, only limited assignments of these bands have been made but further assigning and fitting should be possible and will be attempted in the future. There are also a number of higher-energy bands at 506, 512, 766, 964 and 999 cm^{-1} for which assignments have been made but fitting has not yet been done. In

some of these bands (in particular the 506/512 cm^{-1} bands) there are perturbations that must be accounted for before fitting can be performed.

It is also of considerable interest to investigate the far-IR spectrum of a malonaldehyde isotopologue with deuterium in the tunnelling position (either singly-substituted at H_6 or doubly-substituted at H_6 and H_8). Such species have been investigated in the microwave region **[2]** and the ground state splitting is known to be about 3 cm^{-1}. An infrared study of deuterated malonaldehyde would provide additional information about the tunnelling potential since the deuterium nucleus would occupy a lower-energy position within it. As a result of the reduced splitting, vibrational states corresponding to tunnelling pairs should also be easier to identify. If the tunnelling pair corresponding to the νO···O mode could be identified in one of these isotopologues, this information could be used to identify the corresponding levels in the regular molecule.

Much of the preliminary work has been done in preparation for modeling malonaldehyde using the Generalized Semi-Rigid Bender Hamiltonian, although this was not able to be attempted as part of this thesis project.

Appendix A

Java Code Used for the Minimum Energy Path Calculations in Chapter 5

The following code contains five Java classes which were used in the calculation of the minimum energy path:

Configuration - an object class which contains one set of geometrical parameters describing a configuration of malonaldehyde. These configurations are read in from the input and correspond to the *ab initio* results calculated by Ito **[115]** with fixed rOO and rOH.

LSFitting - contains a number of methods used for performing least squares fitting and evaluating various functions.

MalonPlot - an object class which is used to produce plots for output.

MalonSlice - reads in a set of configurations making up the *ab initio* grid, then fits each energy or geometrical parameter slice of common rOO or rOH to obtain a functional form for the slice. These functions as well as a starting guess for the MEP are then saved as output and used by MalonMEP. A sample input file is provided at the end of the code.

MalonMEP - reads in the slices and guess MEP produced by MalonSlice and iteratively improves each MEP point by finding the minimum of a slice perpendicular to the MEP at that point. The geometrical parameters are also evaluated at each of the MEP points.

To use this code, run MalonSlice to produce the rOO and rOH slices, then run MalonMEP to calculate the MEP. This code makes use of the Apache Commons Math **[117]** and JFreeChart **[118]** libraries.

A.1 - Configuration

```
import java.util.ArrayList;
import java.util.Arrays;

// Contains the geometry of each optimized malonaldehyde configuration with
// fixed R_OO (B7) and R_OH (B8)
public class Configuration {
   // names used in the input files summary1.txt - summary9.txt as provided by Dr. F. Ito [115]
   public static ArrayList<String> PARAM_INPUT_NAMES = new ArrayList<>(Arrays.asList("Eigenvalues",
         "B1", "B2", "B3", "B4", "B5", "B6", "B7", "B8",
         "A1", "A2", "A3", "A4", "A5", "A6", "A7",
         "D1", "D2", "D3", "D4", "D5", "D6"));

   // names of geometrical parameters to be used for output - B9 and A8 are additional non-independent
   // parameters
   public static ArrayList<String> PARAM_OUTPUT_NAMES = new ArrayList<>(Arrays.asList("Energy",
         "B1", "B2", "B3", "B4", "B5", "B6", "R_OO", "R_OH",
         "A1", "A2", "A3", "A4", "A5", "A6", "A7",
         "D1", "D2", "D3", "D4", "D5", "D6",
         "B9", "A8"));

   // list of parameters without R_OO and R_OH
   public static ArrayList<String> REDUCED_PARAM_NAMES = new ArrayList<>(Arrays.asList("Energy",
         "B1", "B2", "B3", "B4", "B5", "B6",
         "A1", "A2", "A3", "A4", "A5", "A6", "A7",
         "D1", "D2", "D3", "D4", "D5", "D6",
         "B9", "A8"));

   private double[] PARAMS = new double[24]; // holds parameters in order of PARAM_OUTPUT_NAMES

   public void setParam(int index, double param){
         PARAMS[index] = param;
   }

   public double getParam(int index) {
         return PARAMS[index];
   }

   public void print(){
      for(int i = 0; i < PARAMS.length; i++){
         System.out.println(PARAM_OUTPUT_NAMES.get(i) + " - " + PARAMS[i]);
      }
   }
}
```

A.2 - LSFitting

```
import org.apache.commons.math3.fitting.leastsquares.LeastSquaresBuilder;
import org.apache.commons.math3.fitting.leastsquares.LeastSquaresProblem;
import org.apache.commons.math3.fitting.leastsquares.MultivariateJacobianFunction;
import org.apache.commons.math3.linear.Array2DRowRealMatrix;
import org.apache.commons.math3.linear.ArrayRealVector;
import org.apache.commons.math3.linear.RealMatrix;
import org.apache.commons.math3.linear.RealVector;
import org.apache.commons.math3.util.Pair;

import java.io.BufferedWriter;
import java.io.IOException;
import java.util.ArrayList;
import java.util.Arrays;

// Contains code for least squares fitting and evaluation of functions
public class LSFitting {

    private BufferedWriter LOG;

    public LSFitting(BufferedWriter log){
        this.LOG = log;
    }

    // creates a least squares problem for a polynomial function
    // fit parameters are in order of a_0, a_1, a_2, ...
    // for a polynomial y = a_0 + a_1*x + a_2*x^2 ...
    // observations: list of x, y points
    // order: order of the fit
    // guess: initial parameters
    public LeastSquaresProblem makePolyLS(ArrayList<double[]> observations, int order, double[] guess){

        if (order < 0){
            log("Invalid order: " + order);
            System.exit(1);
        }

        MultivariateJacobianFunction function = new MultivariateJacobianFunction() {
            public Pair<RealVector, RealMatrix> value(RealVector point) {

                RealVector value = new ArrayRealVector(observations.size());
                RealMatrix jacobian = new Array2DRowRealMatrix(observations.size(), order+1);

                for (int i = 0; i < observations.size(); i++){
                    double modelI = polyEvaluate(observations.get(i)[0], point.toArray());
                    value.setEntry(i, modelI);

                    double[] jac = new double[order+1];
                    for (int j = 0; j <= order; j++){
                        jac[j] = Math.pow(observations.get(i)[0], j);
                    }
                    for (int j = 0; j <= order; j++) jacobian.setEntry(i,j, jac[j]);
                }
                return new Pair<>(value, jacobian);
            }
        };

        double[] target = new double[observations.size()];
        for (int j = 0; j < target.length; j++) target[j] = observations.get(j)[1];
```

```
    return new LeastSquaresBuilder().
            start(guess).
            model(function).
            target(target).
            lazyEvaluation(false).
            maxEvaluations(1000000).
            maxIterations(1000000).
            build();

}

// creates a least squares problem for a potential function
// fit parameters are in order of V_equilibrium, r_equilibrium, a_2, a_3, ...
// for a function V(r) = V_equilibrium + a_2*(r - r_equilibrium)^2 + a_3*(r - r_equilibrium)^3 ...
// observations: list of x, y points
// order: order of the fit
// guess: initial parameters
public LeastSquaresProblem makePotentialLS(ArrayList<double[]> observations, int order, double[] guess){

    if (order < 0 || order == 1){
        log("Invalid order; " + order);
        System.exit(1);
    }

    MultivariateJacobianFunction function = new MultivariateJacobianFunction() {
        public Pair<RealVector, RealMatrix> value(RealVector point) {

            RealVector value = new ArrayRealVector(observations.size());
            RealMatrix jacobian = new Array2DRowRealMatrix(observations.size(), order + 1);

            for (int i = 0; i < observations.size(); i++){
                double modelI = point.getEntry(0);
                for (int j = 2; j <= order; j++){
                    modelI += point.getEntry(j)*Math.pow(observations.get(i)[0] - point.getEntry(1), j);
                }
                value.setEntry(i,modelI);

                double[] jac = new double[order+1];
                jac[0] = 1;
                if (order != 0) jac[1] = 0;

                for (int j = 2; j <= order; j++){
                    jac[j] = Math.pow(observations.get(i)[0] - point.getEntry(1), j);
                    jac[1] += -1*j*point.getEntry(j)*Math.pow(observations.get(i)[0] - point.getEntry(1), j-1);
                }
                for (int j = 0; j <= order; j++) jacobian.setEntry(i,j, jac[j]);
            }
            return new Pair<>(value, jacobian);
        }
    };

    double[] target = new double[observations.size()];
    for (int j = 0; j < target.length; j++) target[j] = observations.get(j)[1];

    return new LeastSquaresBuilder().
            start(guess).
            model(function).
            target(target).
            lazyEvaluation(false).
            maxEvaluations(1000000).
            maxIterations(1000000).
            build();
```

```
}

// creates a least squares problem for a rational function (used to fit the MEP)
// fit parameters are in order of ao, a1, a2... an, b0, b1, b2... bn for order n
// for a function y = (a0 + a1*x + a2*x^2...) / (b0 + b1*x + b2*x^2...)
// observations: list of x, y points
// order: order of the fit
// guess: initial parameters
public LeastSquaresProblem makeMEPLS(ArrayList<double[]> observations, int order, double[] guess){

   if (order < 0){
      log("Invalid order; " + order);
      System.exit(1);
   }

   MultivariateJacobianFunction function = new MultivariateJacobianFunction() {
      public Pair<RealVector, RealMatrix> value(RealVector point) {

         RealVector value = new ArrayRealVector(observations.size());
         RealMatrix jacobian = new Array2DRowRealMatrix(observations.size(), (order + 1)*2);

         for (int i = 0; i < observations.size(); i++){
            double a = 0.0, b = 0.0;
            for (int j = 0; j <= order; j++){
               a += point.getEntry(j)*Math.pow(observations.get(i)[0], j);
               b += point.getEntry(j + order + 1)*Math.pow(observations.get(i)[0], j);
            }
            double modelI = a / b;
            value.setEntry(i,modelI);

            double[] jac = new double[2*(order+1)];
            Arrays.fill(jac, 0);

            for (int j = 0; j <= order; j++){
               jac[j] = b * Math.pow(observations.get(i)[0], j);
               jac[j + order + 1] = -1*a/(b*b) * Math.pow(observations.get(i)[0], j);
            }
            for (int j = 0; j <= 2*order + 1; j++) jacobian.setEntry(i,j, jac[j]);
         }
         return new Pair<>(value, jacobian);
      }
   };

   double[] target = new double[observations.size()];
   for (int j = 0; j < target.length; j++) target[j] = observations.get(j)[1];

   return new LeastSquaresBuilder().
         start(guess).
         model(function).
         target(target).
         lazyEvaluation(false).
         maxEvaluations(1000000).
         maxIterations(1000000).
         build();

}

// returns the point with the lowest y-value
public static double[] getMinPoint (ArrayList<double[]> points){

   double[] current = points.get(0);
```

```
        for (double[] point: points){
            if (point[1] < current[1]) current = point;
        }
        return current;
    }

    // evaluates a polynomial function at x
    // parameters are in order of a_0, a_1, a_2, ...
    // for a polynomial y = a_0 + a_1*x + a_2*x^2 ...
    public static double polyEvaluate(double x, double[] params){

        double y = 0;
        for (int i = 0; i < params.length; i++){
            y += params[i]*Math.pow(x,i);
        }
        return y;
    }

    // evaluates a potential function at r
    // parameters are in order of V_equilibrium, r_equilibrium, a_2, a_3, ...
    // for a function V(r) = V_equilibrium + a_2*(r - r_equilibrium)^2 + a_3*(r - r_equilibrium)^3 ...
    public static double potentialEvaluate(double r, double[] params){

        double v = params[0];
        for (int j = 2; j < params.length; j++){
            v += params[j]*Math.pow(r - params[1], j);
        }
        return v;
    }

    // evaluates a rational function at x
    // parameters are in order of ao, a1, a2... an, b0, b1, b2... bn for order n
    // for a function y = (a0 + a1*x + a2*x^2...) / (b0 + b1*x + b2*x^2...)
    public static double rationalEvaluate(double x, double[] params){

        double a=0.0, b=0.0;
        for (int j = 0; j <= params.length / 2 - 1; j++){
            a += params[j] * Math.pow(x, j);
            b += params[j + (params.length / 2)]*Math.pow(x, j);
        }
        return a / b;
    }

    public void log(String s){
        try{
            LOG.write(s);
            LOG.newLine();
        }catch (IOException ioe){
            System.out.println("Unable to log string: " + s + "\n" + ioe.getMessage());
            System.exit(1);
        }
    }
}
```

A.3 - MalonPlot

```
import org.apache.commons.math3.fitting.WeightedObservedPoint;
import org.jfree.chart.ChartFactory;
import org.jfree.chart.ChartUtilities;
import org.jfree.chart.JFreeChart;
import org.jfree.chart.axis.ValueAxis;
import org.jfree.chart.plot.PlotOrientation;
import org.jfree.chart.plot.XYPlot;
import org.jfree.chart.renderer.xy.XYLineAndShapeRenderer;
import org.jfree.data.xy.XYSeries;
import org.jfree.data.xy.XYSeriesCollection;

import java.awt.*;
import java.io.File;
import java.io.IOException;
import java.util.ArrayList;

// handles plotting for MalonSlice and MalonMEP
public class MalonPlot {

    // R_OH and R_OO ranges for MEP plots
    private static double[] MEP_RANGES = new double[]{0.8,1.3,2.1,3.8};

    private XYSeriesCollection DATASET = new XYSeriesCollection();
    private XYPlot PLOT;
    private JFreeChart CHART;
    private double[] RANGES = new double[4]; // [x_min, x_max, y_min, y_max]

    public MalonPlot(double[] ranges) {
        this.RANGES = ranges;
    }

    public MalonPlot(ArrayList<double[]> points) {
        RANGES = getRanges(points);
    }

    public MalonPlot addPointSeries(ArrayList<WeightedObservedPoint> pointSeries){

        final XYSeries data = new XYSeries("Points_" + DATASET.getSeries().size());
        for (WeightedObservedPoint point: pointSeries){
            data.add(point.getX(), point.getY());
        }
        DATASET.addSeries(data);

        return this;
    }

    public MalonPlot addPoint(double[] point){

        final XYSeries pointSeries = new XYSeries("Point_" + DATASET.getSeries().size());
        pointSeries.add(point[0], point[1]);
        DATASET.addSeries(pointSeries);

        return this;
    }

    public MalonPlot addPolynomial(double[] params, double pointInterval){

        final XYSeries polySeries = new XYSeries("Polynomial_" + DATASET.getSeries().size());
```

```
    double x = RANGES[0];
    while(x < RANGES[1]){
        double y = LSFitting.polyEvaluate(x, params);
        polySeries.add(x, y);
        x += pointInterval;
    }
    DATASET.addSeries(polySeries);

    return this;
}

public MalonPlot addPotential(double[] params, double pointInterval){

    final XYSeries potentialSeries = new XYSeries("Potential_" + DATASET.getSeries().size());

    double x = RANGES[0];
    while(x < RANGES[1]){
        double y = LSFitting.potentialEvaluate(x, params);
        potentialSeries.add(x, y);
        x += pointInterval;
    }
    DATASET.addSeries(potentialSeries);

    return this;
}

public MalonPlot addRational(double[] params, double pointInterval){

    final XYSeries rationalSeries = new XYSeries("Rational_" + DATASET.getSeries().size());

    double x = RANGES[0];
    while(x < RANGES[1]){
        double y = LSFitting.rationalEvaluate(x, params);
        rationalSeries.add(x, y);
        x += pointInterval;
    }
    DATASET.addSeries(rationalSeries);

    return this;
}

public static double[] getRanges(ArrayList<double[]> points){

    double[] p = points.get(0);
    double xMax = p[0], xMin = p[0];
    double yMax = p[1], yMin = p[1];

    for (double[] point: points){
        if (point[0] > xMax) xMax = point[0];
        if (point[0] < xMin) xMin = point[0];
        if (point[1] > yMax) yMax = point[1];
        if (point[1] < yMin) yMin = point[1];
    }

    double dx = xMax - xMin;
    double dy = yMax - yMin;

    xMin = xMin - 0.2*dx;
    yMin = yMin - 0.2*dy;
    xMax = xMax + 0.2*dx;
    yMax = yMax + 0.2*dy;
```

```
    return new double[]{xMin,xMax,yMin,yMax};
}

public XYLineAndShapeRenderer getRenderer(){
    return (XYLineAndShapeRenderer) PLOT.getRenderer();
}

public void createPlot(String name, String xLabel, String yLabel){

    CHART = ChartFactory.createXYLineChart(
            name,
            xLabel,
            yLabel,
            DATASET,
            PlotOrientation.VERTICAL,
            false, false, false);

    PLOT = CHART.getXYPlot();
    PLOT.setRenderer(new XYLineAndShapeRenderer(true, true));
}

public void savePlot(){

    // set range of axes
    ValueAxis domain = PLOT.getDomainAxis();
    domain.setRange(RANGES[0], RANGES[1]);
    ValueAxis range = PLOT.getRangeAxis();
    range.setRange(RANGES[2], RANGES[3]);

    PLOT.setBackgroundPaint(null); // White background

    try {
        save(CHART, CHART.getTitle().getText());
    }catch (IOException ioe){
        System.out.println(ioe.getMessage());
        ioe.printStackTrace();
    }
}

private void save(JFreeChart chart, String name) throws IOException{

    int width = 640;
    int height = 480;

    File XYChart;
    if (new File("out/" + name + ".png").exists()) {
        int c = 2;
        while (new File("out/" + name + "-" + c + ".png").exists()) c++;
        XYChart = new File("out/" + name + "-" + c + ".png");
    } else {
        XYChart = new File("out/" + name + ".png");
    }
    ChartUtilities.saveChartAsPNG(XYChart, chart, width, height);
}

public static ArrayList<WeightedObservedPoint> pointsConvert(ArrayList<double[]> points){

    ArrayList<WeightedObservedPoint> newPoints = new ArrayList<>();

    for (double[] point: points){
        newPoints.add(new WeightedObservedPoint(1,point[0],point[1]));
    }
```

```
    return newPoints;

}

public static ArrayList<double[]> backConvert(ArrayList<WeightedObservedPoint> points){

    ArrayList<double[]> newPoints = new ArrayList<>();

    for (WeightedObservedPoint point: points){
        newPoints.add(new double[]{point.getX(),point.getY()});
    }
    return newPoints;
}

public static void plotPoly(ArrayList<double[]> points, double[] params, String name, String x, String y){

    MalonPlot polyPlot = new MalonPlot(points);
    polyPlot.addPointSeries(pointsConvert(points))
            .addPolynomial(params,0.001)
            .createPlot(name, x, y);
    XYLineAndShapeRenderer renderer = polyPlot.getRenderer();
    renderer.setSeriesLinesVisible(0,false);
    renderer.setSeriesShapesFilled(0,true);
    renderer.setSeriesPaint(0, Color.RED);
    renderer.setSeriesShapesVisible(1,false);
    renderer.setSeriesPaint(1, Color.BLUE);
    polyPlot.savePlot();
}

public static void plotPotential(ArrayList<double[]> points, double[] params, String name, String x, String y){

    MalonPlot potentialPlot = new MalonPlot(points);
    potentialPlot.addPointSeries(pointsConvert(points))
            .addPotential(params,0.001)
            .createPlot(name, x, y);
    XYLineAndShapeRenderer renderer = potentialPlot.getRenderer();
    renderer.setSeriesLinesVisible(0,false);
    renderer.setSeriesShapesFilled(0,true);
    renderer.setSeriesPaint(0, Color.RED);
    renderer.setSeriesShapesVisible(1,false);
    renderer.setSeriesPaint(1, Color.BLUE);
    potentialPlot.savePlot();
}

public static void plotMEP(ArrayList<WeightedObservedPoint> points, double[] params){

    MalonPlot MEPPlot = new MalonPlot(MEP_RANGES);
    MEPPlot.addPointSeries(points)
            .addRational(params,0.01)
            .createPlot("Minimum Energy Path", "rOH", "rOO");
    XYLineAndShapeRenderer MEPRenderer = MEPPlot.getRenderer();
    MEPRenderer.setSeriesLinesVisible(0,false);
    MEPRenderer.setSeriesShapesFilled(0,true);
    MEPRenderer.setSeriesPaint(0, Color.RED);
    MEPRenderer.setSeriesShape(0,new Rectangle(2,2));
    MEPPlot.savePlot();
}

public static void plotPerpSlice(MalonPlot plot, String name, String xAxis, String yAxis){

    plot.createPlot(name, xAxis, yAxis);
    XYLineAndShapeRenderer renderer = plot.getRenderer();
```

```
        renderer.setSeriesLinesVisible(0, false);
        renderer.setSeriesShapesFilled(0, false);
        renderer.setSeriesPaint(0, Color.RED);
        renderer.setSeriesShapesVisible(1, false);
        renderer.setSeriesPaint(1, Color.BLUE);
        renderer.setSeriesLinesVisible(2, false);
        renderer.setSeriesPaint(2, Color.BLACK);
        plot.savePlot();
    }

    public static void plotParamMEP(ArrayList<WeightedObservedPoint> points, String name, String xAxis,
            String yAxis){

        MalonPlot plot = new MalonPlot(backConvert(points));
        plot.addPointSeries(points)
            .createPlot(name, xAxis, yAxis);
        XYLineAndShapeRenderer renderer = plot.getRenderer();
        renderer.setSeriesLinesVisible(0, false);
        renderer.setSeriesShapesFilled(0, false);
        renderer.setSeriesPaint(0, Color.RED);
        plot.savePlot();
    }
}
```

A.4 - MalonSlice

```
import org.apache.commons.math3.fitting.leastsquares.*;
import org.apache.commons.math3.linear.*;
import org.jfree.chart.renderer.xy.XYLineAndShapeRenderer;

import java.awt.*;
import java.io.*;
import java.text.DecimalFormat;
import java.util.ArrayList;
import java.util.Arrays;
import java.util.Collections;

/*
Calculates R_OO and R_OH slices of the potential energy and all other geometrical parameters
Outputs:
log.txt - log file
ConfigurationList_ROO-ROH-Energy.txt - list of R_OO, R_OH and Energy for each input configuration
EnergySliceMinima_*.txt (where * = R_OO and R_OH) - list of minimum energy and R_OH/R_OO for each
slice
**_*_Slices.txt (where * = R_OO and R_OH, ** = each other parameter) - list of fitted functions to each slice
   (for use in MalonMEP)
Plots of each slice, if SAVE_IMAGES is true
*/
public class MalonSlice {

   private static String FILEPATH = "src/summary"; // base name, files are summary1.txt, summary2.txt, etc.
   private static String LOGPATH = "out/";
   private static boolean SAVE_IMAGES = false;

   public static int MAX_REGRESSION_ORDER = 6;
   private static double[] GUESS = new double[]{0,0,0.5,-1.5,1.5,0,0}; // initial fit parameters
   private static int COMMON_PARAM = 8; // 7 (rOO) or 8 (rOH)
   private static int X_PARAM = 7;
   private static int Y_PARAM = 21;

   private static ArrayList<Configuration> ALL_CONFIGS = new ArrayList<>(); // full list of Configurations
   private static ArrayList<Double> SLICE_VALUES = new ArrayList<>(); // all values of COMMON_PARAM
   private static ArrayList<Configuration> CONFIGS = new ArrayList<>();

   private static BufferedWriter[] OUTPUT_WRITER = new BufferedWriter[4];

   // formats for printing output
   private static DecimalFormat R_FORMAT = new DecimalFormat("0.00");
   private static DecimalFormat ENERGY_FORMAT = new DecimalFormat("0.00000");

   public static void main(String[] args){

      createLog("MalonSlice_log", 0);
      createLog("ConfigurationList_ROO-ROH-Energy", 1);
      createLog("MEP_Guess", 2);
      log(1, "R_OO\tR_OH\tEnergy");

      // read in data from all files, populate CONFIGS
      try {
         int i = 1;
         while (new File(FILEPATH + i + ".txt").exists()) {
            log("Reading file: " + FILEPATH + i + ".txt");
            generateCONFIGS(FILEPATH + i + ".txt");
            OUTPUT_WRITER[0].flush();
            i++;
```

```
        }
    }catch(IOException ioe){
        log("Unable to import configurations from file.\n" + ioe.getMessage());
        System.exit(1);
    }
    log("Done reading files!\n\n");

    // for each parameter, generate R_OO and R_OH slices
    for (int i = 0; i < 22; i++){
        if (i == 7 || i == 8) continue;

        Y_PARAM = i;

        // R_OO slices
        COMMON_PARAM = 7;
        X_PARAM = 8;
        calculateSlices();
        CONFIGS.clear();
        CONFIGS.addAll(ALL_CONFIGS);

        // R_OH slices
        COMMON_PARAM = 8;
        X_PARAM = 7;
        calculateSlices();
        CONFIGS.clear();
        CONFIGS.addAll(ALL_CONFIGS);
    }
}

private static void calculateSlices(){

    createLog(Configuration.PARAM_OUTPUT_NAMES.get(Y_PARAM) + "_" +
            Configuration.PARAM_OUTPUT_NAMES.get(COMMON_PARAM) + "_Slices", 3);

    generateSliceValues(); // generates the list of CURRENT_PARAM values
    double[] ranges = getRanges(); // X and Y range for plots

    // for every value of CURRENT_PARAM
    for (Double sliceValue: SLICE_VALUES){
        log("New " + Configuration.PARAM_OUTPUT_NAMES.get(COMMON_PARAM) + ": " + sliceValue);

        ArrayList<double[]> XYpoints = new ArrayList<>();

        ArrayList<Configuration> tempConfigs = new ArrayList<>(); // a copy of CONFIGS to iterate over
        tempConfigs.addAll(CONFIGS);
        for (Configuration c: tempConfigs){
            if (c.getParam(COMMON_PARAM) != sliceValue) continue; // check for correct COMMON_PARAM
            XYpoints.add(new double[]{c.getParam(X_PARAM),c.getParam(Y_PARAM)});
            CONFIGS.remove(c);
        }

        // fit the energy to a potential function, other parameters to a polynomial
        ArrayList<double[]> result;
        if (Y_PARAM == 0 && (X_PARAM == 7 || X_PARAM == 8)) { // Energy vs R_OO or R_OH
            result = doPotentialFitting(XYpoints, null);
        } else {
            result = doPolyFitting(XYpoints, null);
        }

        double[] params = result.get(0);
        double[] sigma = result.get(1);
```

```
        if (Y_PARAM == 0){
            if (X_PARAM == 7 && sliceValue > 1.0) log(2, sliceValue + "\t" + params[1] + "\n");
            if (X_PARAM == 8 && params[1] < 1.0) log(2, params[1] + "\t" + sliceValue + "\n");
        }

        log(3, sliceValue.toString() + " ");
        for (int i = 0; i < params.length; i++) {
            log(3, params[i] + " " + sigma[i] + " ");
        }
        log(3, "\n");

        if (SAVE_IMAGES) {
            String name = Configuration.PARAM_OUTPUT_NAMES.get(Y_PARAM) + " vs " +
                    Configuration.PARAM_OUTPUT_NAMES.get(X_PARAM) + " at " +
                    Configuration.PARAM_OUTPUT_NAMES.get(COMMON_PARAM) + " = " +
                            R_FORMAT.format(sliceValue);
            log("Saving plot: " + name);
            MalonPlot plot = new MalonPlot(ranges);

            plot.addPointSeries(MalonPlot.pointsConvert(XYpoints));

            if (Y_PARAM == 0 && (X_PARAM == 7 || X_PARAM == 8)) {
                plot.addPotential(params, 0.01)
                        .addPoint(new double[]{params[1], params[0]});
            } else {
                plot.addPolynomial(params, 0.01);
            }

            plot.createPlot(name, Configuration.PARAM_OUTPUT_NAMES.get(X_PARAM),
                    Configuration.PARAM_OUTPUT_NAMES.get(Y_PARAM));
            XYLineAndShapeRenderer renderer = plot.getRenderer();
            renderer.setSeriesLinesVisible(0, false);
            renderer.setSeriesShapesFilled(0, false);
            renderer.setSeriesPaint(0, Color.BLACK);
            renderer.setSeriesShapesVisible(1, false);
            plot.savePlot();
        }
        flushLog();
    }
}

// iteratively fits a set of points to a polynomial, decreasing the order each time until all parameters
// are well-defined (or until the polynomial is of order 1)
public static ArrayList<double[]> doPolyFitting(ArrayList<double[]> points, BufferedWriter writer){

    if (writer != null) OUTPUT_WRITER = new BufferedWriter[]{writer};

    boolean fitIsGood;
    int fitNum = 0;
    double[] params;
    RealVector sigma;

    do {
        fitIsGood = true;
        log("Fitting with order: " + String.valueOf(MAX_REGRESSION_ORDER - fitNum));

        double[] guess = new double[MAX_REGRESSION_ORDER - fitNum + 1];
        Arrays.fill(guess, 1);
        LeastSquaresProblem problem = new LSFitting(OUTPUT_WRITER[0]).makePolyLS(points,
                MAX_REGRESSION_ORDER - fitNum, guess);
        LeastSquaresOptimizer.Optimum optimum = new LevenbergMarquardtOptimizer().optimize(problem);
```

```
        params = optimum.getPoint().toArray();
        sigma = optimum.getSigma(0);
        double rms = optimum.getRMS();
        sigma = sigma.mapMultiply(rms);
        log("RMS: " + rms);

        for (int j = 0; j < optimum.getPoint().toArray().length; j++){
            log("a_" + j + " = " + params[j] + "  -  sigma = " + sigma.getEntry(j));
        }

        for (int i = 0; i < params.length; i++){
            if (params[i] == 0 || Double.isNaN(sigma.getEntry(i)) || sigma.getEntry(i) > Math.abs(params[i]))
                fitIsGood = false;
        }

        fitNum++;
    } while (!fitIsGood && fitNum < MAX_REGRESSION_ORDER);

    ArrayList<double[]> result = new ArrayList<>();
    result.add(params);
    result.add(sigma.toArray());
    flushLog();
    return result;
}

// iteratively fits a set of points to a potential function, decreasing the order each time until all parameters
// are well-defined (or until the function is of order 2)
public static ArrayList<double[]> doPotentialFitting(ArrayList<double[]> points, BufferedWriter writer){

    if (writer != null) OUTPUT_WRITER = new BufferedWriter[]{writer};

    boolean fitIsGood;
    int fitNum = 0;
    double[] params;
    RealVector sigma;

    do {
        int order = MAX_REGRESSION_ORDER - 2 * fitNum;
        log("Fitting with order: " + String.valueOf(order));
        fitIsGood = true;

        double[] guess = new double[order+1];
        for (int j = 0; j <= order; j++) guess[j] = GUESS[j];
        double[] minPoint = LSFitting.getMinPoint(points);
        guess[0] = minPoint[1];
        if (order != 0) guess[1] = minPoint[0];

        LeastSquaresProblem problem = new LSFitting(OUTPUT_WRITER[0])
                .makePotentialLS(points, MAX_REGRESSION_ORDER - 2 * fitNum, guess);
        LeastSquaresOptimizer.Optimum optimum = new LevenbergMarquardtOptimizer().optimize(problem);

        params = optimum.getPoint().toArray();
        sigma = optimum.getSigma(0);
        double rms = optimum.getRMS();
        sigma = sigma.mapMultiply(rms);

        log("RMS: " + rms);

        for (int j = 0; j < optimum.getPoint().toArray().length; j++){
            if (j == 0) log("V_equilibrium = " + params[j] + "  -  sigma = " + sigma.getEntry(j));
            else if (j == 1) log("r_equilibrium = " + params[j] + "  -  sigma = " + sigma.getEntry(j));
            else log("a_" + j + " = " + params[j] + "  -  sigma = " + sigma.getEntry(j));
```

```
        }

        for (int i = 0; i < params.length; i++){
            if (i == 1) continue; // don't check for r_equilibrium
            if (params[i] == 0 || Double.isNaN(sigma.getEntry(i)) || sigma.getEntry(i) > Math.abs(params[i]))
                fitIsGood = false;
        }

        fitNum++;
    } while (!fitIsGood && fitNum < MAX_REGRESSION_ORDER / 2);

    ArrayList<double[]> result = new ArrayList<>();
    result.add(params);
    result.add(sigma.toArray());
    flushLog();
    return result;
}

private static double[] getRanges(){

    ArrayList<double[]> points = new ArrayList<>();
    for (Configuration c: ALL_CONFIGS){
        points.add(new double[]{c.getParam(X_PARAM), c.getParam(Y_PARAM)});
    }

    if (points.size() > 0){
        return MalonPlot.getRanges(points);
    }
    else return new double[]{0,1,0,1};
}

private static void generateCONFIGS(String fileName) throws IOException{

    BufferedReader reader = new BufferedReader(new FileReader(new File(fileName)));

    // check that the first line is of the correct form
    String[] firstLine = reader.readLine().split("\\s+");
    if (Configuration.PARAM_INPUT_NAMES.contains(firstLine[1]))
        throw new IOException("First line not properly formatted: " + fileName);

    int configsInRow = firstLine.length - 1;
    Configuration[] configurationRow; // holds each row of configurations from the file
    configurationRow = new Configuration[configsInRow];
    for(int i = 0; i < configsInRow; i++){
        configurationRow[i] = new Configuration();
    }

    while(reader.ready()){
        String[] line = reader.readLine().split("\\s+");

        // at the end of each row of configurations, add contents of array to CONFIGS and create a new array
        if (!Configuration.PARAM_INPUT_NAMES.contains(line[1])){
            CONFIGS.addAll(Arrays.asList(configurationRow));
            ALL_CONFIGS.addAll(Arrays.asList(configurationRow));
            configsInRow = line.length - 1;

            configurationRow = new Configuration[configsInRow];
            for(int i = 0; i < configsInRow; i++){
                configurationRow[i] = new Configuration();
            }
        } else{
            //Eigenvalues line needs additional processing since they are not separated by spaces
```

```
            if (line[1].equals(Configuration.PARAM_INPUT_NAMES.get(0))) line = processEVLine(line);
            for(int i = 0; i < configsInRow; i++){
               configurationRow[i].setParam(Configuration.PARAM_INPUT_NAMES.indexOf(line[1]),
                     Double.parseDouble(line[i+2]));
            }
         }
      }

      for (Configuration c: configurationRow){
         log(1, "\n");
         log(1,R_FORMAT.format(c.getParam(7)) + "\t" +
               R_FORMAT.format(c.getParam(8)) + "\t" + ENERGY_FORMAT.format(c.getParam(0)));
      }

      CONFIGS.addAll(Arrays.asList(configurationRow)); // add last row of configurations
      ALL_CONFIGS.addAll(Arrays.asList(configurationRow));
      reader.close();
   }

   private static String[] processEVLine(String[] line){
      String processLine = line[0] + " " + line[1] + " " + line[3];
      processLine = processLine.replaceAll("-", " -");
      return processLine.split("\\s+");
   }

   private static void generateSliceValues(){

      SLICE_VALUES = new ArrayList<>();
      for (Configuration configuration: ALL_CONFIGS) {
         if (!SLICE_VALUES.contains(configuration.getParam(COMMON_PARAM)))
            SLICE_VALUES.add(configuration.getParam(COMMON_PARAM));
      }
      Collections.sort(SLICE_VALUES);
   }

   // creates an output writer to name.txt, numbering the files if it already exists
   private static void createLog(String name, int index){
      try {
         File logFile;
         if (new File(LOGPATH + name + ".txt").exists()) {
            int c = 2;
            while (new File(LOGPATH + name + "-" + c + ".txt").exists()) c++;
            logFile = new File(LOGPATH + name + "-" + c + ".txt");
         } else {
            logFile = new File(LOGPATH + name + ".txt");
         }
         OUTPUT_WRITER[index] = new BufferedWriter(new FileWriter(logFile));
      }catch (IOException ioe){
         System.out.println("Unable to create log file writer.\n" + ioe.getMessage());
         System.exit(1);
      }
   }

   // writes s to OUTPUT_WRITER[0]
   public static void log(String s){
      try{
         OUTPUT_WRITER[0].write(s);
         OUTPUT_WRITER[0].newLine();
      }catch (IOException ioe){
         System.out.println("Unable to log string: " + s + "\n" + ioe.getMessage());
         System.exit(1);
      }
```

```
    }

    // writes s to OUTPUT_WRITER[index]
    public static void log(int index, String s){
        try{
            OUTPUT_WRITER[index].write(s);
        }catch (IOException ioe){
            System.out.println("Unable to log string: " + s + "\n" + ioe.getMessage());
            System.exit(1);
        }
    }

    private static void flushLog(){
        try{
            for (int i = 0; i < OUTPUT_WRITER.length; i++){
                OUTPUT_WRITER[i].flush();
            }
            OUTPUT_WRITER[0].newLine();

        }catch (IOException ioe){
            System.out.println("Unable to flush log.\n" + ioe.getMessage());
            System.exit(1);
        }
    }
}
```

A.5 - MalonMEP

```
import org.apache.commons.math3.fitting.WeightedObservedPoint;
import org.apache.commons.math3.fitting.leastsquares.*;
import java.io.*;
import java.util.ArrayList;

public class MalonMEP {

   private static String INPUT_PATH = "src/MEP_Input/";
   private static String LOGPATH = "out/";

   private static boolean SAVE_IMAGES = false;
   private static int ITERNUM = 20; // number of iterations
   private static double FILLLIMIT = 0.01; // maximum rOO-rOH distance between calculated MEP points
   private static double ROH_UPPER_LIMIT = 1.18; // calculation of the MEP is not good above this rOH value
   private static double[] RANGES = new double[]{0.88,1.2,2.16,3.52}; // range to calculate the MEP
   private static int FITORDER = 1;
   private static double[] GUESS = new double[]{-1.64,1.72,-0.71,0.74};

   private static ArrayList<ArrayList<ArrayList<Double>>> SLICES = new ArrayList<>();
   // index (0 for OH slice, 1 for OO slice), slice value, param1, sigma1, param2, sigma2...
   private static ArrayList<WeightedObservedPoint> MEP = new ArrayList<>(); // x = rOH, y = rOO
   private static ArrayList<ArrayList<WeightedObservedPoint>> PARAM_RHO = new ArrayList<>();
   // (RHO, Parameter) points
   private static ArrayList<ArrayList<double[]>> PARAM_COORDINATES = new ArrayList<>();
   // (rOO, rOH, Parameter) points

   private static BufferedWriter[] OUTPUT_WRITER = new BufferedWriter[3];

   public static void main(String[] args){

      createAllLogs();
      String logTitle = "rOH rOO";
      for (String param: Configuration.REDUCED_PARAM_NAMES) logTitle = logTitle + " " + param;
      log(1, logTitle);

      for (int i = 0; i < 20; i++) PARAM_COORDINATES.add(new ArrayList<>());

      // read in data from all files, populate SLICES and MEP
      try {
         log("Reading files: " + INPUT_PATH + "MEP_Guess.txt");
         generateMEPGuess(INPUT_PATH + "MEP_Guess.txt");

         for (int i = 0; i < 22; i++){
            if (i == 7 || i == 8) continue; // skip R_OO and R_OH
            SLICES.add(new ArrayList<>());
            String name = INPUT_PATH + Configuration.PARAM_OUTPUT_NAMES.get(i);
            log("Reading files: " + name +"_R_OH_Slices.txt \nand "
                  + name + "_R_OO_Slices.txt");
            generateSLICES(name +"_R_OH_Slices.txt", 0);
            generateSLICES(name +"_R_OO_Slices.txt", 1);
         }
         flushLog();
      }catch(IOException ioe){
         System.out.println("Unable to import configurations from file.\n" + ioe.getMessage());
         log("Unable to import configurations from file.\n" + ioe.getMessage());
         System.exit(1);
      }
      log("Done reading files!\n\n");
```

```
    LeastSquaresProblem problem = new LSFitting(OUTPUT_WRITER[0])
            .makeMEPLS(MalonPlot.backConvert(MEP), FITORDER, GUESS);
    LeastSquaresOptimizer.Optimum optimum = new LevenbergMarquardtOptimizer().optimize(problem);

    double[] results = optimum.getPoint().toArray();

    System.out.println(MEP.size());
    MalonPlot.plotMEP(MEP, results);
    fillMEP();
    System.out.println(MEP.size());
    MalonPlot.plotMEP(MEP, results);

    for (int i = 0; i < ITERNUM; i++){
        boolean finalIteration = (i == ITERNUM - 1);
        ArrayList<WeightedObservedPoint> newMEP = generateNextMEP(results, finalIteration);
        MEP = newMEP;

        problem = new LSFitting(OUTPUT_WRITER[0])
                .makeMEPLS(MalonPlot.backConvert(MEP), FITORDER, GUESS);
        optimum = new LevenbergMarquardtOptimizer().optimize(problem);
        results = optimum.getPoint().toArray();
        MalonPlot.plotMEP(newMEP,results);
    }
    flushLog();

    addNewParams();
    makeParamRHO();
    for (int i = 0; i < 20; i++) {
        MalonPlot.plotParamMEP(PARAM_RHO.get(i), Configuration.REDUCED_PARAM_NAMES.get(i)+
            " vs MEP", "MEP", Configuration.REDUCED_PARAM_NAMES.get(i));
    }
}

// Changes MEP axis to RHO, defined as: B5 - B3
private static void makeParamRHO(){

    for (int i = 0; i < 22; i++){
        log(2,Configuration.REDUCED_PARAM_NAMES.get(i));

        PARAM_RHO.add(new ArrayList<>());
        for (int k = 0; k < PARAM_COORDINATES.get(i).size(); k++){
            double x = PARAM_COORDINATES.get(5).get(k)[2] - PARAM_COORDINATES.get(3).get(k)[2];
            PARAM_RHO.get(i).add(new WeightedObservedPoint(1, x, PARAM_COORDINATES.get(i).get(k)[2]));

            log(2, x + "    " + PARAM_COORDINATES.get(i).get(k)[2] + "   " +
                        PARAM_COORDINATES.get(i).get(k)[0] + "   " + PARAM_COORDINATES.get(i).get(k)[1]);
            flushLog();

            if (i == 0){ // for energy, add the other side of the transition state symmetrically
                PARAM_RHO.get(i).add(new WeightedObservedPoint(1 ,-1*x,
                        PARAM_COORDINATES.get(i).get(k)[2]));
            }
        }
        log(2, "");
    }
}

private static void addNewParams(){

    PARAM_COORDINATES.add(new ArrayList<>());
    PARAM_COORDINATES.add(new ArrayList<>());
```

```
    for (int i = 0; i < PARAM_COORDINATES.get(0).size(); i++) {
        double B5 = PARAM_COORDINATES.get(5).get(i)[2];
        double[] A = new double[]{-1.0*B5, 0};

        double A4 = PARAM_COORDINATES.get(10).get(i)[2] * (Math.PI / 180.0);
        double B3 = PARAM_COORDINATES.get(3).get(i)[2];
        double[] C = new double[]{-1.0*B3*Math.cos(A4), B3*Math.sin(A4)};

        double A2 = PARAM_COORDINATES.get(8).get(i)[2] * (Math.PI / 180.0);
        double alpha = A2 + A4 - Math.PI;

        double B2 = PARAM_COORDINATES.get(2).get(i)[2];
        double[] D = new double[]{C[0] - B2*Math.cos(alpha), C[1] + B2*Math.sin(alpha)};

        double[] R = new double[]{A[0] - D[0], A[1] - D[1]};
        double R_mag = Math.sqrt(R[0]*R[0] + R[1]*R[1]);

        double B7 = PARAM_COORDINATES.get(0).get(i)[0];
        double A6 = PARAM_COORDINATES.get(12).get(i)[2] * (Math.PI / 180.0);
        double B9 = Math.sqrt(B7*B7 + R_mag*R_mag - 2*B7*R_mag*Math.cos(A6));

        double beta = Math.asin(B7*Math.sin(A6)/B9);

        double AdD = A[0]*R[0] + A[1]*R[1];
        double A_mag = Math.sqrt(A[0]*A[0] + A[1]*A[1]);
        double D_mag = Math.sqrt(R[0]*R[0] + R[1]*R[1]);
        double gamma = Math.acos(AdD/(A_mag*D_mag));
        double A8 = beta + gamma;
        double A8deg = A8 * (180.0 / Math.PI);

        double B8 = PARAM_COORDINATES.get(0).get(i)[1];
        PARAM_COORDINATES.get(PARAM_COORDINATES.size()-2).add(new double[]{B7, B8, B9});
        PARAM_COORDINATES.get(PARAM_COORDINATES.size()-1).add(new double[]{B7, B8, A8deg});
    }
}

// adds interpolated points to guess MEP
private static void fillMEP(){
    boolean done;
    do {
        done = true;
        for (int i = 1; i < MEP.size(); i++) {
            double dist = Math.sqrt(Math.pow(MEP.get(i).getX() - MEP.get(i - 1).getX(), 2) +
                    Math.pow(MEP.get(i).getY() - MEP.get(i - 1).getY(), 2));
            if (dist > FILLLIMIT) {
                MEP.add(i, new WeightedObservedPoint(1, (MEP.get(i).getX() + MEP.get(i - 1).getX()) / 2.0,
                        (MEP.get(i).getY() + MEP.get(i - 1).getY()) / 2.0));
                done = false;
            }
        }
    } while (!done);
}

private static ArrayList<WeightedObservedPoint> generateNextMEP(double[] MEPfitParam, boolean
        finalIteration){

    // Points along each perpendicular slice (all parameters)
    ArrayList<ArrayList<double[]>> points = new ArrayList<>();
    for (int i = 0; i < 20; i++) points.add(new ArrayList<>());

    ArrayList<WeightedObservedPoint> nextMEP = new ArrayList<>(); //Min along each slice - new MEP points
```

```
for (WeightedObservedPoint point: MEP){
   log("New MEP Point: " + point.getX() + ", " + point.getY());

   double[] line = getPerpLine(point,MEPfitParam);
   for (int i = 0; i < 20; i++) points.get(i).clear();

   for (ArrayList<Double> slice: SLICES.get(0)){ // each energy slice
      log("Checking Slice: " + slice.get(0) + ", " + slice.get(1));

      // find rOH and rOO of intersection of slice with line
      int index = slice.get(0).intValue(); // 0 for rOH slice, 1 for rOO slice
      double[] position = new double[2];
      position[index] = slice.get(1);
      position[1 - index] = (1 - index) * (line[0] + position[0] * line[1]) +
            (index) * (position[1] - line[0]) / line[1];

      if (position[0] < RANGES[0] || position[0] > RANGES[1] ||
            position[1] < RANGES[2] || position[1] > RANGES[3]) continue;

      double[] subSlice = new double[(slice.size() - 2) / 2];
      for (int i = 2; i < slice.size(); i = i + 2){
         subSlice[i/2 - 1] = slice.get(i); // slice parameters without uncertainty
      }

      // calculate position of the intersection as a distance along the line
      double linePosition = Math.sqrt(Math.pow(position[0]-point.getX(),2) +
            Math.pow(position[1] - point.getY(),2));
      if (position[0] < point.getX()) linePosition *= -1;
      linePosition += -1; // -1 for offset, so that the minimum is far from zero

      // potential energy at the intersection
      double v = LSFitting.potentialEvaluate(position[1 - index], subSlice);

      log("Point Found: " + position[0] + ", " + position[1] + ", " + v +
            ", position on line: " + linePosition);
      points.get(0).add(new double[]{linePosition,v});

      // calculate the value of each parameter at the intersection using the equivalent slice
      if (finalIteration && point.getX() < ROH_UPPER_LIMIT){
         for (int i = 1; i < 20; i++){
            ArrayList<ArrayList<Double>> paramSlices = SLICES.get(i);
            for (ArrayList<Double> paramSlice: paramSlices){
               if (paramSlice.get(0).intValue() == index &&
                     Math.abs(paramSlice.get(1) - position[index]) < FILLLIMIT/10000.0){
                  double[] subParamSlice = new double[(paramSlice.size() - 2) / 2];
                  for (int j = 2; j < paramSlice.size(); j = j + 2){
                     subParamSlice[j/2 - 1] = paramSlice.get(j);
                  }
                  double paramValue = LSFitting.polyEvaluate(position[1 - index], subParamSlice);
                  points.get(i).add(new double[]{linePosition,paramValue});
                  break;
               }
            }
         }
      }
      flushLog();
   }
   if (points.get(0).size() < 5){
      log("Not Enough Points to Fit: " + point.getX() + ", " + point.getY());
      continue;
   }
```

```
        // fitting the energy
        log("Fitting slice... " + points.size() + " / " + SLICES.size() + " slices used");
        ArrayList<double[]> fitResults = MalonSlice.doPotentialFitting(points.get(0), OUTPUT_WRITER[0]);

        double[] reg = fitResults.get(0);
        double min = reg[1] + 1; // +1 for offset
        double vMin = reg[0];

        double theta = Math.atan(line[1]);
        double newROH = point.getX() + min*Math.cos(theta);
        double newROO = point.getY() + min*Math.sin(theta);
        nextMEP.add(new WeightedObservedPoint(reg[0],newROH,newROO));

        //fitting the other parameters
        if (finalIteration && point.getX() < ROH_UPPER_LIMIT){
           PARAM_COORDINATES.get(0).add(new double[]{newROO,newROH,vMin});
           String logString = point.getX() + " " + point.getY() + " " + point.getWeight();
           for(int k = 1; k < 20; k++){
              ArrayList parPoint = points.get(k);
              ArrayList<double[]> paramResults = MalonSlice.doPolyFitting(parPoint,OUTPUT_WRITER[0]);
              double[] paramReg = paramResults.get(0);
              double paramValue = LSFitting.polyEvaluate(reg[1],paramReg);
              PARAM_COORDINATES.get(k).add(new double[]{newROO,newROH,paramValue});
              logString = logString + " " + paramValue;
           }
           log(1,logString);
        }

        if (SAVE_IMAGES){
           log("Saving fitted plots..");

           MalonPlot slicePlot = new MalonPlot(RANGES)
                 .addPointSeries(MEP)
                 .addPolynomial(line, 0.01)
                 .addPoint(new double[]{newROH, newROO});
           MalonPlot.plotPerpSlice(slicePlot, "MEP with slice at - " + point.getX() + ", " + point.getY(),
                 "rOH", "rOO");

           MalonPlot potentialPlot = new MalonPlot(points.get(0))
                 .addPointSeries(MalonPlot.pointsConvert(points.get(0)))
                 .addPotential(reg, 0.01)
                 .addPoint(new double[]{reg[1], reg[0]});
           MalonPlot.plotPerpSlice(potentialPlot, "Potential Slice at - " + point.getX() + ", " + point.getY(),
                 "Position on Line", "Energy");
        }
        flushLog();
     }
     return nextMEP;
  }

  private static double[] getPerpLine(WeightedObservedPoint point, double[] fitParam){

     double x = point.getX();
     double num = 0.0, denom = 0.0;
     double a = 0.0, b = 0.0;
     for (int j = 0; j <= (fitParam.length / 2) - 1; j++){
        num += fitParam[j] * Math.pow(x, j);
        denom += fitParam[j + (fitParam.length / 2)] * Math.pow(x, j);

        a += j * fitParam[j] * Math.pow(x, j - 1);
        b += j * fitParam[j + (fitParam.length / 2)] * Math.pow(x, j - 1);
     }
```

```
    a = a / denom;
    b = -1 * num / (denom * denom) * b;

    double d = a + b;
    double slope = -1.0 / d;
    double yint = point.getY() - (slope * x);

    return new double[]{yint, slope};
}

private static void generateSLICES(String fileName, int index) throws IOException{

    BufferedReader reader = new BufferedReader(new FileReader(new File(fileName)));

    while(reader.ready()){
        String[] line = reader.readLine().split("\\s+");
        ArrayList<Double> slice = new ArrayList<>();

        slice.add((double)index);
        for (String s: line){
            if (s == null) continue;
            slice.add(Double.parseDouble(s));
        }
        SLICES.get(SLICES.size() - 1).add(slice);
    }
    reader.close();
}

private static void generateMEPGuess(String fileName) throws IOException{

    BufferedReader reader = new BufferedReader(new FileReader(new File(fileName)));

    if (MEP.size() == 0) {
        String[] line = reader.readLine().split("\\s+");
        double x = Double.parseDouble(line[0]);
        double y = Double.parseDouble(line[1]);
        MEP.add(new WeightedObservedPoint(1, x, y));
    }

    while(reader.ready()){
        String[] line = reader.readLine().split("\\s+");
        double x = Double.parseDouble(line[0]);
        double y = Double.parseDouble(line[1]);

        for (int i = 0; i < MEP.size(); i++){
            if (MEP.get(i).getY() < y) {
                MEP.add(i,new WeightedObservedPoint(1, x, y));
                break;
            }
            if (i == MEP.size() - 1){
                MEP.add(i+1,new WeightedObservedPoint(1, x, y));
                break;
            }
        }
    }
    reader.close();
}

private static void createAllLogs() {
    createLog("MalonMEP_log", 0);
    createLog("MEPWithParams",1);
```

```
        createLog("MalonParam_Input",2);
    }

    // creates an output writer to name.txt, numbering the files if it already exists
    private static void createLog(String name, int index){
        try {
            File logFile;
            if (new File(LOGPATH + name + ".txt").exists()) {
                int c = 2;
                while (new File(LOGPATH + name + "-" + c + ".txt").exists()) c++;
                logFile = new File(LOGPATH + name + "-" + c + ".txt");
            } else {
                logFile = new File(LOGPATH + name + ".txt");
            }
            OUTPUT_WRITER[index] = new BufferedWriter(new FileWriter(logFile));
        }catch (IOException ioe){
            System.out.println("Unable to create log file writer.\n" + ioe.getMessage());
            System.exit(1);
        }
    }

    // writes s to OUTPUT_WRITER[0]
    public static void log(String s){
        try{
            OUTPUT_WRITER[0].write(s);
            OUTPUT_WRITER[0].newLine();
        }catch (IOException ioe){
            System.out.println("Unable to log string: " + s + "\n" + ioe.getMessage());
            System.exit(1);
        }
    }

    // writes s to OUTPUT_WRITER[index]
    public static void log(int index, String s){
        try{
            OUTPUT_WRITER[index].write(s);
            OUTPUT_WRITER[index].newLine();
        }catch (IOException ioe){
            System.out.println("Unable to log string: " + s + "\n" + ioe.getMessage());
            System.exit(1);
        }
    }

    private static void flushLog(){
        try{
            for (int i = 0; i < OUTPUT_WRITER.length; i++){
                OUTPUT_WRITER[i].flush();
            }
            OUTPUT_WRITER[0].newLine();

        }catch (IOException ioe){
            System.out.println("Unable to flush log.\n" + ioe.getMessage());
            System.exit(1);
        }
    }
}
```

*A.6 - Sample Input for MalonSlice (from Dr. F. Ito **[115]**)*
See table 5.1.1 for descriptions of parameters.

		1	2	3	4	5
Eigenvalues	**--**	**-267.18593**	**-267.18588**	**-267.18581**	**-267.18571**	**-267.18558**
B1		**1.10651**	**1.10668**	**1.10684**	**1.10703**	**1.10720**
B2		**1.23198**	**1.23156**	**1.23114**	**1.23068**	**1.23026**
B3		**1.44527**	**1.44594**	**1.44666**	**1.44732**	**1.44797**
B4		**1.08277**	**1.08291**	**1.08299**	**1.08313**	**1.08325**
B5		**1.35976**	**1.35947**	**1.35922**	**1.35899**	**1.35876**
B6		**1.08643**	**1.08639**	**1.08641**	**1.08637**	**1.08636**
B7		**2.66000**	**2.68000**	**2.70000**	**2.72000**	**2.74000**
B8		**0.92000**	**0.92000**	**0.92000**	**0.92000**	**0.92000**
A1		**119.35755**	**119.34512**	**119.33360**	**119.31772**	**119.30301**
A2		**123.89143**	**124.06511**	**124.23643**	**124.40727**	**124.57596**
A3		**119.70730**	**119.51445**	**119.34717**	**119.16554**	**118.98725**
A4		**120.95845**	**121.30572**	**121.64227**	**121.99104**	**122.33732**
A5		**122.48622**	**122.39822**	**122.29761**	**122.20526**	**122.10721**
A6		**27.67430**	**27.56032**	**27.44175**	**27.32774**	**27.21129**
A7		**108.57830**	**108.60775**	**108.65282**	**108.68641**	**108.73063**
D1		**180.00000**	**180.00000**	**180.00000**	**180.00000**	**180.00000**
D2		**180.00000**	**180.00000**	**180.00000**	**180.00000**	**180.00000**
D3		**0.00000**	**0.00000**	**0.00000**	**0.00000**	**0.00000**
D4		**180.00000**	**180.00000**	**180.00000**	**180.00000**	**180.00000**
D5		**180.00000**	**180.00000**	**180.00000**	**180.00000**	**180.00000**
D6		**0.00000**	**0.00000**	**0.00000**	**0.00000**	**0.00000**
		6	**7**	**8**	**9**	**10**
Eigenvalues	**--**	**-267.18543**	**-267.18526**	**-267.18507**	**-267.18485**	**-267.18462**
B1		**1.10736**	**1.10753**	**1.10768**	**1.10784**	**1.10799**
B2		**1.22985**	**1.22945**	**1.22906**	**1.22867**	**1.22830**
B3		**1.44863**	**1.44927**	**1.44991**	**1.45055**	**1.45118**
B4		**1.08337**	**1.08349**	**1.08361**	**1.08373**	**1.08385**
B5		**1.35855**	**1.35835**	**1.35816**	**1.35799**	**1.35783**
B6		**1.08634**	**1.08633**	**1.08632**	**1.08631**	**1.08630**
B7		**2.76000**	**2.78000**	**2.80000**	**2.82000**	**2.84000**
B8		**0.92000**	**0.92000**	**0.92000**	**0.92000**	**0.92000**
A1		**119.28730**	**119.27098**	**119.25407**	**119.23658**	**119.21854**
A2		**124.74352**	**124.91019**	**125.07616**	**125.24156**	**125.40646**
A3		**118.80894**	**118.62957**	**118.44919**	**118.26804**	**118.08625**
A4		**122.68402**	**123.03182**	**123.38083**	**123.73098**	**124.08223**
A5		**122.00701**	**121.90586**	**121.80388**	**121.70100**	**121.59721**
A6		**27.09389**	**26.97611**	**26.85804**	**26.73963**	**26.62087**
A7		**108.77890**	**108.82960**	**108.88189**	**108.93533**	**108.98967**
D1		**180.00000**	**180.00000**	**180.00000**	**180.00000**	**180.00000**
D2		**180.00000**	**180.00000**	**180.00000**	**180.00000**	**180.00000**
D3		**0.00000**	**0.00000**	**0.00000**	**0.00000**	**0.00000**

D4		180.00000	180.00000	180.00000	180.00000	180.00000
D5		180.00000	180.00000	180.00000	180.00000	180.00000
D6		0.00000	0.00000	0.00000	0.00000	0.00000
		11	12	13	14	15
Eigenvalues	--	-267.18437	-267.18635	-267.18662	-267.18687	-267.18710
B1		1.10813	1.10801	1.10784	1.10768	1.10752
B2		1.22794	1.22857	1.22904	1.22947	1.22981
B3		1.45181	1.45123	1.45049	1.44982	1.44920
B4		1.08398	1.08394	1.08381	1.08368	1.08357
B5		1.35769	1.35820	1.35855	1.35874	1.35882
B6		1.08629	1.08651	1.08652	1.08653	1.08654
B7		2.86000	2.86000	2.84000	2.82000	2.80000
B8		0.92000	0.94000	0.94000	0.94000	0.94000
A1		119.19905	119.13792	119.15310	119.16906	119.18366
A2		125.57169	125.61061	125.45374	125.29423	125.12397
A3		117.91327	117.89496	118.12181	118.29516	118.45425
A4		124.43052	124.41512	124.04980	123.70519	123.36297
A5		121.49219	121.46677	121.56253	121.67181	121.77581
A6		26.49992	26.48893	26.60438	26.71993	26.84128
A7		109.04864	108.61695	108.59702	108.54288	108.45295
D1		180.00000	180.00000	180.00000	180.00000	180.00000
D2		180.00000	180.00000	180.00000	180.00000	180.00000
D3		0.00000	0.00000	0.00000	0.00000	0.00000
D4		180.00000	180.00000	180.00000	180.00000	180.00000
D5		180.00000	180.00000	180.00000	180.00000	180.00000
D6		0.00000	0.00000	0.00000	0.00000	0.00000
		16	17	18	19	20
Eigenvalues	--	-267.18731	-267.18750	-267.18767	-267.18782	-267.18794
B1		1.10737	1.10720	1.10702	1.10684	1.10666
B2		1.23021	1.23063	1.23107	1.23153	1.23200
B3		1.44857	1.44790	1.44722	1.44652	1.44581
B4		1.08345	1.08333	1.08321	1.08309	1.08297
B5		1.35899	1.35921	1.35945	1.35971	1.35999
B6		1.08656	1.08657	1.08659	1.08661	1.08663
B7		2.78000	2.76000	2.74000	2.72000	2.70000
B8		0.94000	0.94000	0.94000	0.94000	0.94000
A1		119.19825	119.21157	119.22403	119.23570	119.24669
A2		124.95744	124.79144	124.62519	124.45823	124.29036
A3		118.62333	118.79981	118.97797	119.15563	119.33236
A4		123.01612	122.66908	122.32316	121.97845	121.63490
A5		121.87545	121.97438	122.07269	122.16985	122.26566
A6		26.95904	27.07553	27.19155	27.30721	27.42243
A7		108.38653	108.32868	108.27424	108.22165	108.17083
D1		180.00000	180.00000	180.00000	180.00000	180.00000
D2		180.00000	180.00000	180.00000	180.00000	180.00000
D3		0.00000	0.00000	0.00000	0.00000	0.00000

D4		180.00000	180.00000	180.00000	180.00000	180.00000
D5		180.00000	180.00000	180.00000	180.00000	180.00000
D6		0.00000	0.00000	0.00000	0.00000	0.00000
		21	22	23	24	25
Eigenvalues	--	-267.18804	-267.18810	-267.18947	-267.18938	-267.18926
B1		1.10647	1.10628	1.10606	1.10625	1.10645
B2		1.23249	1.23298	1.23397	1.23346	1.23295
B3		1.44509	1.44435	1.44344	1.44420	1.44494
B4		1.08284	1.08272	1.08267	1.08280	1.08292
B5		1.36028	1.36059	1.36147	1.36113	1.36079
B6		1.08665	1.08668	1.08693	1.08690	1.08688
B7		2.68000	2.66000	2.66000	2.68000	2.70000
B8		0.94000	0.94000	0.96000	0.96000	0.96000
A1		119.25710	119.26709	119.17509	119.16602	119.15599
A2		124.12154	123.95173	124.01171	124.17897	124.34530
A3		119.50823	119.68336	119.68041	119.49970	119.31631
A4		121.29251	120.95131	120.94098	121.28218	121.62525
A5		122.36007	122.45309	122.41883	122.31996	122.22753
A6		27.53719	27.65148	27.62184	27.51023	27.39749
A7		108.12205	108.07565	107.58051	107.62809	107.68126
D1		180.00000	180.00000	180.00000	180.00000	180.00000
D2		180.00000	180.00000	180.00000	180.00000	180.00000
D3		0.00000	0.00000	0.00000	0.00000	0.00000
D4		180.00000	180.00000	180.00000	180.00000	180.00000
D5		180.00000	180.00000	180.00000	180.00000	180.00000
D6		0.00000	0.00000	0.00000	0.00000	0.00000
		26	27	28	29	30
Eigenvalues	--	-267.18911	-267.18894	-267.18874	-267.18853	-267.18829
B1		1.10664	1.10683	1.10701	1.10719	1.10737
B2		1.23245	1.23195	1.23147	1.23101	1.23056
B3		1.44569	1.44642	1.44714	1.44784	1.44854
B4		1.08305	1.08317	1.08329	1.08342	1.08354
B5		1.36048	1.36019	1.35992	1.35966	1.35942
B6		1.08685	1.08683	1.08681	1.08679	1.08677
B7		2.72000	2.74000	2.76000	2.78000	2.80000
B8		0.96000	0.96000	0.96000	0.96000	0.96000
A1		119.14781	119.13929	119.13003	119.11993	119.10895
A2		124.51149	124.67737	124.84249	125.00679	125.17031
A3		119.13933	118.96356	118.78745	118.61058	118.43296
A4		121.96813	122.31172	122.65641	123.00226	123.34925
A5		122.13323	122.03831	121.94218	121.84473	121.74599
A6		27.28385	27.16955	27.05472	26.93941	26.82361
A7		107.73795	107.79725	107.85854	107.92157	107.98619
D1		180.00000	180.00000	180.00000	180.00000	180.00000
D2		180.00000	180.00000	180.00000	180.00000	180.00000
D3		0.00000	0.00000	0.00000	0.00000	0.00000

D4		180.00000	180.00000	180.00000	180.00000	180.00000
D5		180.00000	180.00000	180.00000	180.00000	180.00000
D6		0.00000	0.00000	0.00000	0.00000	0.00000
		31	32	33	34	35
Eigenvalues	--	-267.18804	-267.18777	-267.18749	-267.18790	-267.18820
B1		1.10754	1.10770	1.10787	1.10770	1.10754
B2		1.23012	1.22969	1.22928	1.23004	1.23046
B3		1.44923	1.44991	1.45058	1.44991	1.44922
B4		1.08366	1.08378	1.08390	1.08387	1.08375
B5		1.35920	1.35899	1.35880	1.35943	1.35964
B6		1.08676	1.08674	1.08673	1.08695	1.08697
B7		2.82000	2.84000	2.86000	2.86000	2.84000
B8		0.96000	0.96000	0.96000	0.98000	0.98000
A1		119.09711	119.08445	119.07104	118.99724	119.00899
A2		125.33315	125.49541	125.65716	125.70693	125.54224
A3		118.25463	118.07560	117.89585	117.89374	118.06949
A4		123.69735	124.04657	124.39691	124.37933	124.02688
A5		121.64607	121.54506	121.44303	121.41876	121.51389
A6		26.70733	26.59057	26.47334	26.45486	26.57420
A7		108.05220	108.11938	108.18752	107.73059	107.65344
D1		180.00000	180.00000	180.00000	180.00000	180.00000
D2		180.00000	180.00000	180.00000	180.00000	180.00000
D3		0.00000	0.00000	0.00000	0.00000	0.00000
D4		180.00000	180.00000	180.00000	180.00000	180.00000
D5		180.00000	180.00000	180.00000	180.00000	180.00000
D6		0.00000	0.00000	0.00000	0.00000	0.00000
		36	37	38	39	40
Eigenvalues	--	-267.18849	-267.18877	-267.18903	-267.18927	-267.18949
B1		1.10737	1.10719	1.10700	1.10681	1.10661
B2		1.23093	1.23140	1.23189	1.23240	1.23291
B3		1.44851	1.44778	1.44705	1.44631	1.44555
B4		1.08362	1.08350	1.08337	1.08325	1.08312
B5		1.35987	1.36013	1.36040	1.36069	1.36100
B6		1.08699	1.08701	1.08704	1.08706	1.08708
B7		2.82000	2.80000	2.78000	2.76000	2.74000
B8		0.98000	0.98000	0.98000	0.98000	0.98000
A1		119.01787	119.02640	119.03405	119.04086	119.04685
A2		125.38479	125.22362	125.06168	124.89876	124.73491
A3		118.24032	118.41797	118.59533	118.77174	118.94718
A4		123.68377	123.33691	122.99086	122.64589	122.30213
A5		121.61535	121.71354	121.81049	121.90602	122.00004
A6		26.68797	26.80322	26.91776	27.03166	27.14499
A7		107.57651	107.50357	107.43225	107.36263	107.29479
D1		180.00000	180.00000	180.00000	180.00000	180.00000
D2		180.00000	180.00000	180.00000	180.00000	180.00000
D3		0.00000	0.00000	0.00000	0.00000	0.00000

D4		180.00000	180.00000	180.00000	180.00000	180.00000
D5		180.00000	180.00000	180.00000	180.00000	180.00000
D6		0.00000	0.00000	0.00000	0.00000	0.00000
		41	42	43	44	45
Eigenvalues	--	-267.18970	-267.18987	-267.19003	-267.19015	-267.19025
B1		1.10641	1.10621	1.10599	1.10578	1.10553
B2		1.23345	1.23400	1.23456	1.23515	1.23626
B3		1.44478	1.44400	1.44320	1.44238	1.44138
B4		1.08300	1.08288	1.08275	1.08263	1.08257
B5		1.36133	1.36168	1.36204	1.36243	1.36341
B6		1.08711	1.08715	1.08718	1.08722	1.08749
B7		2.72000	2.70000	2.68000	2.66000	2.66000
B8		0.98000	0.98000	0.98000	0.98000	1.00000
A1		119.05204	119.05651	119.06034	119.06367	118.95827
A2		124.57015	124.40444	124.23771	124.06989	124.13259
A3		119.12185	119.29584	119.46920	119.64193	119.62344
A4		121.95958	121.61823	121.27808	120.93913	120.93315
A5		122.09254	122.18350	122.27287	122.36060	122.31611
A6		27.25775	27.36993	27.48150	27.59246	27.55697
A7		107.22893	107.16535	107.10438	107.04635	106.50540
D1		180.00000	180.00000	180.00000	180.00000	180.00000
D2		180.00000	180.00000	180.00000	180.00000	180.00000
D3		0.00000	0.00000	0.00000	0.00000	0.00000
D4		180.00000	180.00000	180.00000	180.00000	180.00000
D5		180.00000	180.00000	180.00000	180.00000	180.00000
D6		0.00000	0.00000	0.00000	0.00000	0.00000
		46	47	48	49	50
Eigenvalues	--	-267.19009	-267.18990	-267.18969	-267.18945	-267.18920
B1		1.10573	1.10595	1.10617	1.10638	1.10659
B2		1.23573	1.23513	1.23453	1.23395	1.23339
B3		1.44219	1.44299	1.44382	1.44464	1.44543
B4		1.08271	1.08283	1.08295	1.08308	1.08320
B5		1.36304	1.36264	1.36225	1.36188	1.36153
B6		1.08746	1.08742	1.08738	1.08735	1.08732
B7		2.68000	2.70000	2.72000	2.74000	2.76000
B8		1.00000	1.00000	1.00000	1.00000	1.00000
A1		118.95437	118.95074	118.94989	118.94835	118.94590
A2		124.30135	124.46639	124.63110	124.79486	124.95766
A3		119.44515	119.27609	119.10290	118.92898	118.75470
A4		121.27364	121.61192	121.95222	122.29361	122.63618
A5		122.22251	122.13625	122.04811	121.95827	121.86683
A6		27.44853	27.33852	27.22808	27.11702	27.00527
A7		106.57939	106.63724	106.70659	106.77870	106.85320
D1		180.00000	180.00000	180.00000	180.00000	180.00000
D2		180.00000	180.00000	180.00000	180.00000	180.00000
D3		0.00000	0.00000	0.00000	0.00000	0.00000

D4		180.00000	180.00000	180.00000	180.00000	180.00000
D5		180.00000	180.00000	180.00000	180.00000	180.00000
D6		0.00000	0.00000	0.00000	0.00000	0.00000
		51	52	53	54	55
Eigenvalues	--	-267.18892	-267.18864	-267.18833	-267.18801	-267.18768
B1		1.10679	1.10699	1.10718	1.10736	1.10754
B2		1.23285	1.23232	1.23181	1.23132	1.23083
B3		1.44621	1.44698	1.44773	1.44848	1.44921
B4		1.08333	1.08345	1.08358	1.08370	1.08382
B5		1.36120	1.36090	1.36061	1.36034	1.36009
B6		1.08729	1.08726	1.08724	1.08722	1.08720
B7		2.78000	2.80000	2.82000	2.84000	2.86000
B8		1.00000	1.00000	1.00000	1.00000	1.00000
A1		118.94252	118.93821	118.93297	118.92678	118.91964
A2		125.11955	125.28061	125.44087	125.60043	125.75936
A3		118.57994	118.40455	118.22849	118.05171	117.87421
A4		122.97995	123.32490	123.67103	124.01831	124.36675
A5		121.77385	121.67939	121.58350	121.48624	121.38769
A6		26.89285	26.77981	26.66615	26.55189	26.43705
A7		106.92977	107.00817	107.08819	107.16961	107.25219
D1		180.00000	180.00000	180.00000	180.00000	180.00000
D2		180.00000	180.00000	180.00000	180.00000	180.00000
D3		0.00000	0.00000	0.00000	0.00000	0.00000
D4		180.00000	180.00000	180.00000	180.00000	180.00000
D5		180.00000	180.00000	180.00000	180.00000	180.00000
D6		0.00000	0.00000	0.00000	0.00000	0.00000

Appendix B

Supplementary Material - Line Lists

The full sets of lines and combination differences used in the multi-state fitting (as summarized in figure 4.9.1), as well as some assigned lines that were not used, are available in a separate document hosted by the University of New Brunswick library at "https://unbscholar.lib.unb.ca/islandora/object/unbscholar%3A7951".

References

[1] W. F. Rowe, R. W. Duerst, and E. B. Wilson, *J. Am. Chem. Soc.* **98**, 4021 (1976).

[2] S. L. Baughcum, R. W. Duerst, W. F. Rowe, Z. Smith, and E. B. Wilson, *J. Am. Chem. Soc.* **103**, 6296 (1981).

[3] S. L. Baughcum, Z. Smith, E. B. Wilson, and R. W. Duerst, *J. Am. Chem. Soc.* **106**, 2260 (1984).

[4] P. Turner, S. L. Baughcum, S. L. Coy, and Z. Smith, *J. Am. Chem. Soc.* **106**, 2265 (1984).

[5] W. F. Rowe, Ph.D. Thesis, Harvard University, 1975.

[6] J. E. Del Bene and W. L. Kochenour, *J. Am. Chem. Soc.* **98**, 2041 (1976).

[7] E. M. Fluder and J. R. de la Vega, *J. Am. Chem. Soc.* **100**, 5265 (1978).

[8] J. Catalán, M. Yáñez, and J. I. Fernández-Alonso, *J. Am. Chem. Soc.* **100**, 6917 (1978).

[9] G. Karlström, H. Wennerström, B. Jönsson, S. Forsén, J. Almlöf, and B. Roos, *J. Am. Chem. Soc.* **97**, 4188 (1975).

[10] P. Schuster, *Chem. Phys. Lett.* **3**, 433 (1969).

[11] S. Kato, H. Kato, and K. Fukui, *J. Am. Chem. Soc.* **99**, 684 (1977).

[12] D. L. Breen, *J. Phys. Chem.* **82**, 714 (1978).

[13] A. D. Isaacson and K. Morokuma, *J. Am. Chem. Soc.* **97**, 4453 (1975).

[14] C. J. Seliskar and R. E. Hoffmann, *J. Am. Chem. Soc.* **99**, 7072 (1977).

[15] R. S. Brown, *J. Am. Chem. Soc.* **99**, 5497 (1977).

[16] R. S. Brown, A. Tse, T. Nakashima, and R. C. Haddon, *J. Am. Chem. Soc.* **101**, 3157 (1979).

[17] Z. Smith, E. B. Wilson, and R. W. Duerst, *Spectroc. Acta Pt. A-Molec. Biomolec. Spectr.* **39**, 1117 (1983).

[18] M. J. Frisch, A. C. Scheiner, H. F. Schaefer III, and J. S. Binkley, *J. Chem. Phys.* **82**, 4194 (1985).

[19] J. S. Binkley, M. J. Frisch, and H. F. Schaefer III, *Chem. Phys. Lett.* **126**, 1 (1986).

[20] J. Bicerano, H. F. Schaefer III, and W. H. Miller, *J. Am. Chem. Soc.* **105**, 2550 (1983).

[21] C. J. Seliskar and R. E. Hoffman, *Chem. Phys. Lett.* **43**, 481 (1976).

[22] C. J. Seliskar and R. E. Hoffmann, *J. Mol. Spectrosc.* **88**, 30 (1981).

[23] A. A. Arias, T. A. W. Wasserman, and P. H. Vaccaro, *J. Chem. Phys.* **107**. 5617 (1997).

[24] C. J. Seliskar and R. E. Hoffmann, *J. Mol. Spectrosc.* **96**, 146 (1982).

[25] D. W. Firth, K. Beyer, M. A. Dvorak, S. W. Reeve, A. Grushow, and K. R. Leopold, *J. Chem. Phys.* **94**, 1812 (1991).

[26] T. Baba, T. Tanaka, I. Morino, K. M. T. Yamada, and K. Tanaka, *J. Chem. Phys.* **110**, 4131 (1999).

[27] C. Duan and D. Luckhaus, *Chem. Phys. Lett.* **391**, 129 (2004).

[28] D. W. Firth, P. F. Barbara, and H. P. Trommsdorff, *Chem. Phys.* **136**, 349 (1989).

[29] T. Chiavassa, P. Roubin, L. Pizzala, P. Verlaque, A. Allouche, and F. Marinelli, *J. Phys. Chem.* **96**, 10659 (1992).

[30] T. N. Wassermann, D. Luckhaus, S. Coussan, and M. A. Suhm, *Phys. Chem. Chem. Phys.* **8**, 2344 (2006).

[31] T. D. Sewell, Y. Guo, and D. L. Thompson, *J. Chem. Phys.* **103**, 8557 (1995).

[32] V. A. Benderskii, E. V. Vetoshkin, and H. P. Trommsdorff, *Chem. Phys.* **271**, 165 (2001).

[33] R. Meyer and T. Ha, *Mol. Phys.* **101**, 3263 (2003).

[34] D. P. Tew, N. C. Handy, and S. Carter, *Mol. Phys.* **102**, 2217 (2004).

[35] N. O. B. Lüettschwager, T. N. Wassermann, S. Coussan, and M. A. Suhm, *Phys. Chem. Chem. Phys.* **12**, 8201 (2010).

[36] N. O. B. Lüettschwager, T. N. Wassermann, S. Coussan, and M. A. Suhm, *Mol. Phys.* **111**, 2211 (2013).

[37] T. Hammer and U. Manthe, *J. Chem. Phys.* **136**, 054105 (2012).

[38] N. Makri and W. H. Miller, *J. Chem. Phys.* **91**, 4026 (1989).

[39] J. O. Richardson and S. C. Althorpe, *J. Chem. Phys.* **134**, 054109 (2011)

[40] Z. Smedarchina, W. Siebrand, and A Fernández-Ramos, *J. Chem. Phys.* **137**, 224105 (2012)

[41] T. D. Sewell and D. L. Thompson, *Chem. Phys. Lett.* **193**, 347 (1992)

[42] Z. Smedarchina, W. Siebrand, and M. Z. Zgierski, *J. Chem. Phys.* **103**, 5326 (1995)

[43] Y. Guo, T. D. Sewell, and D. L. Thompson, *Chem. Phys. Lett.* **224**, 470 (1994)

[44] G. V. Mil'nikov, K. Yagi, T. Taketsugu, H. Nakamura, and K. Hirao, *J. Chem. Phys.* **119**, 10 (2003)

[45] G. V. Mil'nikov, K. Yagi, T. Taketsugu, H. Nakamura, and K. Hirao, *J. Chem. Phys.* **120**, 5036 (2004)

[46] V. A. Benderskii, E. V. Vetoshkin, S. Y. Grebenshchikov, L. von Laue, and H. P. Trommsdorff, *Chem. Phys.* **219**, 119 (1997)

[47] V. A. Benderskii, E. V. Vetoshkin, L. von Laue, and H. P. Trommsdorff, *Chem. Phys.* **219**, 143 (1997)

[48] V. A. Benderskii, E. V. Vetoshkin, I. S. Irgibaeva, and H. P. Trommsdorff, *Chem. Phys.* **262**, 393 (2000)

[49] C. S. Tautermann, A. F. Voegele, T. Loerting, and K. R. Liedl, *J. Chem. Phys.* **117**, 1962 (2002)

[50] C. S. Tautermann, A. F. Voegele, T. Loerting, and K. R. Liedl, *J. Chem. Phys.* **117**, 1967 (2002)

[51] E. Bosch, M. Moreno, and L. M. Lluch, *Chem. Phys.* **159**, 99 (1992)

[52] E. Bosch, M. Moreno, and L. M. Lluch, *Chem. Phys. Lett.* **196**, 73 (1992)

[53] K. Yagi, T. Taketsugu, and K. Hirao, *J. Chem. Phys.* **115**, 10647 (2001)

[54] G. V. Mil'nikov and H. Nakamura, *J. Chem. Phys.* **115**, 6881 (2001)

[55] K. Yagi, G. V. Mil'nikov, T. Taketsugu, K. Hirao, and H. Nakamura, *Chem. Phys. Lett.* **397**, 435 (2004)

[56] T. Carrington and W. H. Miller, *J. Chem. Phys.* **84**, 4364 (1986)

[57] N. Shida, P. F. Barbara, and J. E. Almlöf, *J. Chem. Phys.* **91**, 4061 (1989)

[58] N. Shida, J. E. Almlöf, and P. F. Barbara, *J. Phys. Chem.* **95**, 10457 (1991)

[59] E. Bosch, M. Moreno, J. M. Lluch, and J. Bertrán, *J. Chem. Phys.* **93**, 5685 (1990)

[60] V. Aquilanti, G. Capecchi, S. Cavalli, C. Adamo, and V. Barone, *Phys. Chem. Chem. Phys.* **2**, 4095 (2000)

[61] D. Babić, S. D. Bosanac, N. Došlić, *Chem. Phys. Lett.* **358**, 337 (2002)

[62] G. Kovačević, T. Hrenar, and N Došlić, *Chem. Phys.* **293**, 41 (2003)

[63] T. Hayashi and S. Mukamel, *J. Phys. Chem. A* **107**, 9113 (2003)

[64] D. P. Tew, N. C. Handy, and S. Carter, *J. Chem. Phys.* **125**, 084313 (2006)

[65] M. E. Tuckerman and D. Marx, *Phys. Rev. Lett.* **86**, 4946 (2001)

[66] W. Siebrand, Z. Smedarchina, and A. Fernández-Ramos, *J. Chem. Phys.* **139**, 021101 (2013)

[67] S. F. Tayyari and F. Milani-Nejad, *Spectrochimica Acta Part A* **54**, 255 (1998)

[68] J. Spanget-Larsen, *Chem. Phys.* **240**, 51 (1999)

[69] S. F. Tayyari, M. Z. Tabrizi, F. Tayyari and F. Milani-Nejad, *Journal of Molecular Structure (Theochem)* **637**, 171 (2003)

[70] Y. Wang, B. J. Braams, J. M. Bowman, S. Carter, and D. P. Tew, *J. Chem. Phys.* **128**, 224314 (2008)

[71] M. Schröder and H. Meyer, *J. Chem. Phys.* **141**, 034116 (2014)

[72] T. Hammer, M. D. Coutinho-Neto, A. Viel, and U. Manthe, *J. Chem. Phys.* **131**, 224109 (2009)

[73] T. Hammer and U. Manthe, *J. Chem. Phys.* **134**, 224305 (2011)

[74] M. Schröder, F. Gatti, and H. Meyer, *J. Chem. Phys.* **134**, 234307 (2011)

[75] W. Mizukami, S. Habershon, and D. P. Tew, *J. Chem. Phys.* **141**, 144310 (2014)

[76] Z. Latajka and S. Scheiner, *J. Phys. Chem.* **96**, 9764 (1992)

[77] K. Luth and S. Scheiner, *J. Phys. Chem.* **98**, 3582 (1994)

[78] G. Buemi and F. Zuccarello, *J. Chem. Soc., Faraday Trans.* **92**, 347 (1996)

[79] V. Barone and C. Adamo, *J. Chem. Phys.* **105**, 11007 (1996)

[80] K. Wolf, W. Mikenda, E. Nusterer, and K. Schwarz, *J. Mol. Struct.* **448**, 201 (1998)

[81] X. Krokidis, V. Goncalves, A. Savin, and B. Silvi, *J. Phys. Chem. A* **102**, 5065 (1998)

[82] A. L. Sobolewski and W. Domcke, *J. Phys. Chem. A* **103**, 4494 (1999)

[83] S. Sadhukhan, D. Muñoz, C. Adamo, and G. E. Scuseria, *Chem. Phys. Lett.* **306**, 83 (1999)

[84] D. P. Tew, N. C. Handy, S. Carter, S. Irle, and J. Bowman, *Mol. Phys.* **101**, 3513 (2003)

[85] A. Alparone and S. Millefiori, *Chem. Phys.* **290**, 15 (2003)

[86] M. D. Coutinho-Neto, A. Viel, and U. Manthe, *J. Chem. Phys.* **121**, 9207 (2004)

[87] R. Meyer and T. Ha, *Mol. Phys.* **103**, 2687 (2005)

[88] F. Fillaux and B. Nicolaï, *Chem. Phys. Lett.* **415**, 357 (2005)

[89] Ł. Walewski, D. Krachtus, S. Fischer, J. C. Smith, P. Bała, and B. Lesyng, *Int. J. Quantum Chem.* **106**, 636 (2006)

[90] A. Miani, P. Carloni, and S. Raugei, *Chem. Phys. Lett.* **427**, 230 (2006)

[91] J. N. Woodford, *J. Phys. Chem. A* **111**, 8519 (2007)

[92] A. Viel, M. D. Coutinho-Neto, and U. Manthe, *J. Chem. Phys.* **126**, 024308 (2007)

[93] J. Stare, *J. Chem. Inf. Model.* **47**, 840 (2007)

[94] P. P. Schmidt, *Mol. Phys.* **105**, 1217 (2007)

[95] E. Kamarchik, D. A. Mazziotti, *Phys. Rev. A* **79**, 012502 (2009)

[96] A. Hazra, J. H. Skone, and S. Hammes-Schiffer, *J. Chem. Phys.* **130**, 054108 (2009)

[97] Y. Yang and M. Meuwly, *J. Chem. Phys.* **133**, 064503 (2010)

[98] P. Hamm and G. Stock, *Phys. Rev. Lett.* **109**, 173201 (2012)

[99] Y. Wang and J. M. Bowman, *J. Chem. Phys.* **139**, 154303 (2013)

[100] A. Fernández-Ramos, Z. Smedarchina, and W. Siebrand, *Phys. Rev. E* **90**, 033306 (2014)

[101] B. P. Winnewisser, M. Winnewisser, I. R. Medvedev, F. C. De Lucia, S. C. Ross, J. Koput, *Phys. Chem. Chem. Phys.* **12**, 8158 (2010)

[102] P. R. Bunker and P. Jensen, "Molecular Symmetry and Spectroscopy", 2nd edition. NRC Research Press, Ottawa, Ontario, Canada. 2006.

[103] E. B. Wilson, J. C. Decius, and P. C. Cross, "Molecular Vibrations: The Theory of Infrared and Raman Vibrational Spectra". Dover Publications, Inc. New York. 1955.

[104] J. K. G. Watson, in “Vibrational Spectra and Structures” (James R. Durig, Ed.), Vol. 6, pp. 1-89. Dekker, New York, 1977.

[105] A. Trivella, S. Coussan, and T. Chiavassa, *Synthetic Communications* **38**, 3285 (2008)

[106] M. Winnewisser, B. P. Winnewisser, F. C. De Lucia, D. W. Tokaryk, S. C. Ross, and B. E. Billinghurst, *Phys. Chem. Chem. Phys.* **16**, 17373 (2014)

[107] B. E. Billinghurst, Staff Scientist - Far-Infrared Beamline, Canadian Light Source Inc. (personal communication)

[108] OPUS Version 7.0, Bruker Corporation, 2011

[109] Igor Pro Version 6.3.7.2, WaveMetrics, Inc., 2014

[110] C. F. Neese, An interactive LOOMISWOOD package for spectral assignment in Igor Pro, version 2.0, 56th Ohio State University International Symposium on Molecular Spectroscopy (The Ohio State University, Columbus, Ohio, 2001).

[111] H. M. Pickett, *J. Mol. Spectrosc.* **148**, 371 (1991).

[112] PGOPHER, a Program for Simulating Rotational Structure, C. M. Western, University of Bristol, http://pgopher.chm.bris.ac.uk

[113] M. Niedenhoff, G. Winnewisser, K. M. T. Yamada, and S. P. Belov, *J. Mol. Spectrosc.* **169**, 224 (1995)

[114] M. Niedenhoff, K. M. T. Yamada, and G. Winnewisser, *J. Mol. Spectrosc.* **183**, 176 (1997)

[115] Personal communication with Dr. S. Ross from Dr. Fumiyuki Ito, Senior Researcher Atmospheric Environment Research Group, EMRI, AIST, Tsukuba-West, Tsukuba, Ibaraki, Japan.

[116] M. J. Frisch, G. W. Trucks, H. B. Schlegel, G. E. Scuseria, M. A. Robb, J. R. Cheeseman, G. Scalmani, V. Barone, B. Mennucci, G. A. Petersson, H. Nakatsuji, M. Caricato, X. Li, H. P. Hratchian, A. F. Izmaylov, J. Bloino, G. Zheng, J. L. Sonnenberg, M. Hada, M. Ehara, K. Toyota, R. Fukuda, J. Hasegawa, M. Ishida, T. Nakajima, Y. Honda, O. Kitao, H. Nakai, T. Vreven, J. A. Montgomery, Jr., J. E. Peralta, F. Ogliaro, M. Bearpark, J. J. Heyd, E. Brothers, K. N. Kudin, V. N. Staroverov, R. Kobayashi, J. Normand, K. Raghavachari, A. Rendell, J. C. Burant, S. S. Iyengar, J. Tomasi, M. Cossi, N. Rega, J. M. Millam, M. Klene, J. E. Knox, J. B. Cross, V. Bakken, C. Adamo, J. Jaramillo, R. Gomperts, R. E. Stratmann, O. Yazyev, A. J. Austin, R. Cammi, C. Pomelli, J. W. Ochterski, R. L. Martin, K. Morokuma, V. G. Zakrzewski, G. A. Voth, P. Salvador, J. J. Dannenberg, S. Dapprich, A. D. Daniels, Farkas, J. B. Foresman, J. V. Ortiz, J. Cioslowski, D. J. Fox, Gaussian 09, Revision A.02, gaussian Inc. Wallingford CT, 2009.

[117] Apache Commons Math (commons-math3-3.5), The Apache Software Foundation. http://commons.apache.org/proper/commons-math/index.html

[118] JFreeChart (Version 1.0.19), Object Refinery Limited. http://www.jfree.org/jfreechart/

Curriculum Vitae
Edward Scott Goudreau

Degrees

2014/9 - 2016/10 Master of Science (MSc.)
Physics
University of New Brunswick
Thesis: "Far-Infrared Synchrotron-Based Spectroscopy of Proton Tunnelling in Malonaldehyde"

2009/9 - 2014/5 Bachelor of Science (BSc.), Honours
Chemistry, Physics (Mathematics minor)
University of New Brunswick
Thesis: "Rotationally Resolved High-resolution Laser Spectroscopy of NiB"

Publications and Presentations

Journal Publications

[1] E. S. Goudreau, A. G. Adam, D. W. Tokaryk, and C. Linton, *J. Mol. Spectrosc.* **314**, 13 (2015) - "High resolution laser spectroscopy of the [20.6]0.5–$X^2\Sigma^+$ transition of nickel monoboride, NiB"

Presentations
(The underlined name indicates the presenter)

2016/9 E. S. Goudreau, D. W. Tokaryk, S. C. Ross, and B. E. Billinghurst
International Symposium for Molecular Spectroscopy (ISMS)
"Progress in the Rotational Analysis of the Ground and Low-Lying Vibrationally Excited States of Malonaldehyde"

2016/9 E. S. Goudreau, D. W. Tokaryk, and S. C. Ross
CSC Canadian Chemistry Conference and Exhibition
"Far-infrared Synchrotron-based Spectroscopy of Proton Tunnelling in Malonaldehyde"

2015/9 E. S. Goudreau, D. W. Tokaryk, and S. C. Ross
International Symposium for Molecular Spectroscopy (ISMS)
"Far-infrared Synchrotron-based Spectroscopy of Proton Tunnelling in Malonaldehyde"

2015/9 E. S. Goudreau, C. Linton, D. W. Tokaryk, and A. G. Adam
International Symposium for Molecular Spectroscopy (ISMS)
"High Resolution Laser Spectroscopy of Nickel Monoboride, NiB"

Conference Publications

A. Riazanov, M. M. Hindle, E. S. Goudreau, C. J. Martyniuk, and C. J. O. Baker
Semantic Web Applications and Tools for Life Sciences 2012 (SWAT4LS 2012)
"Ecotoxicology Data Federation with SADI Semantic Web Services"